TOWARDS BIO-INTEGRATING INTERFACES IN ORGANIC NEUROTECHNOLGY DEVELOPMENT

by

Takashi Daniel Yoshida Kozai

A dissertation submitted in partial fulfillment
of the requirements for the degree of
Doctor of Philosophy
(Biomedical Engineering)
in The University of Michigan
2011

Doctoral Committee:

Professor Daryl R. Kipke, Chair
Professor Nicholas A. Kotov
Associate Professor Joerg Lahann
Associate Professor Jan P. Stegemann

Microelectrodes

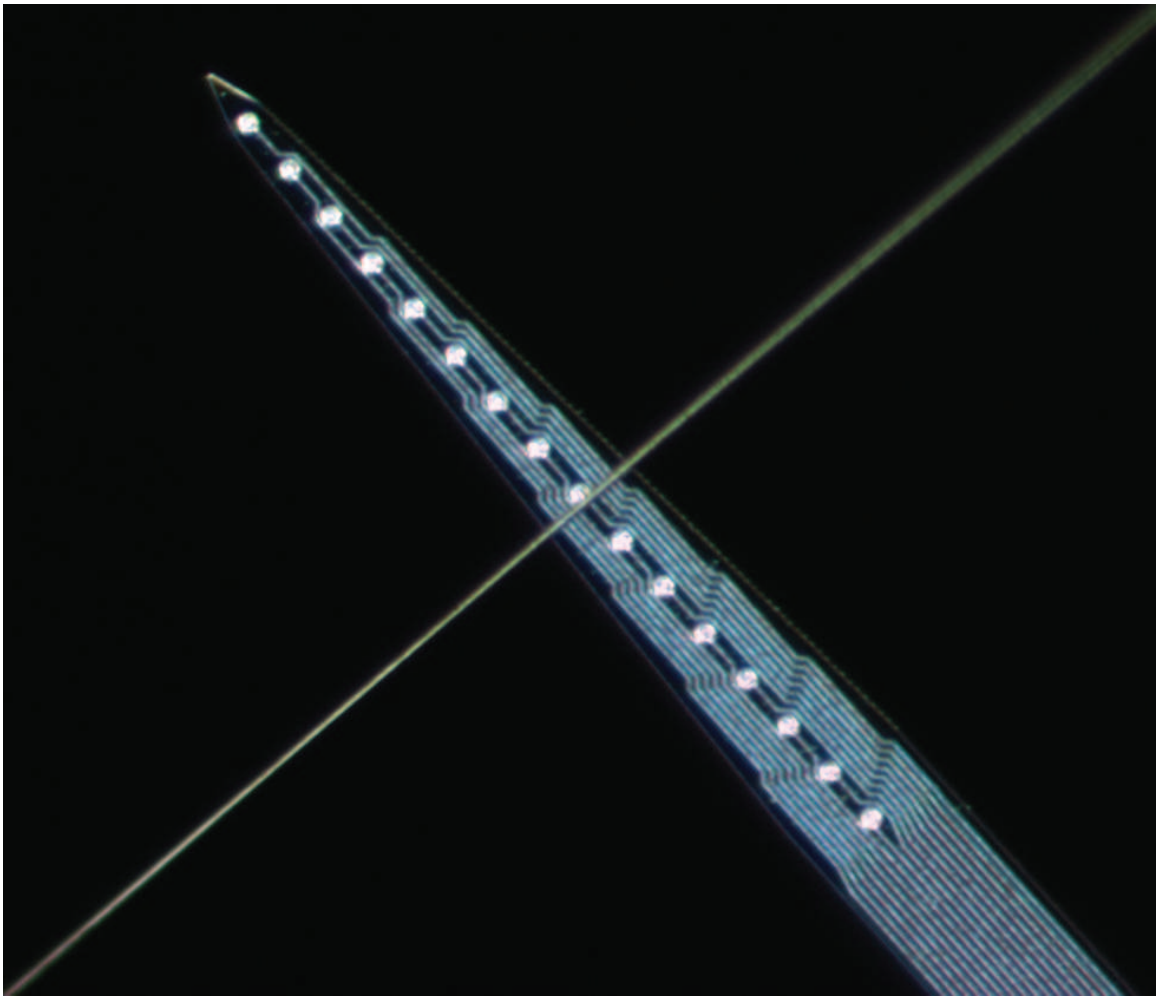

Dedicated to :
To my parents
&
Andrea

PREFACE

In the 1770's, an Italian physician Luigi Alyisio Galvani accidentally discovered that the muscles of a dead frog leg twitched when an electrical spark stuck an exposed nerve. This phenomena was further investigated by Count Alessandro Giuseppe Antonio Anastasio Volta, shortly after he failed out of chemistry of gasses. His studies led to the invention of the Voltaic Pile (the first electric battery) and perhaps the first demonstration of a neural interface. Around 1790, Volta applied his invention on his own ears and found that electrical stimulation can create a perception of sound which he described as "a thick boiling soup." When applied to his tongue, he noticed sensations of tastes. When they touched the eye, they created a sensation of light.

Influenced by Galvani, Carlo Matteucci began a series of experiments in 1830 that showed that injured excitable biological tissue generated electrical currents. This work on bioelectricity formed the cornerstone for Emil du Bois-Reymond's research starting in 1840 that led to the discovery of action potentials. Around 1870, in what was perhaps a controversial study, Eduard Hitzig assisted by Gustav Fritsch, electrically stimulated different regions of the cortex of a dog without anesthesia. They discovered that stimulating specific regions of the brain caused contractions in different muscle groups.

Later, Edgar Douglas Adrian observed that sense organs and nerve cells discharge a series of impulses. In a key publication in 1928, he stated that excitation of the skin under a constant stimuli is initially strong, but gradually decreases. He further characterized the nature of the diminishing sensation noting that the impulses along the nerves are constant in strength, yet reduced in frequency. This discovery earned him a share in the 1932 Nobel Prize in Medicine. Another group of researchers, Joseph Erlanger and Herber Spencer Gasser, around the same time measured conduction velocities and characterized the action potential waveform of nerve fibers. Erlanger and Herber recieved the Nobel Prize in 1944 for their discoveries through the characterization and classification of highly differentiated functions of nerve fibers. In 1939, Hodgkin and Huxley recorded the first intracellular action potential from a giant axon of a squid. The discoveries that resulted from this experimental setup earned them the 1963 Nobel Prize. In 1958, Strumwasser published the first long-term extracellular recordings using bundles of microwire in hibernating squirrels, marking the beginning of chronically implanted neuroprosthetics.

ACKNOWLEDGEMENTS

Daryl Kipke has allowed me the freedom to pursue my scientific ideas. I am grateful for the patience he has shown me during my research and personal struggles early on and the opportunities to pursue crazy exploratory projects at Rochester and high-risk technology development projects. I will always be awed by Daryl's ability to take a single crazy idea and turn it into a vision. He has also opened countless doors for me and provided me with many opportunities for professional growth and success, at times taking a risk on himself. Especially in this past year, he has provided me with family and career advice and guidance that goes much farther beyond his lab. In addition, I'd like to thank Dr. Joerg Lahann and Dr. Nicholas Kotov who gave me the chance and opportunity to champion the microthread project as well as devoting time to discuss and evolve the project. I would also like to thank my committee member Dr. Jan Stegemann for his time and effort. I would also like to thank Dr. Michael Mayer who provided a critical eye on the science and spent time with me discussing what I really had to do to make a successful career.

During my early academic struggles Aileen Huang-Saad was really the one faculty that came down a couple of levels to speak to me eye to eye. The things I learned from her class and the following year (in which Fontis Biotechnology was funded by the National Collegiate Inventors and Innovators Alliance E-teams grant) changed my professional life. I naively thought that for a successful research career, you

needed the ability to do research and research experience. I am forever grateful and amazed at her ability to teach and convey the importance of communication skills, networking skills, and presentation skills as well as the dedication and commitment to never give up on us. While I'm still not 'good' at these skills, I have learned a lot in the 2 years that she closely mentored us through BME599 and Fontis Biotechnology. While this experience may have delayed my graduation and may not have cashed out in a large sum of money, I would never trade this experience for anything.

There are many individuals in the Neural Engineering Lab (NEL) that I would not be here without, but none more so than Nick Langhals. As Fontis Biotechnology came to a close and I began to devote my full attention to the NEL, Nick was the only person that bought into my ideas. What I naively thought would be a short 2 week paper, turned into 4 weeks, 3 months, 6 months and ultimately remains unpublished due to a lack of precision instrumentation technology. Throughout the process, he was never discouraged, but continued to bring experience and technical expertise to the table. He spent many late hours on Fridays and weekend discussing projects, which I'm glad to say has lead to multiple manuscripts and a grant. He has been a strong professional ally in the ever changing terrain of the lab and a very good personal friend. His contributions helped in the characterization for ch 3 and played a key role in the conception and execution of ch 4, especially in the *in vivo* experiments.

Paras Patel really helped me run things behind the scenes. There is no one else I would trust more to get things done precisely and timely. He has helped me tremendously, especially during those times when I physically did not have enough time and was running on 3 hours of sleep a day. Most importantly though, I appreciated his ability to provide honest critical feedback when asked for it. He helped process data

in ch 3 and played a key role in the *in vitro* characterization of ch 4.

Jey Subbaroyan was really the one who secured me a place in this lab. Not only did he entertain an idea that many people instantly dismissed, but he really enabled me in the lab by helping me get or showing me how to get the resources I needed to test that idea. He taught me how to do surgeries as well as discussed many things with me from the inner workings of the lab to philosophy. For these things, I will always be grateful. His guidance ultimately lead me to ch 2.

I would also like to thank Kip Ludwig. He and I never really worked on a project together, and really only started discussing lab projects after he had graduated. However, he has continued to selflessly sacrifice time in his busy day to provide advice from the perspective a graduate student, a critical eye to review my scientific writing, and mentorship as a professional who still can relate to making that transition from being a student.

Tim Marzullo gave me the chance to go with him to the University of Rochester to piggyback a series of exploratory experiments off of his pilot study. That was probably the first time I ever worked that hard for that long continuously/consecutively. I'm grateful he put up with me (and my almost type B personality that week) and for the chats we had at that pub Elmwood Inn, which was the only place still open serving food that late at night. I am also grateful to Dr. Ania K. Majewska and Dr. Edward B Brown for training us and letting us use their equipment. Ania and Tim also spent many hours critically reviewing the manuscript (ch 3) and taught me how to put together a good manuscript.

Xiaopei Deng played a key role in the planning and execution of ch 4, particularly around the parylene component. She coordinated the efforts of Amanda L. Ryan, Dr. Sampa Saha, and Dr. Hsien-Yeh Chen. Huanan Zhang also contributed the ch

4 through SEM and EDX analysis. Amisha Agarwal and Firas S. Midani assisted in preparing chronic assembled devices in ch 4 and helped run the chronically implanted animals. Karen Smith with the help of Dr. Leah Hains at Wadsworth Center Advanced Light Microscopy and Image Analysis Core conducted the 4 label histology near the end of ch 4.

I would also like to thank Badri Roysam for helpful project discussions, as well as providing a generous introduction on our behalf to Ed and Ania. Anna Devor shared helpful two-photon vascular imaging discussions. Shadi Dayeh provided insightful discussion on nanoscale electro-neural interfaces.

I am very grateful to Paras Patel, Karen Schroeder, Kip Ludwig, Nick Langhals, Lena Chang Hall and Andrea Brown for their critical readings of the manuscript. Also, I would like to thank the other members of the NEL: Dr. Greg Gage, Dr. Erin Purcell, Matt Gibson, Azadeh Yazdan, Dr. Mark L Lehmkuhle, Dr. John Seymour, Dr. Hirak Parikh, Pratik Rohatgi, Kyle Ronquist, Dr. Taegyun Moon, Rachel Miriani, Taneev Mackert, Dr. Liz Nunamaker, Dave Turer, and Louis Salas for the full NEL experience as well as a special thanks to Vera Williams and Tonya Thompson for their fast turnaround precision work behind the scene. In addition, I would like to thank Chris Edwards and the rest of the Microscope Imaging Lab (MIL).

I would also like to thank Dr. Michael Stowell who took me in as an undergraduate student and helped me learn numerous techniques to prepare me for graduate school along with Maria Pagratis. I am also humbled by Dr. Mark Winey who really opened doors for me during my undergraduate career as well as Dr. Tom Cech who taught me how to use an electron microscope. Most importantly, I would like to thank David C. Knight of University High School (Irvine, CA) who showed me

that biological processes are a complex network of efficient and precise miniaturized nanomachinery. His class lead me to discover a love for learning.

Finally, I would like to thank my friends and family: Ken Wakabayashi, a sempai empathic to the struggles of graduate students. Fongming Hooi, who put up with me in one of my darkest times with her bright and cheerful sometimes seemingly unrealistic and annoying optimism that rubbed off on me making life bearable. Her work with code has also helped me on numerous occasions. For these things, I am eternally grateful and glad to have her as a friend, and happy to have an authored a paper with her (ch 3). Lena Chang Hall, who has always been an older sister to me: always encouraging me when things weren't going well and always celebrating when things worked out. My grandfather who taught me that learning is fun. Lastly, I'd like to acknowledge the loving and patient support of my fiancée, Andrea Brown.

TABLE OF CONTENTS

LIST OF FIGURES

Figure

LIST OF TABLES

Table

ABSTRACT

TOWARDS BIO-INTEGRATING INTERFACES IN ORGANIC NEUROTECHNOLGY DEVELOPMENT

by
Takashi Daniel Yoshida Kozai

Chair: Daryl R. Kipke

Penetrating electrodes allow investigators and clinicians direct access to the underlying neural pathway via stimulation and recording. While demonstrating acute reliability, chronic implants exhibit variability and limited reliability in recording performances and inflammatory tissue responses. Although flexible probe technology has been developed for many years, penetrating microscale microelectrodes made from flexible polymers tend to bend or deflect and may fail to reach their target location. In the first study, we investigate the use of an electronegative self-assembled monolayer (SAM) as a coating on a stiff insertion shuttle to carry a polymer probe into the cerebral cortex without deflection, and then detach the shuttle from the probe by altering the shuttle's hydrophobicity. The average relative displacement of PDMS and polyimide probes was (2.1±1.1)% and (1.0±0.66)% with the SAM and 100% and (26.5±3.7)% without the SAM, respectively.

While advances in technology are pointing to incremental improvements for solving this longstanding reactive tissue response, understanding the role of vascular

disruption on implants have been limited by challenges *in vivo*. During insertion, the highly-regulated blood brain barrier is compromised leading to plasma release into the surrounding parenchyma and adsorbtion onto the electrode surface. In the second study, we investigate localized bleeding resulting from inserting microscale neural probes into the cortex using *in vivo* 3D multi-photon vascular mapping to explore an approach to minimize blood vessel disruption. An (82.8±14.3)% reduction in neurovascular damage was observed when probes were inserted in regions devoid of major sub-surface vessels.

These findings combined with the growing literature emphasize novel penetrating electrode designs for improving chronic recordings. Here, we report an integrated composite electrode consisting of a carbon fiber core, poly(p-xylylene)-based thin-film coating that acts as dielectric barrier and is functionalized to control intrinsic biological processes, and a poly(thiophene)-based recording pad. The resulting implants are an order of magnitude smaller and more mechanically compliant with brain tissue than traditional recording electrodes, were found to elicit negligible chronic reactive tissue responses, and have excellent recording characteristics in acute and chronic experiments in rats. This technology establishes a new development path for highly selective and long-lasting stealthy neural interface materials and devices.

CHAPTER I

Introduction

Neural prosthetics, sometimes referred to as brain-machine interfaces (BMIs), or brain-computer interfaces (BCIs), are systems that interface directly with the nervous system, often substituting for a damaged neural function such as a motor output, sensory input, or cognition. In their most common form, BMIs rely on electrodes sampling electrical signals from the brain and inputting electrical signals to the brain. Despite the early success of BMI systems, clinical relevance of these devices are hampered by the intermittent reliability of chronic recording/stimulating electrodes. The three studies outlined in this dissertation are focused on improving the reliability of long-term chronic recording/stimulating electrodes in order to improve the clinical efficacy of BMIs.

1.1 Neuroprosthetics

The neural interface is the key component of the BMI that detects and sends signals between the brain and the computer system that controls a functional modality. Perhaps the most common neural prosthesis is the cochlear implant (Figure 1.1C). These devices restore limited hearing to individuals who retain an auditory nerve fiber. According to the Food and Drug Administration (FDA) ∼188,000 people have received cochlear implants worldwide, including over 41,000 adults and 25,000 chil-

dren in the US. An emerging sensory implant is the retinal implant (Figure 1.1E). In two clinical studies, Second Sight has implanted 24 patients with retinal prostheses and provided these patients with basic object recognition. Deep brain stimulators are neural prosthetic devices that provide therapeutic benefits for Parkinson's disease, epilepsy, dystonia, and chronic pain. These devices have been implanted in over 80,000 patients according to Medtronic (Figure 1.1G). They are also being investigated in treating severe levels of obesity and depression (Sani et al., 2007; Lehmkuhle et al., 2010; Mayberg et al., 2005; Mayberg, 2009).

An example of a non-invasive neural interface is the electroencephalographic (EEG) scalp electrode (Figure 1.1A), which has allowed over 20 locked-in patients to spell words on a screen by utilizing an event-related potential which occurs around 300 ms after a stimulus, such as a flashing light (Kaper et al., 2004; Schalk et al., 2004). Electrocorticographic (ECoG) electrodes, which are surgically positioned under the skull and on top of the brain surface have recently gained renewed momentum (Leuthardt et al., 2004, 2009; Yanagisawa et al., 2009; Kim et al., 2010; Pei et al., 2011). While there are many types of neural interfaces with different capabilities and limitations, this dissertation focuses on intracortical neural interfaces which utilize microelectrode arrays that are implanted into the cortex of the brain, often in movement-related areas (Figure 1.1B, D, F) (Strumwasser, 1958; Georgopoulos et al., 1986; Schwartz and Moran, 1999, 2000; Taylor et al., 2002; Schwartz et al., 2006; Wessberg et al., 2000; Velliste et al., 2008). Currently there are many types of wire, silicon, and polymer-based implantable neural interface technologies at various stages of development that are advancing front-end neural interface capabilities across many dimensions, including channel count, site and substrate materials, and the ability to precisely target locations in the neocortex, deep brain, and spinal

Figure 1.1: Examples of prosthetic devices. (A) EEG P300 speller for locked-in patients. (B) Prosthetic leg with a controlled knee joint. (C) Cochlear Implant. (D) New 22 degrees of freedom prosthetic arm. (E) Second Sight retinal implant. (F) Prosthetic arm being used.(G) Medtronic deep brain stimulator. (Images were provided by DARPA, Medtronic, and Second Sight.)

cord (Figure 1.2) (Bartels et al., 2008; Hetke and Anderson, 2002; McCreery et al., 2006; McNaughton et al., 1983; Motta and Judy, 2005; Musallam et al., 2007; Neves and Ruther, 2007; Nicolelis et al., 2003; Nordhausen et al., 1996; Schwartz, 2004; Polikov et al., 2005; Rennaker et al., 2005; Schwartz, 2004; Wise et al., 2004; Grand et al., 2010).

1.2 Overview

Long-term functional neuroprosthetic devices that record from large populations of neurons reliably and reproducibly over the course of a human lifetime are necessary for neural prostheses to be useful in clinical settings (Kipke et al., 2008; Lebedev and Nicolelis, 2006). Despite initial promising results, there remains a large variability in microelectrode performance from implant to implant (Figure 1.3) (Williams et al., 2007; Ward et al., 2009), even within the same patient (Rousche and Normann, 1998) and the same probe shank (Stensaas and Stensaas, 1976). Chronic microelectrode implants induce a reactive tissue response in the surrounding tissue (Rousche and Normann, 1998; Biran et al., 2005; McConnell et al., 2009). This tissue response eventually degrades the electrical characteristics of the recording site over time (Rousche and Normann, 1998; Liu et al., 1999; Williams et al., 1999; Nicolelis et al., 2003; Polikov et al., 2005; Liu et al., 2006; Schwartz et al., 2006; Ward et al., 2009).

There is an ongoing need for higher fidelity and longer-lasting implantable microscale neural interfaces for recording and stimulation in both scientific and emerging clinical applications (Brown et al., 1998; Dobelle, 2000; Fetz and Finocchio, 1975; Gage et al., 2005; Georgopoulos et al., 1986; Kargo and Nitz, 2003; Kipke et al., 2008; Nicolelis et al., 2003; Schwartz and Moran, 1999; Taylor et al., 2002). For

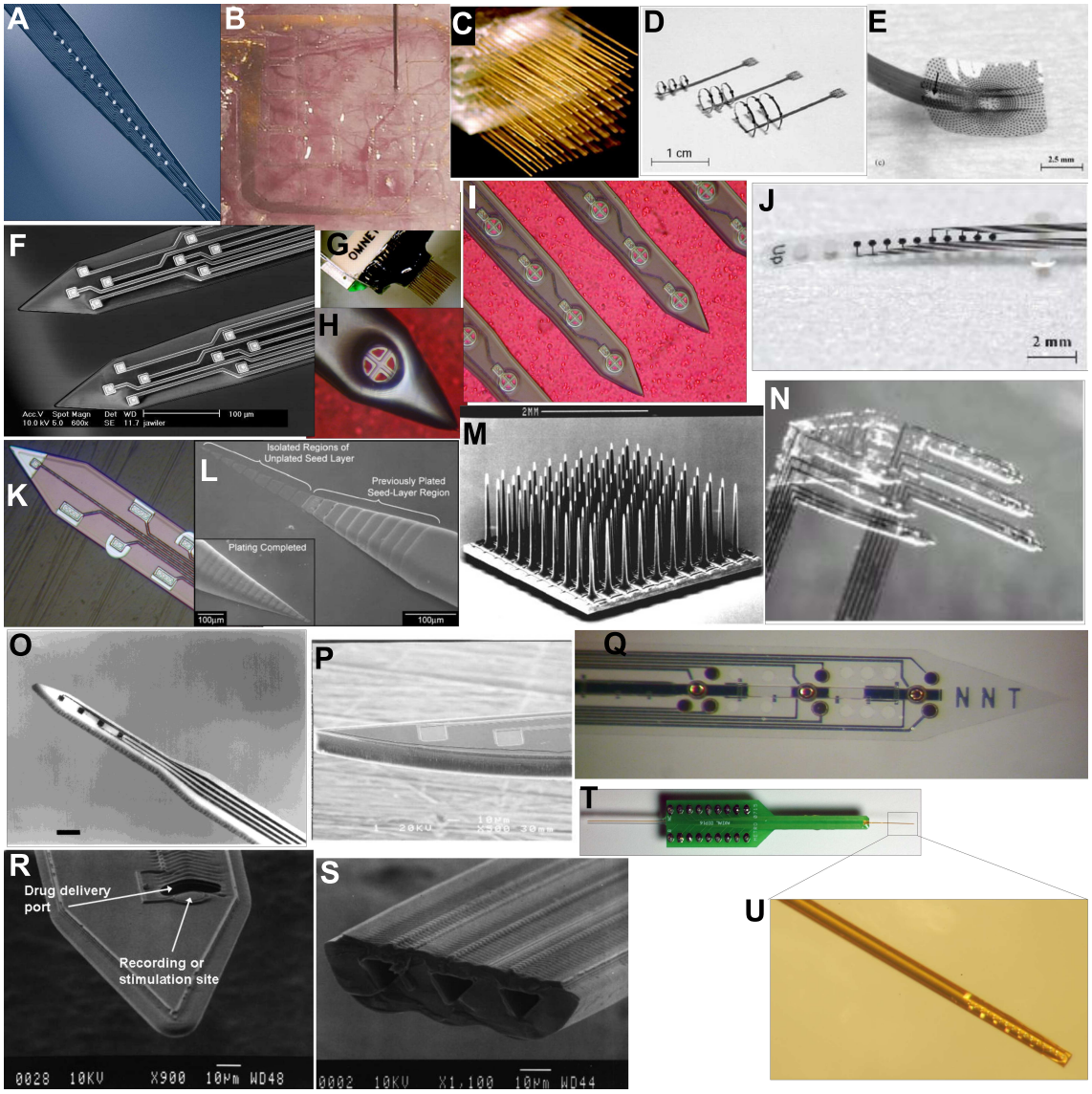

Figure 1.2: Examples of implantable neural interfaces. (A) Traditional silicon Michigan probes. (B) Parylene ECoG probe with penetrating tungsten microwire (Toda et al., 2011). (C) Microwire Array (Nicolelis et al., 2003). (D) Polymer nerve cuff electrode. (Stieglitz et al., 2005). (E) Implantable parylene ECoG (Rodger et al., 2008). (F) Michigan two-shank tetrode microelectrode. (G) Same as C with Omnetic packaging. (H) Open Architecture Cathedral Probe. (I) Same as H in four-shake arrangement. (J) Planar parylene probe (Rodger et al., 2008). (K) Michigan edge electrode. (L) Electroplated Ni-Au-Silicon nitride probe (Motta and Judy, 2005). (M) Utah Array (Nordhausen et al., 1996). (N) Planar polyimide probe (Rousche et al., 2001). (O) Ceramic probe (Burmeister et al., 2002; Moxon et al., 2004). (P) SOI Probe (Cheung et al., 2003). (Q) Polyimide probe with microfluidic channel (N2T). (R)&(S) Chevron RIE etched microfluidic Silicon Probe (Chen et al., 2004; Rathnasingham et al., 2004). (T)&(U) Acute Michigan probe with fused-silica microfluidic channel (Rohatgi et al., 2009).

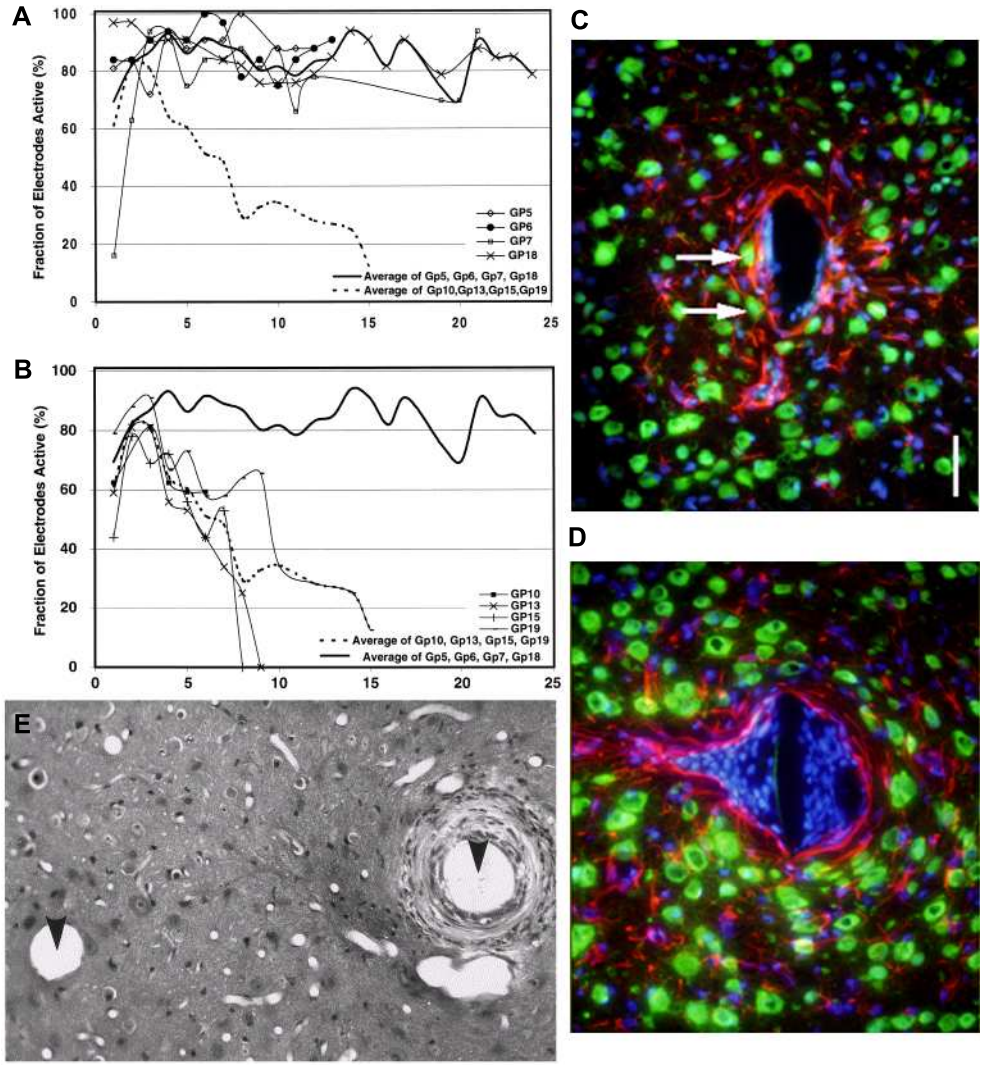

Figure 1.3: Variability in chronically implanted neural probes. A) Chronically stable electrode. B) Chronically implanted electrodes that rapidly degrade and fail in the first two weeks. C) Tissue interface with minimal reactive response. D) Highly reactive tissue response. E) *Left;* minimal tissue reaction. *Right;* Reactive tissue response from an identical type of probe shank implanted into the same animal. (Williams et al., 1999; Subbaroyan, 2007; Rousche and Normann, 1998)

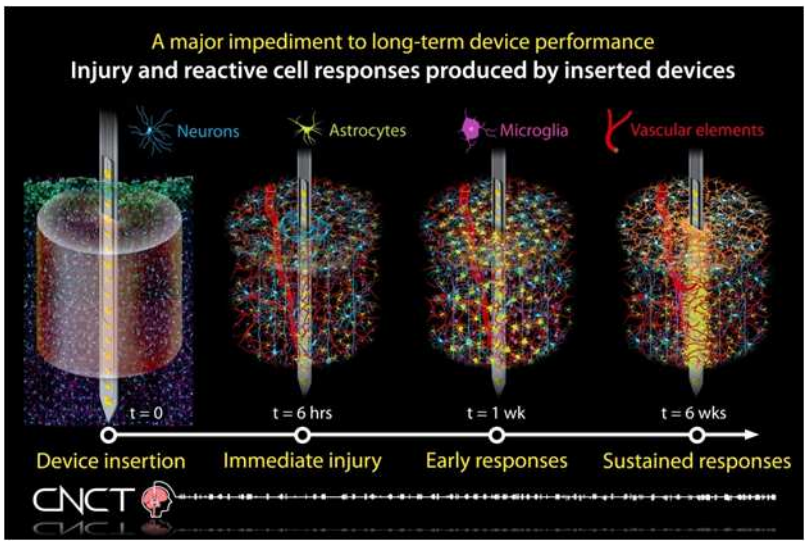

Figure 1.4: Illustration of increasing reactive tissue response over-time.

chronically implanted probes, one challenge is to improve and/or control the degree to which the probe integrates with the surrounding tissue to meet particular performance requirements, such as high signal-to-noise ratio and long-term stability (Liu et al., 2006; Nicolelis et al., 2003; Polikov et al., 2005; Rousche and Normann, 1998; Schwartz et al., 2006; Williams et al., 1999; Ward et al., 2009).

1.3 Reactive tissue response

Chronic microelectrode implants induce inflammatory responses in the tissue which degrade the electrical characteristics of the electrode site over time (Figure 1.4). Cellular encapsulation by microglia and reactive astrocytes isolates the device from surrounding tissues (Edell et al., 1992; Turner et al., 1999; Szarowski et al., 2003; Kim et al., 2004b; Biran et al., 2005; Polikov et al., 2005; Biran et al., 2005). Within 24 hours after probe implantation, the device becomes surrounded by activated microglia, which form a thin cellular sheath encapsulating the device over the following week (Szarowski et al., 2003; Purcell et al., 2009c). During this first week, astrocytes are maximally activated, then form a compact sheath approximately three

weeks later (Szarowski et al., 2003; Biran et al., 2005; McConnell et al., 2009).

Impedance magnitude at 1kHz is used to evaluate encapsulation *in vivo* as it increases at recording sites with extensive glial reactivity (Williams et al., 2007). This phenomenon may be explained by the fact that glial cells form tight junctions with each other to create a sheath leading to a diffusion barrier that limits transmission of ions through the extracellular space (Roitbak and Sykov, 1999). Additionally, neuronal cell death can occur (Kim et al., 2004b; McConnell et al., 2009) causing neuronal density to be reduced by 40% within 100 μm of the probe, increasing the electrode distance from the recording source (Biran et al., 2005). The neural source that generates a recordable spike is typically located within 50 μm of the electrode site and cannot be recorded beyond 140 μm (Henze et al., 2000; Biran et al., 2005; Purcell et al., 2009c). Before investigators can develop intervention strategies to improve the chronic interface, they need to first understand the causes of the reactive tissue response.

1.4 Possible factors that illicit reactive tissue response

Neuronal loss and glial encapsulation around implants are well documented phenomena. However, the underlying mechanisms of this cellular response remain unknown. Here we discuss several factors that may affect the reactive tissue response to chronically implanted electrodes.

1.4.1 Mechanical stressors

Mechanical acute trauma

Details of insertions, such as tip shape, size, position, and speed are known to affect acute tissue trauma (Edell et al., 1992; Bjornsson et al., 2006; Johnson et al., 2007; Kozai et al., 2010). It is known that rupture of vasculature occurs during

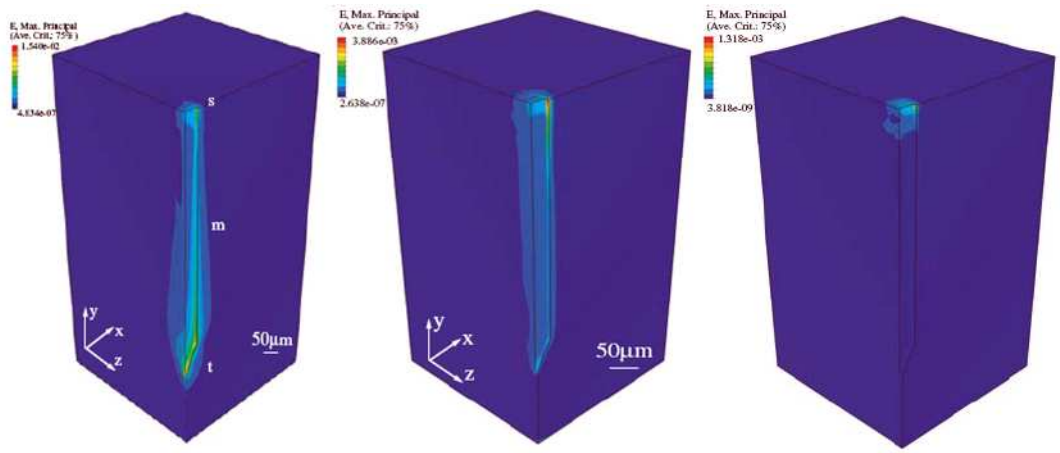

Figure 1.5: Finite-Element Model demonstrating tissue strain from implanted silicon *(left)*, polyimide *(center)*, and 'soft' *(right)* probes. (Subbaroyan et al., 2005)

probe implantation and has been observed up to 300 μm from the probe tip *ex vivo* (Bjornsson et al., 2006). As the probe is inserted into the tissue, it is generally accepted that the probe tears the extracellular matrix and cell membranes as well as drags, compresses, and even punctures distant cells and vasculature. The damage to neural arbor may cause neurons that have healthy somas (via histological staining) to become silent (Henze et al., 2000). Studies using a cell membrane impermeable dye demonstrated that insertion combined with tissue displacement from probe volume and vasogenic edema can cause damage to cell membranes multiple cell layers thick (Retterer et al., 2008; Rohatgi et al., 2009).

Mechanical mismatch

The inflammatory response may be exacerbated by the sustained tissue response due to the motion of the brain with respect to the rigid microelectrodes implanted anchored to the skull (Edell et al., 1992; Kim et al., 2004b; Subbaroyan et al., 2005; Gilletti and Muthuswamy, 2006; Lee et al., 2005; Biran et al., 2005; Goldstein and Salcman, 1973; Bartels, 1976; Hoogerwerf and Wise, 1994;

Niparko et al., 1989). This phenomenon is often referred to as micromotion. Finite elemental modeling has shown that polymer probes are more flexible and produce less strain on the tissue, which can result in closer proximity of healthier neurons to the electrode for improved recordings (Figure 1.5) (Lee et al., 2005; Subbaroyan et al., 2005). *In vitro* experiments have shown that constant mechanical strain on neural tissue results in upregulation of molecular stress markers which may in turn perpetuate the chronic tissue response (Neary et al., 2003; LaPlaca et al., 2005). Additionally, *in vitro* studies have shown that the mechanical response in living brain tissue is dependent on the total strain history (Morrison et al., 1998). Therefore, perpetual mechanical strain from chronically implanted electrodes may continuously produce strain to the surrounding tissue and continue to build a chronic immune response. However, there is a conflict between a probe's flexibility, softness, and feature size that are hypothesized to be important for long-term tissue integration and the largely opposite mechanical characteristics that are thought to be important for reliable and minimally damaging insertion in the brain.

Steric (size & shape)

Tissue displacement or changes in pressure on the tissue caused by the implanted probe volume and vasogenic edema resulting from insertion may affect short and long-term tissue responses. This increase in pressure may affect transmembrane proteins, such as ion channels, and disrupt their normal function. Qualitatively, after probe insertion, it is sometimes observed that a settling period of 5-15 minutes is required before single unit neuronal spikes return. Additionally, the increase in pressure may trigger inflammation molecule and shock protein synthesis. Also, the substrate of the probe physically and sterically blocks electrical and chemical signals from passing through it. These factors are relatively difficult to examine and quantify

independently from some of the other factors listed here. Lastly, surface shape, roughness, micropore size, or texture have been shown to influence cell adhesion (Hallab et al., 2001; Deligianni et al., 2001; Ratner and Bryant, 2004).

Studies comparing several different electrodes with cross-sectional areas ranging from 1,450 μm^2 (3mm Michigan Probe)-16,900 μm^2 (Cornell Probe) showed that at long time points (4+ weeks), the tissue response was similar for all devices (Szarowski et al., 2003). While for earlier time points, the reactive response was proportional to the cross-sectional area, the sustained response appeared to be independant of device size, geometry, and surface roughness.

Although small changes in large stiff probes show no difference in histological outcomes, studies in biomaterials point to new strategies and information regarding size. Particles of up to 20 μm in diameter can be phagocytosed (Brandwood et al., 1992; Shanbhag et al., 1994). Depending on the concentration and material composition these particles may cause problems to the cells if the phagocytosed materials cannot be digested. These cells can release inflammation molecules, lose their shapes, detach from substrates, and undergo lysis (Brandwood et al., 1992; Shanbhag et al., 1994). Larger particles that can not be phagocytosed by a single cell, become surrounded by aggregations of macrophages some of which migrate to the surface (Brandwood et al., 1992).

While particles can be ingested, long fibreous substrates with small diameters cannot be phagocytosed by single cells. While fibers with diameters greater than 20 μm show substantial encapsulation, fibers with subcellular diameters ($<$12 μm) show only scarce glial cells with filopodia extensions on the surface of the fibers (Bernatchez et al., 1996).

1.4.2 Electro-biochemical stressors

Soluble signals

Decrease in survival signal. Brain injury models have shown that following an injury, an inflammatory tissue response occurs involving an upregulation of cyclin-dependent kinases causing glial cells to re-enter the cell-cycle and proliferate while causing neurons to undergo caspase-mediated apoptosis (Verdaguer et al., 2004; Cernak et al., 2005; Giovanni et al., 2005; Appert-Collin et al., 2006; Hugel et al., 2006; Alvira et al., 2007; Byrnes et al., 2007; Cernak et al., 2005). Active cells are known to naturally release neuroprotective molecules (Lindholm, 1994; Morrison and Mason, 1998). For implanted probes with large feature sizes, steric blockade of electrochemical signals may reduce neuroprotective molecule release by decreasing neuronal input signals and ultimately leading to apoptosis. A very clear example of this phenomenon was demonstrated by Korsching and Thoenen (1983). They showed that removing cells that secrete neural growth factors (NGFs) resulted in apoptosis of the neurons that would normally innervate those cells. Further studies in developmental neuroscience showed that neurons naturally compete for growth factors during embryonic development (Colman et al., 1997), and more than 50% of the neurons undergo apoptosis during development (Kuida et al., 1995, 1998). Knocking out the ability for neurons to undergo apoptosis from NGF competition results in perinatal death characterized by an enlarged and malformed cerebrum (Kuida et al., 1998). This emphasizes the importance of apoptosis in neurons and demonstrates that there is a relatively small window for maintaining neural health, which may be disrupted by an implanted electrode.

On the other hand, further investigation of neural regeneration shows that endogenous cyclic adenosine monophosphate (cAMP) in the dorsal root ganglia (DRG) de-

creases at the end of the developmental stage, which coincides with neurons becoming unable to exhibit spontaneous regeneration (Cai et al., 2001). Further investigation is ongoing to determine if and how to create specific conditions in adult systems to temporarily reactivate regenerative properties observed during the developmental stage (Gonzalez-Perez et al., 2010; Hui-Chou et al., 2011).

Increase in inflammatory signal. The inflammatory tissue response can be traced back to the disruption of the highly controlled blood-brain barrier (BBB) during microelectrode insertion (Groothuis et al., 1998; Kimelberg, 1995). It is known that rupture of vasculature occurs during probe implantation and has been observed up to 300 μm from the probe tip *ex vivo* (Bjornsson et al., 2006). Details of probe insertion impact chemical trauma on tissue (Johnson et al., 2007), as the implantation of microelectrodes puncture and tear neural vasculature (House et al., 2006). During this time, the highly regulated BBB is compromised, depositing molecules foreign to the central nervous system (CNS) into the brain tissue, such as albumin (40mg/ml), immunoglobulins (IgG) (10mg/ml), and fibrinogen (3mg/ml) (Cao et al., 2007). Therefore, one focus of research is on the BBB during and after microelectrode implantation, particularly on its role in vasogenic brain edema and cytotoxic swelling (Betz et al., 1989; Klatzo, 1967; Marmarou, 1994; Kimelberg, 1995; Dirnagl et al., 1999; Kempski, 2001). This response leads to a modification of the extracellular matrix (Kim et al., 2004b) and a change in cellular composition surrounding the implant (Kim et al., 2004b; Biran et al., 2005).

Examples. IgG are largely not found within the parenchyma and anti-host secondary antibodies can be used to detect BBB integrity (Alafuzoff et al., 1983; Winslow et al., 2010). Increased IgG in the CNS is often associated with problems in the brain, such as multiple sclerosis (Wilson et al., 1979; Poser et al., 1983;

Hanly et al., 1994). Albumin is the most common blood plasma protein consisting of 60% of the blood plasma. Albumin is known to reversibly increase calcium activity in glial cells and has been shown to mildly affect neurons over short time periods (Nadal et al., 1995, 1998). More recently, albumin has been found to affect astrocytes through TGF-β receptors (Ivens et al., 2007). These responses lead to a modification of the extracellular matrix (Kim et al., 2004b) and changes in the cellular composition surrounding the implant (Kim et al., 2004b; Biran et al., 2005). However, neuronal loss appears to be minimal from stab wounds caused by microelectrode insertions (Biran et al., 2005). This may be because stab wounds can quickly heal while mechanical mismatch of the physical probe perpetuates disruption to nearby vasculature resulting in a chronically leaky BBB.

Surface-bound signals

Another explanation for the stab wound observation may be that a chemical property of the microelectrode surface is likely to perpetuate the acute tissue response. Silicon is a hydrophobic material and non-specifically adsorbs proteins onto its' surface. These proteins may be inflammatory molecules or plasma proteins that are normally not found in healthy CNS tissue. Once adsorbed onto the probe, these molecules may remain on the surface perpetuating an inflammation response into an immune response. Adhesion of these non-specific proteins to the implant material is called bio-fouling. Inflammatory cytokines have been found attached to explanted probes, and the inhibition of astrogliosis and increasing impedance by anti-inflammatory drugs suggest an important role in the reactive tissue response (Shain et al., 2003; Szarowski et al., 2003; Spataro et al., 2005; Kim et al., 2006; Zhong and Bellamkonda, 2007; Purcell et al., 2009c).

1.5 Recent advances in science and technology

1.5.1 Electrophysiological interface strategies

Depolarizing stimulation

Functional recovery of neurons is often very poor. After an injury, axons typically regenerate poorly into mixed nerve pathways. Electrical stimulation and functional stimulation of nerve targets have been shown to promote the speed and accuracy of axonal regeneration and reinnervation (Al-Majed et al., 2000b; Protas et al., 2001; Colombo et al., 2000; Field-Fote, 2001). Stimulation has also been shown to modulate a neuron to react more strongly in the presence of a neurotrophic gradient (Ming et al., 2001). Electrical stimulation induces specific NGF and neuroprotective molecule upregulation (Lindholm, 1994; Morrison and Mason, 1998) and results in safer reinnervation than an NGF injection (Al-Majed et al., 2000a). Neurons are capable of significant activity-dependant reorganization (Muir and Steeves, 1997), which can be driven by electrical stimulation activity.

Electrical field stimulation

During the development of an embryo's nervous system, there is a natural voltage gradient along the neural tube (Shi and Borgens, 1995). This voltage gradient only appears when neurulation begins and disappears after it ends. Experimental tests determined that these extracellular electric fields serve as morphological cues and pattern coordinates in the developing embryo (Shi and Borgens, 1995). The disappearance of this voltage gradient may contribute to the poor accuracy of neural regeneration and reinnervation. Neurites have demonstrated a preferential growth towards cathodic electric fields (Figure 1.6) (McCaig et al., 2002). This may be due to the electric field generating a local intracellular Ca^{+2} gradient (Schubert et al., 1978; Robinson and McCaig, 1980; Cohan et al., 1987;

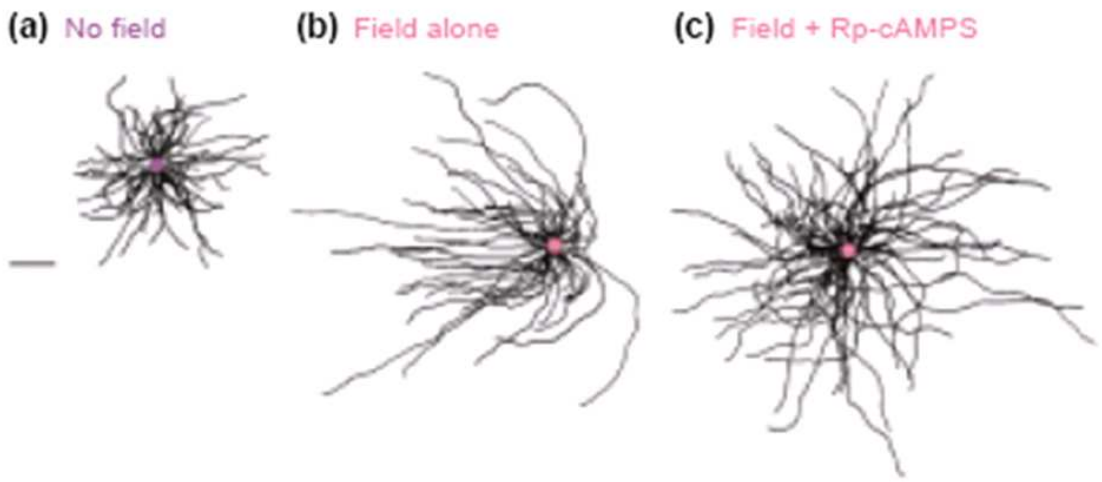

Figure 1.6: Growth of neurites towards a cathode in an electric field (EF). The directional responses of neurite growth are traced in black from the cell body (red). A) Neurites grow evenly in all direction in the absense of EF. B) In a field of 150mV/mm neurites grow towards the cathode (left). C) Direction reponses are inhibited by a cAMP antagonist, Rp-cAMPS. Scale bar is 100 μm. (McCaig et al., 2002)

Bedlack et al., 1992; Wood and Willits, 2009). Local increases in calcium have been shown to coincide with neurite growth (Hong et al., 2000). Rp-cAMP, a cAMP antagonist, has also been shown to inhibit directional responses (Figure 1.6C) (McCaig et al., 2002), perhaps by modulating its effect on actin and microtubules (Schubert et al., 1978; Lohof et al., 1992; Moon and Drubin, 1995). Similar effects have also been observed for magnetic fields (Blackman et al., 1993; Macias et al., 2000). Additionally, astrocytes align themselves in the presence of an electric field, and may assist in promoting neurite growth (Alexander et al., 2006).

1.5.2 Mechanical interface strategies

Flexibility

Flexible neural probes have been around for over a decade (Rousche and Normann, 1998). However, flexible implantable neural microelectrode technologies have met an impasse because investigators lack a precise and efficient method to implant these flexible neural microelectrodes *in vivo*. Further development of smaller, more flexible

microelectrodes requires new approaches to handle the probes and insert them into the brain.

In particular, thin-film, microscale polymer probes that have desirable flexibility for long-term implantation tend to buckle before penetrating the pia mater or deflect while being directed to the target area. Existing methods to suitably strengthen polymer probes for insertion restrict the design of the probe, limit its functionality, or negate its flexibility. One approach is to integrate a rigid insertion device during fabrication (O'Brien et al., 2001), however this technique restricts probe design and presents challenges in precise implantations. Another approach is to coat a flexible or small probe with stiff biodegradable polymers or crystals (Foley et al., 2006; Suzuki et al., 2003), but these present significant challenges to achieve the appropriate stiffness, reproducibility, and sharpness in a small conformal coating. An alternative approach is to create channels in the substrate which can be filled with stiff biodegradable polymers or crystals (Takeuchi et al., 2004). These electrode designs require a larger fluid channel to fill with biodegradable material to reach a critical stiffness for insertion. This larger channel then results in a larger implanted footprint, potentially creating more damage. Other methods include a polymer substrate integrated with a stiff silicon backbone (Lee et al., 2004), but this negates the flexibility of the polymer substrate. Perhaps the most clever approach is to use a Gauss gun or a coil gun to insert (Jaroch et al., 2009). *(This technology is often mistakenly called a rail-gun inserter)* However, this approach does limit the profile of the electrode and MRI compatibility. Additionally, this technology currently has issues with precise targeting, though there are promises of improvement.

Another approach is to shuttle the soft probe into the brain using a stiff shuttle. However, materials such as polymers, metals, and silicon adhere to each other in

an aqueous environment due to surface energies (Johnson et al., 1971). In an aqueous environment, two hydrophobic substrates in contact, such as glass and metal, demonstrate strong adhesive forces (Mcfarlane and Tabor, 1950). This adhesive force is formed by a convex-shaped menisci which creates a lower pressure inside the meniscus resulting in an intrinsic attractive force, and during separation the viscosity of the liquid causes an additional attractive force (Cai and Bhushan, 2008a,b). In the case of a polymer probe and silicon shuttle in the brain, this thin aqueous meniscus is formed at the triple junction between polymer, silicon, and extracellular fluid. Therefore, polymer probes stick to metallic and silicon surfaces through hydrophobic interactions, causing a polymer probe to be carried out of the brain when the insertion shuttle is removed.

Steric (size & shape)

Leveraging the findings that cells react substantially less to subcellular-sized fibers, chronically implanted advanced architecture style electrodes with subcellular sized lattice features (4-10 μm) have be shown to elicit smaller reactive tissue responses (Seymour and Kipke, 2006, 2007; Clark et al., 2010). These findings have lead to advanced cathedral architecture recording sites for planar silicon probes which have a round hollow hole with a cross-shaped recording lattice inside (Figure 1.2H, I) (Kipke et al., 2008). These strategies have also been applied to dopamine sensing electrodes (Clark et al., 2010). Additionally, Ken Wise and Patrick Tresco have been developing and testing planar silicon lattice probes (unpublished data).

Insertion

In the course of developing more reliable and longer lasting implantable microelectrodes, there has been increased motivation to reduce size and improve flexibility of

the electrodes. As devices become smaller and more flexible, insertion strategies and packaging will become more important. The non-linear, inhomogeneity of the brain will become much larger relative to the probe, and their roles in the reactive tissue responses may become more evident. Empirical evidence suggests that stiff, sharp, and straight probes should be inserted relatively fast, but under control for a minimally damaging insertion (Bjornsson et al., 2006; Edell et al., 1992; Johnson et al., 2007).

1.5.3 Biochemical interface strategies

Soluble or diffusing molecules

Currently, there are three principle strategies for delivering soluble cues or drugs into tissue:

1) *Drug releasing polymer matrix or hydrogels.* Soluble poly(ethylene glycol) (PEG) has been used to control drug delivery diffusion from implantable neural microelectrodes, such as in hydrogel coatings (Zhong et al., 2001; Saul et al., 2003). Other examples of drug eluting coatings have been nitrocellulose coatings (Zhong and Bellamkonda, 2005), electrostatic layer-by-layer (LbL) assembled drug hydrogels (He and Bellamkonda, 2005), poly(ethyl-vinyl) acetate (Shain et al., 2003), microcontact printing (James et al., 2004), alginate (Kim et al., 2004a), electrospinning of silk-like polymer containing the laminin fragment IKVAV (Wu et al., 2006), and sol-gel (Pierce et al., 2009).

Dexamethasone and α-MSH are anti-inflammatory drugs that have been used in drug-eluting microelectrode coatings (Shain et al., 2003; Golde et al., 2003; Zhong and Bellamkonda, 2005; Wadhwa et al., 2006; Kim and Martin, 2006; Zhong and Bellamkonda, 2007). Another approach is to fill a cone or a well with neurotrophic factors that are slowly released to attract neurite growth (Kennedy,

1989; Kennedy et al., 1992; Satish et al., 2004; Williams et al., 2005; Bartels et al., 2008). More recent strategies include trapping stem cells in scaffold matrices so they can release growth factors to the injured tissue (Purcell et al., 2009a,b).

2) *Microfluidic injection.* Perhaps the simplest microfluidic drug delivery for neural prosthetic is a subcutaneous injection of anti-inflammatory drugs, such as dexamethasone, coinciding with the device implantation (Spataro et al., 2005). More elegant drug delivery systems have also been developed to deliver small volumes of drugs directly to the region of interest in the brain. Planar silicon microelectrodes with fluidic channels have been made utilizing chevron slits and deep reactive-ion etching (DRIE) (Chen et al., 1997). Polyimide based (Rousche et al., 2001; Pellinen et al., 2005; Metz et al., 2004) and parylene based (Suzuki et al., 2004; Takeuchi et al., 2005) flexible polymer microelectrodes containing microfluidic channels have also been designed. The biggest limitation for chronic microfluidic implants is that microfluidic ports can easily collapse or be blocked by debris/cells during insertion or over time. Fused-silica tubes mounted onto planar silicon microelectrodes help address the issue of collapsing (Rohatgi et al., 2009), but still suffer from occasional clogging. The other limitation of microfluidic devices for chronic neural interfaces is that these devices lack a reliable microscale gating mechanism to close and open the fluidic port.

3) *Caged soluble cues.* The last technique is to develop strategies that deliver small volumes of drug at some timepoint after implantation. The most common technique is to cage or trap drugs until they receive some cue to be released. Several examples include reservoirs covered with a thin gold film which can be dissolved to release drugs (Santini et al., 1999), ultrasound activated drug release (Langer, 2000), photoactivated ligands (Dormn and Prestwich, 2000), sponge-like nanostructured con-

ducting polymers that release drugs when electrically stimulated (Isaksson et al., 2007; Simon et al., 2009; Luo and Cui, 2009), and enzyme activated drugs (Ulijn, 2006; Zhou et al., 2009).

Surface material

Many groups have investigated different methods of improving the performance of the chronic neuron-implant interface by modifying these implants using novel biomaterial designs. These groups examined biocompatibility of these alternative materials, such as polyimide (Schmidt et al., 1993) and parylene-C (Winslow et al., 2010) in neural tissue. These materials demonstrated biocompatibility, but did not show substantial improvement over the current silicon standard.

In vitro study of Arg-Gly-Asp amino-silane modified silicon substrates showed enhanced cell proliferation and bioactivity (Davis et al., 2002). In addition to silicon, polyimide and gold surfaces with immobilized bioactive laminin-derived peptides and dextran-coatings showed that chemical surface modifications could be utilized to establish a better tissue interface (Massia et al., 2004). Most recently, surface immobilized neural adhesion molecule L1 has been demonstrated *in vivo* to promote neurite outgrowth and neuronal survival around chronically implanted microelectrodes, and at the same time reduce glial reactivity (Azemi et al., 2011).

Recently, there has also been an increasing appreciation for reducing protein adsorption (Horbett and Brash, 1995) on the surface of implantable neural microelectrodes. It is thought that coatings that prevent blood plasma molecule adsorption minimize damage of the acute tissue response, which in turn reduces the chronic tissue response. However, the mechanisms underlying the tissue response are still largely unknown. A direct relationship between *in vivo* recording quality and tissue response metrics has also not been characterized. Furthermore, while PEG and

laminin immobilization have been demonstrated on silicon neural microelectrodes, anti-biofouling contribution to the chronic reactive tissue response has not yet been characterized (Azemi et al., 2008).

Other anti-biofouling coating technology. While PEG hydrogel coatings may rapidly dissolve (Sommakia et al., 2009), tethered PEG coatings, such as PEG-terminated alkanethiols or PEG-terminated methacrylate (PEGMA) *in vivo*, have been recognized for many years for their ability to prevent non-specific protein adsorption and cell adhesion in implantable biomedical applications (Harris, 1992). It is believed that the protein resistance is controlled by terminal hydrophilicity of the head group combined with the formation of dense but disordered poly(ethylene glycol) brush (Wang et al., 1997; Pertsin et al., 2002; Schwendel et al., 2003; Herrwerth et al., 2003). While self-assembled monolayer (SAM) PEG coated planar microelectrode arrays have been developed (Azemi et al., 2008), an advanced variation on PEG SAM is the self-assembled monolayers of oligo(ethylene glycol) methyl methacrylate (OEGMA) (Ma et al., 2004) that promise improved robustness over PEG SAM coatings (Mrksich et al., 1997; Mrksich and Whitesides, 1997). The trade off with OEGMA is decreased density for increased robustness. In general, protein adsorption resistant coatings typically have hydrophilic head groups or kosmotropes. Some other examples include but are not limited to oligosaccharides, tri(propyl sulfoxide), hydroxyl glycerol, phosphorylcholine, tri(sarcosine), N-acetylpiperazine, permethylated sorbitol, hexamethylphophoramide, intramolecular zwitterion, mannitol, oligo(phosphocholine), sulfobetaine, carboxybetaine (Kane et al., 2003; Zhang et al., 2008; Love et al., 2005). It is important to note, however, that small changes in polymer structure can significantly influence the adsorption behavior of proteins (Weber et al., 2004).

Another protein adsorption resistant coating is 2-methacryloyloxyethyl phosphorylcholine (MPC) (Ueda et al., 1992; Inoue et al., 2004; Goda et al., 2007). MPC is composed of a hydrophilic side chain with phospholipid polar groups and has been shown to significantly reduce adsorption of fibrinogen and lysozymes on silicon (Feng et al., 2005) as well as fibrinogen and albumin on parylene-C (Goda et al., 2007). MPC has also been reported to show phospholipid adsorption. This is believed to occur from colliding cells, and the amount adsorbed correlates with the amount of MPC grafted on the device (Ishihara et al., 1992). The adsorbed phospholipids are believed to provide an additional biocompatible surface.

Other biofunctional coatings. Surfaces can further be biologically functionalized by immobilizing proteins and other signaling molecules. This can be done though functionalized polymer coating (Lahann et al., 2001), vapor-based initiator coating for atom transfer radical polymerization (Jiang et al., 2008), or through click chemistry (Nandivada et al., 2007). NCAM (CD56), and L1CAM (CD171) are glycoproteins on cell surfaces involved in neuronal survival and growth (Marchase et al., 1975; Faissner et al., 1984). Chondoitinase ABC has also been shown to promote axon regeneration and reactivates plasticity by removing chondoitin sulfate that is produced by microglia after CNS injury (Yin et al., 2009; Kwok et al., 2008; Bradbury et al., 2002). Other candidate biomolecules are dexamethasone and IL-10, which have been shown to have anti-inflammatory effects while BDNF is a known neurotrophic factor.

1.5.4 Electrochemical interface strategies

Electrical stimulation

The electrochemical nature of an electrode-tissue interface has been well-described, particularly for electrodes during recording (Venugopalan, 1994; Merrill et al., 2005; Cogan, 2008). Electrodes undergo reduction or oxidation and reach an equilibrium

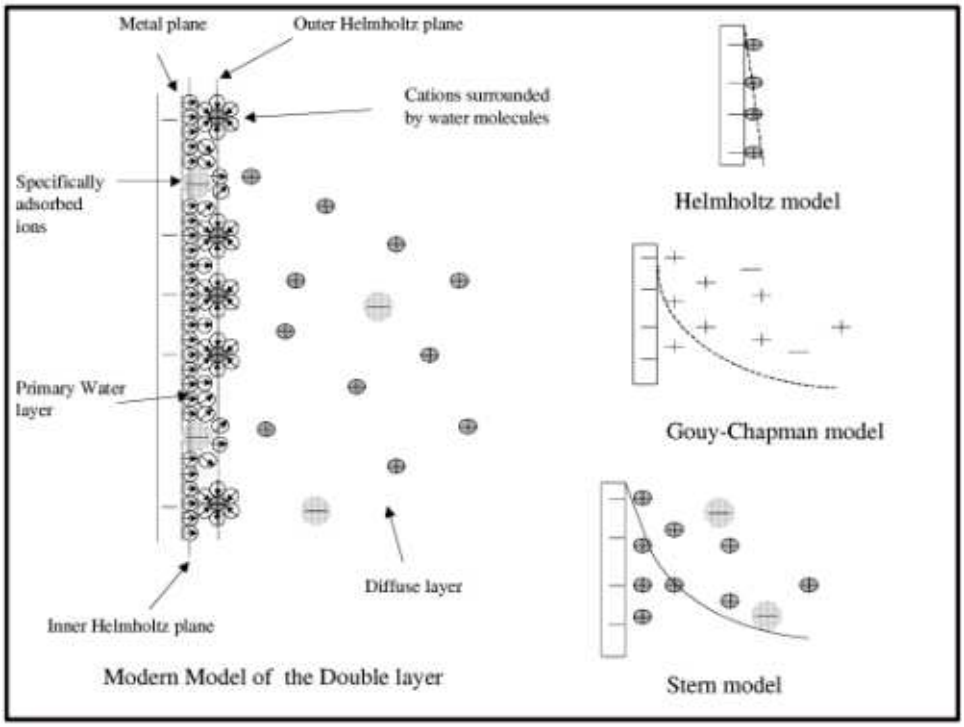

Figure 1.7: Detailed illustration of an electrochemical model of an implanted electrode *(left)*. Top, Helmholtz model assumes a linear double layer potential profile. Middle, Gouy-Chapman model assumes that charges decay rapidly and continuously from conductive material to electroyle without distinct layers. Bottom, Gouy-Chapman-Stern combines the first two models. Left, additionally depicts adsorption of water molecules and counter ions. (Zuleta, 2005)

that balances the charge transfer from the reduction-oxidation (redox) with the electrochemical potential across the interface. As electrodes become smaller, they are more influenced by *Helmholtz plane* or Gouy-Chapman-Stern "diffuse-layer" than their macro scale electrode counterparts (Figure 1.7). While DC electrical stimulation for microelectrodes has been well described (Mayer et al., 2004), AC stimulation is complicated by the formation of multiple diffusion layers or shells, especially as the electrode site becomes smaller.

At the electrochemical interface, there are two methods for transducing an electrical signal; 1) capacitive, and 2) redox reaction. In a capacitive signal transfer, electrical charges are displaced through the *Helmholtz plane* double layer capaci-

tance. In a redox (or Faradaic) reaction, a chemical reaction takes place which alters the electrode by dispelling the electrode material as ions or depositing ionic molecules in the electrolye solution to the surface of the electrode. While both forms of signal transfer always occur, their rates of reaction can be greatly controlled by strategically selecting the electrode material and electrical stimulation parameters.

While Faradaic reactions are unavoidable, their reaction rate kinetics and mass influence their reversibility (Bard and Faulkner, 1980). A Faradaic reaction with very fast kinetics or very low diffusion rate can reverse back to its initial form before it disperses out of range. For this reason, a heavy non-toxic metal, iridium, is a preferred electrode material, particularly for stimulation. Another popular stimulation electrode material is platinum. Platinum, in addition to its double layer capacitance, has a pseudocapacitance (Reading, 1975; Rand and Woods, 1971). In a pseudocapacitor, the products of the the redox reaction remain temporarily bound to the surface of the electrode, and by applying a rapid charge balanced stimulation in the opposite direction, the reaction can be reversed and ions may be recovered. Iridium also has this psuedocapacitive behavior (Grupioni et al., 2002).

(It is important to note that in a chemical *equilibrium*, the net reaction is zero which is distinct from having a zero forward or backward reaction. Additionally, *in vivo*, a system is never truly in equilibrium.)

Direct current (DC) or cyclic voltammetry (CV) electrical stimulation has also been used to disrupt protein and cellular encapsulation (Johnson et al., 2005; Merrill and Tresco, 2005; Sommakia et al., 2009). This results in an immediate decrease in 1kHz impedance, which gradually increases again over time. However, it is important to note that *in vivo* studies show that the relationship between electrode impedance and recording quality do not exactly correlate. Poor recording quality

with low impedance electrodes suggest that there are other variables that affect recording quality (Suner et al., 2005).

Because implantable microelectrodes have very small surface area electrode sites, an electrical stimulation with a high charge density can easily be applied that lesions the tissue (Townsend et al., 2002; Brozoski et al., 2006) or even evolve gasses, for example, through hydrolysis (Venugopalan, 1994). While this can be used to determine the location of electrode sites in the brain post mortem, these high levels of stimulation should be avoided during the lifetime of a chronic implant in a patient. Shannon (1992) used the data from McCreery et al. (1990) to generate the following expression for safe stimulation:

$$log\left(\frac{Q}{A}\right) = k - log(Q) \tag{1.1}$$

where Q is charge (μC) per phase, Q/A is charge density per phase (μC/cm^2) and $k \lesssim 1.7$ (Merrill et al., 2005; McCreery et al., 1990; Yuen et al., 1981; Agnew et al., 1989; Bhargava, 1993).

Electrode material

Metals. Many metals have been tested in the brain for biocompatibility (Dymond et al., 1970; Stensaas and Stensaas, 1976; Merrill et al., 2005; Cogan, 2008). Stainless steel, gold, iridium oxide, platinum, platinum-iridium, and tungsten are perhaps the more common electrode sites among currently commercially available electrodes (Cogan, 2008; Dymond et al., 1970; Stensaas and Stensaas, 1976; Babb and Kupfer, 1984; Chouard and Pialoux, 1995; Majji et al., 1999; Niparko et al., 1989). Other non-toxic electrode materials tested for neuroprosthetics are aluminum, gold-nickel-chromium, gold nickel-rhodium, nickle-chrome-

molybdenum, nitinol, platinum-nickel, platinum-rhodium, platinum-tungsten, platinum black, rhenium, titanium. (Dymond et al., 1970; Stensaas and Stensaas, 1976; Ryhnen et al., 1998; Bogdanski et al., 2002; Chouard and Pialoux, 1995).

Cobalt, copper, iron, silver, and germanium have been classified toxic, while molybdenum, nichrome, and tantalum have been classified as mildly reactive (Stensaas and Stensaas, 1976; Dymond et al., 1970; Fisher et al., 1961; Sawyer and Srinivasan, 1974; Babb and Kupfer, 1984).

For platinized or electroplated metals, such as platinum black, applying ultrasonic vibrations during deposition may improve the stability and impedance of the electrode sites (Desai et al., 2010).

As a side note, low shunt capacitance combined with high impedance electrodes may reduce the electrode's high-frequency response by forming a low-pass filter (Robinson, 1968). This can be compensated by coupling a negative capacitor amplifier to the electrode (Thomas, 1977).

Capacitive. Capacitive electrodes are attractive for electrical stimulation (McCreery et al., 1988; Rose et al., 1985; Guyton and Hambrecht, 1973), particularly because they prevent or limit Faradaic reactions. Several examples of capacitive electrodes are tantalum pentoxide, titanium dioxide, and titanium nitride (Cogan, 2008; McCreery et al., 1988; Rose et al., 1985; Guyton and Hambrecht, 1973; Gabay et al., 2007; Fromherz and Stett, 1995; Schoen and Fromherz, 2008). As mentioned earlier, tantalum is known to be reactive to the brain tissue. The challenge with capacitive electrodes is generating enough current for meaningful stimulation, or that a high dielectric material can compromise bandgaps during high current stimulation leading to larger leakage currents.

Polymer/Composite. Electrochemical deposition of conductive polymers such

as polypyrrol and poly(3,4-ethylenedioxythiophene) (PEDOT) have been used to improve the recording characteristics of small, high-impedance recording sites (Cui et al., 2001; Cui and Martin, 2003; Ludwig et al., 2006, 2011). These materials typically make good recording sites, but rapidly breakdown during stimulation (Wilks et al., 2009). Carbon nanotubes have also been shown to improve recording sites when electrochemically deposited (Keefer et al., 2008). Another method to apply carbon nanotube recording sites is to use LbL deposition (Jan et al., 2009) or grow vertically aligned carbon nanotubes from the electrode site (Yu et al., 2007).

These electrode sites can also be further bioactivated by applying surface-immobilized cues to improve the attachment and growth of neurons including electrochemical deposition of conducting polymers and neuron-promoting biomolecules on the electrodes (Cui et al., 2001; Stauffer and Cui, 2006; Cui et al., 2003; Buchko et al., 2001; Cui and Martin, 2003).

Chemical. Microdialysis offers advantages in sensitivity and multi-chemical selectivity (Parrot et al., 2003; Shackman et al., 2007). However, microdialysis lack high temporal and spatial resolutions necessary for behavioral neuroscience. To this end, microelectrodes with recording sites (typically, but not always carbon or platinum) have been developed that are further modified to preferentially detect specific neurochemicals on the order of seconds (Burmeister and Gerhardt, 2001; Pomerleau et al., 2003; McMahon et al., 2006; Kulagina and Michael, 2003; Khan, 2003; Schuvalio et al., 2006; Yoshida, 1995; Johnson et al., 2006, 2007). This is done by applying a voltage to the working electrode to cause a redox reaction which can be detected as a current proportional to the concentration of analyte. The two most common techniques are constant potential amperometry and cyclic voltammetry. In order to make the electrodes sensitive and selective to one chemical three strate-

gies are employed: 1) permselective membrane, 2) enzymatic coatings that breakdown a neurochemical molecule into a reactive species, typically hydrogen peroxide (Wilson and Gifford, 2005; Qin et al., 2008; Robinson et al., 2008), 3) implant into a region of the brain where an interfering neurochemical molecule is known to be absent. Until recently, electrodes have been dip coated, which precludes selective coating of small sites that may be closely spaced (Hu et al., 1994; Xin and Wightman, 1997; Schuvailo et al., 2005; Garguilo et al., 1993; Ryan et al., 1997). This has been addressed by site selective electrochemical deposition of enzymes (Frey et al., 2007, 2010a,b), allowing for a single probe to detect multiple chemicals, and even multiple modes. However, enzymatic coatings suffer from relatively rapid degradation at body temperature. On the other hand, chronic chemical sensing electrodes have been developed for chemical sensors that only require a permselective membrane (Clark et al., 2010; Ferguson et al., 2011; Flagel et al., 2011).

1.5.5 Electomechanical interface strategies

For the most part, electromechanical interfaces have been non-invasive or minimally invasive (subdural). Vibrotactile feedback has been used for the blind (Filin and Kosichkin, 1970; Ide and Obata, 1975) and certain deaf patients (Blamey et al., 1985; Dowell et al., 1985). It has also been applied to posture (O'brien and Azrin, 1970), and more recently to provide feedback for vestibular disorders (Young et al., 2001, 2003; Weinberg et al., 2006; Sienko et al., 2010). Functional electrical stimulation (FES) has been used to bypass the spine and activate muscle groups directly (Merletti et al., 1975; Reswick, 1976; Hambrecht, 1989; Peckham, 1992). Vibrotactile has also been applied to provide other information such as pressure in myoelectric limbs (Patterson and Katz, 1992; Schultz et al., 2009).

On the other hand, there are few mechanoelectic electrodes (Liao et al., 2008).

These devices typically have well defined surface properties. The electrode detects specific molecules by reversibly binding the target molecule and changing conformation. Conformation changes can be detected either through changes in resistance or capacitance of the electrode surface.

Alternative interface paradigms

An emerging technique is *optogenetics* in which specific types of neurons (or other cells) are genetically modified to express the membrane protein called channel rhodopsin (Boyden et al., 2005; Miller, 2006; Zhang et al., 2010; Deisseroth, 2011). This has lead to the development of microfabricated electrodes with optical channels for stimulation (Zorzos et al., 2010; Im et al., 2011).

On the other hand, calcium sensitive dyes or voltage sensitive dyes can be used to detect neuron activity (Hong et al., 2000). Combined with *in vivo* multiphoton imaging, slow neuronal activity can be tracked ~500 μm into the brain (Histed et al., 2009). Genetically inducible calcium indicators are currently being developed (Roderick and Bootman, 2006).

1.6 Dissertation Organization

This dissertation studies the technology and biology of implantable cortical neural interfaces and advances the concept and theory behind designing long-term implantable neural interfaces. Chapter II-IV include three research studies that are either in press or in preparation for submission to peer-reviewed journals.

In chapter II, we discuss the development and characterization of an insertion strategy for implanting ultra-flexible polymer neural probes into soft brain tissue. Polymer probes stick to metallic and silicon shuttles through hydrophobic interactions, causing a polymer probe to be carried out of the brain when the insertion

shuttle is removed. For hydrophilic surfaces, a phenomenon described as "capillary action" leads to a separation of the two surfaces in an aqueous solution (Cai and Bhushan, 2008a). Therefore, separation can be achieved by converting one of the hydrophobic surfaces (the shuttle) to a highly hydrophilic surface with a coating such that the meniscus force along the new hydrophilic surface overcomes the meniscus force along the hydrophobic probe surface. This study applied the use of an electronegative self-assembled monolayer (SAM) as a coating on a stiff insertion shuttle to carry a polymer probe into the cerebral cortex, and then the detachment of the shuttle from the probe. The results show that polydimethylsiloxane (PDMS) and polyimide probes could be inserted into an agarose *in vitro* brain model using the SAM coated silicon insertion shuttles. SAM-coated shuttles were further validated through their use to reliably insert PDMS probes in the cerebral cortex of rodents. This study found that SAM-coated silicon shuttles are a viable method for accurately and precisely inserting flexible neural probes in the brain and has been published in the *Journal of Neuroscience Methods* (Kozai and Kipke, 2009). This technology has also been filed under United States Patent Application 20090312770.

In Chapter III, we study the acute tissue damage caused by implantation of cortical probes with specific focus on the vasculature disruption during probe implantation. This trauma can cause abnormal electrophysiological responses, temporary increases in neurotransmitter levels, and perpetuate chronic immune responses. This study overcame the challenges for investigators to examine neurovascular features below the surface of the brain *in vivo* by employing 3D multiphoton imaging. Localized bleeding resulting from inserting microscale neural probes into cortex was investigated and approaches were explored to minimize blood vessel disruption through insertion methods. 3D two-photon microscopy (TPM) images of cortical neurovas-

culature were obtained from mice and used to select preferred insertion positions for probe insertion to reduce neurovasculature damage. The results show significant reduction in neurovascular damage for probes inserted in regions devoid of major sub-surface vessels. Also, the deviation of surface vessels from the vector normal to the surface as a function of depth and vessel diameter were measured and characterized. 68% of the major vessels were found to deviate less than 49 μm from their surface origin up to a depth of 500 μm. Inserting probes more than 49 μm from major surface vessels can reduce chances of severing major sub-surface neurovasculature without using TPM. This study was published in the *Journal of Neural Engineering* (Kozai et al., 2010).

Chapter IV reports an integrated composite electrode consisting of a carbon fiber core, a poly(p-xylylene)-based thin-film coating that acts as dielectric barrier which is functionalized to control intrinsic biological processes, and a poly(thiophene)-based recording pad. The resulting devices are an order of magnitude smaller than currently available neural interfaces and more mechanically compliant with brain tissue than traditional recording electrodes. These microthread electrodes were found to elicit negligible chronic reactive tissue responses and have excellent recording characteristics in acute and chronic experiments in rats. Developing smaller and more flexible neural probes with advanced surface materials for long-term, high quality and selective neural recording could potentially lead to paradigm shifts in both neuroscience research and clinical neurotechnologies by allowing researchers to explore new paradigms in novel ways. This technology has been filed under United States Provisional Patent Application 61/356,482.

Chapter V summarizes the findings of the previous chapters and discusses the impacts to the field of neural engineering. Additionally, it explores new opportunities,

emerging technologies, and the overall direction of the field.

1.7 References

Agnew, W. F., McCreery, D. B., Yuen, T. G., and Bullara, L. A. (1989). Histologic and physiologic evaluation of electrically stimulated peripheral nerve: considerations for the selection of parameters. *Ann Biomed Eng*, 17(1):39–60.

Al-Majed, A. A., Brushart, T. M., and Gordon, T. (2000a). Electrical stimulation accelerates and increases expression of bdnf and trkb mrna in regenerating rat femoral motoneurons. *Eur J Neurosci*, 12(12):4381–4390.

Al-Majed, A. A., Neumann, C. M., Brushart, T. M., and Gordon, T. (2000b). Brief electrical stimulation promotes the speed and accuracy of motor axonal regeneration. *J Neurosci*, 20(7):2602–2608.

Alafuzoff, I., Adolfsson, R., Bucht, G., and Winblad, B. (1983). Albumin and immunoglobulin in plasma and cerebrospinal fluid, and blood-cerebrospinal fluid barrier function in patients with dementia of alzheimer type and multi-infarct dementia. *J Neurol Sci*, 60(3):465–472.

Alexander, J. K., Fuss, B., and Colello, R. J. (2006). Electric field-induced astrocyte alignment directs neurite outgrowth. *Neuron Glia Biol*, 2(2):93–103.

Alvira, D., Tajes, M., Verdaguer, E., de Arriba, S. G., Allgaier, C., Matute, C., Trullas, R., Jimnez, A., Palls, M., and Camins, A. (2007). Inhibition of cyclin-dependent kinases is neuroprotective in 1-methyl-4-phenylpyridinium-induced apoptosis in neurons. *Neuroscience*, 146(1):350–365.

Appert-Collin, A., Hugel, B., Levy, R., Niederhoffer, N., Coupin, G., Lombard, Y., Andr, P., Poindron, P., and Gies, J. P. (2006). Cyclin dependent kinase inhibitors prevent apoptosis of postmitotic mouse motoneurons. *Life Sci*, 79(5):484–490.

Azemi, E., Lagenaur, C. F., and Cui, X. T. (2011). The surface immobilization of the neural adhesion molecule l1 on neural probes and its effect on neuronal density and gliosis at the probe/tissue interface. *Biomaterials*, 32(2011):681–92.

Azemi, E., Stauffer, W. R., Gostock, M. S., Lagenaur, C. F., and Cui, X. T. (2008). Surface immobilization of neural adhesion molecule l1 for improving the biocompatibility of chronic neural probes: In vitro characterization. *Acta Biomater*, 4(5):1208–1217.

Babb, T. L. and Kupfer, W. (1984). Phagocytic and metabolic reactions to chronically implanted metal brain electrodes. *Exp Neurol*, 86(2):171–182.

Bard, A. J. and Faulkner, L. R., editors (1980). *Electrochemical methods.* Wiley, New York.

Bartels, J., Andreasen, D., Ehirim, P., Mao, H., Seibert, S., Wright, E. J., and Kennedy, P. (2008). Neurotrophic electrode: Method of assembly and implantation into human motor speech cortex. *Journal of Neuroscience Methods*, 174(2):168 – 176.

Bartels, K. E. (1976). Surgical implantation of electroencephalographic electrodes in the dog. *Am J Vet Res*, 37(1):83–85.

Bedlack, R. S., Wei, M., and Loew, L. M. (1992). Localized membrane depolarizations and localized calcium influx during electric field-guided neurite growth. *Neuron*, 9(3):393–403.

Bernatchez, S. F., Parks, P. J., and Gibbons, D. F. (1996). Interaction of macrophages with fibrous materials in vitro. *Biomaterials*, 17(21):2077–2086.

Betz, A. L., Iannotti, F., and Hoff, J. T. (1989). Brain edema: a classification based on blood-brain barrier integrity. *Cerebrovasc Brain Metab Rev*, 1(2):133–154.

Bhargava, A. (1993). Long-term effects of quasi-trapezoidal pulses on the structure and function of sacral anterior roots. Master's thesis, Case Western Reserve University, Cleveland, OH.

Biran, R., Martin, D. C., and Tresco, P. A. (2005). Neuronal cell loss accompanies the brain tissue response to chronically implanted silicon microelectrode arrays. *Experimental Neurology*, 195(1):115 – 126.

Bjornsson, C. S., Oh, S. J., Al-Kofahi, Y. A., Lim, Y. J., Smith, K. L., Turner, J. N., De, S., Roysam, B., Shain, W., and Kim, S. J. (2006). Effects of insertion conditions on tissue strain and vascular damage during neuroprosthetic device insertion. *J Neural Eng*, 3(3):196–207.

Blackman, C. F., Benane, S. G., and House, D. E. (1993). Evidence for direct effect of magnetic fields on neurite outgrowth. *FASEB J*, 7(9):801–806.

Blamey, P. J., Dowell, R. C., Brown, A. M., and Clark, G. M. (1985). Clinical results with a hearing aid and a single-channel vibrotactile device for profoundly deaf adults. *Br J Audiol*, 19(3):203–210.

Bogdanski, D., Kller, M., Mller, D., Muhr, G., Bram, M., Buchkremer, H. P., Stver, D., Choi, J., and Epple, M. (2002). Easy assessment of the biocompatibility of ni-ti alloys by in vitro cell culture experiments on a functionally graded ni-niti-ti material. *Biomaterials*, 23(23):4549–4555.

Boyden, E. S., Zhang, F., Bamberg, E., Nagel, G., and Deisseroth, K. (2005). Millisecond-timescale, genetically targeted optical control of neural activity. *Nat Neurosci*, 8(9):1263–1268.

Bradbury, E. J., Moon, L. D. F., Popat, R. J., King, V. R., Bennett, G. S., Patel, P. N., Fawcett, J. W., and McMahon, S. B. (2002). Chondroitinase abc promotes functional recovery after spinal cord injury. *Nature*, 416(6881):636–640.

Brandwood, A., Noble, K. R., and Schindhelm, K. (1992). Phagocytosis of carbon particles by macrophages in vitro. *Biomaterials*, 13(9):646–648.

Brown, E. N., Frank, L. M., Tang, D., Quirk, M. C., and Wilson, M. A. (1998). A statistical paradigm for neural spike train decoding applied to position prediction from ensemble firing patterns of rat hippocampal place cells. *J Neurosci*, 18(18):7411–7425.

Brozoski, T. J., Caspary, D. M., and Bauer, C. A. (2006). Marking multi-channel silicon-substrate electrode recording sites using radiofrequency lesions. *J Neurosci Methods*, 150(2):185–191.

Buchko, C. J., Kozloff, K. M., and Martin, D. C. (2001). Surface characterization of porous, biocompatible protein polymer thin films. *Biomaterials*, 22(11):1289–1300.

Burmeister, J. J. and Gerhardt, G. A. (2001). Self-referencing ceramic-based multisite microelectrodes for the detection and elimination of interferences from the measurement of l-glutamate and other analytes. *Anal Chem*, 73(5):1037–1042.

Burmeister, J. J., Pomerleau, F., Palmer, M., Day, B. K., Huettl, P., and Gerhardt, G. A. (2002). Improved ceramic-based multisite microelectrode for rapid measurements of l-glutamate in the cns. *J Neurosci Methods*, 119(2):163–171.

Byrnes, K. R., Stoica, B. A., Fricke, S., Giovanni, S. D., and Faden, A. I. (2007). Cell cycle activation contributes to post-mitotic cell death and secondary damage after spinal cord injury. *Brain*, 130(Pt 11):2977–2992.

Cai, D., Qiu, J., Cao, Z., McAtee, M., Bregman, B. S., and Filbin, M. T. (2001). Neuronal cyclic amp controls the developmental loss in ability of axons to regenerate. *J Neurosci*, 21(13):4731–4739.

Cai, S. and Bhushan, B. (2008a). Meniscus and viscous forces during separation of hydrophilic and hydrophobic surfaces with liquid-mediated contacts. *Materials Science and Engineering: R: Reports*, 61(1-6):78 – 106.

Cai, S. and Bhushan, B. (2008b). Viscous force during tangential separation of meniscus bridges. *Philosophical Magazine*, 88:449–461.

Cao, L., Chang, M., Lee, C.-Y., Castner, D. G., Sukavaneshvar, S., Ratner, B. D., and Horbett, T. A. (2007). Plasma-deposited tetraglyme surfaces greatly reduce total blood protein adsorption, contact activation, platelet adhesion, platelet procoagulant activity, and in vitro thrombus deposition. *J Biomed Mater Res A*, 81(4):827–837.

Cernak, I., Stoica, B., Byrnes, K. R., Giovanni, S. D., and Faden, A. I. (2005). Role of the cell cycle in the pathobiology of central nervous system trauma. *Cell Cycle*, 4(9):1286–1293.

Chen, C. S., Mrksich, M., Huang, S., Whitesides, G. M., and Ingber, D. E. (1997). Geometric control of cell life and death. *Science*, 276(5317):1425–1428.

Chen, Z.-J., Gillies, G. T., Broaddus, W. C., Prabhu, S. S., Fillmore, H., Mitchell, R. M., Corwin, F. D., and Fatouros, P. P. (2004). A realistic brain tissue phantom for intraparenchymal infusion studies. *J Neurosurg*, 101(2):314–322.

Cheung, K., Djupsund, K., Dan, Y., and Lee, L. (2003). Implantable multichannel electrode array based on soi technology. *Journal of Microelectromechanical Systems*, 12(2):179–184.

Chouard, C. H. and Pialoux, P. (1995). [biocompatibility of cochlear implants]. *Bull Acad Natl Med*, 179(3):549–555.

Clark, J. J., Sandberg, S. G., Wanat, M. J., Gan, J. O., Horne, E. A., Hart, A. S., Akers, C. A., Parker, J. G., Willuhn, I., Martinez, V., Evans, S. B., Stella, N., and Phillips, P. E. M. (2010). Chronic microsensors for longitudinal, subsecond dopamine detection in behaving animals. *Nat Methods*, 7(2):126–129.

Cogan, S. F. (2008). Neural stimulation and recording electrodes. *Annu Rev Biomed Eng*, 10:275–309.

Cohan, C. S., Connor, J. A., and Kater, S. B. (1987). Electrically and chemically mediated increases in intracellular calcium in neuronal growth cones. *J Neurosci*, 7(11):3588–3599.

Colman, H., Nabekura, J., and Lichtman, J. W. (1997). Alterations in synaptic strength preceding axon withdrawal. *Science*, 275(5298):356–361.

Colombo, G., Joerg, M., Schreier, R., and Dietz, V. (2000). Treadmill training of paraplegic patients using a robotic orthosis. *J Rehabil Res Dev*, 37(6):693–700.

Cui, X., Lee, V. A., Raphael, Y., Wiler, J. A., Hetke, J. F., Anderson, D. J., and Martin, D. C. (2001). Surface modification of neural recording electrodes with conducting polymer/biomolecule blends. *J Biomed Mater Res*, 56(2):261–272.

Cui, X. and Martin, D. C. (2003). Electrochemical deposition and characterization of poly(3,4-ethylenedioxythiophene) on neural microelectrode arrays. *Sensors and Actuators B: Chemical*, 89(1-2):92–102.

Cui, X., Wiler, J., Dzaman, M., Altschuler, R. A., and Martin, D. C. (2003). In vivo studies of polypyrrole/peptide coated neural probes. *Biomaterials*, 24(5):777–87.

Davis, D. H., Giannoulis, C. S., Johnson, R. W., and Desai, T. A. (2002). Immobilization of rgd to 111 silicon surfaces for enhanced cell adhesion and proliferation. *Biomaterials*, 23(19):4019–4027.

Deisseroth, K. (2011). Optogenetics. *Nat Methods*, 8(1):26–29.

Deligianni, D. D., Katsala, N. D., Koutsoukos, P. G., and Missirlis, Y. F. (2001). Effect of surface roughness of hydroxyapatite on human bone marrow cell adhesion, proliferation, differentiation and detachment strength. *Biomaterials*, 22(1):87–96.

Desai, S. A., Rolston, J. D., Guo, L., and Potter, S. M. (2010). Improving impedance of implantable microwire multi-electrode arrays by ultrasonic electroplating of durable platinum black. *Front Neuroengineering*, 3:5.

Dirnagl, U., Iadecola, C., and Moskowitz, M. A. (1999). Pathobiology of ischaemic stroke: an integrated view. *Trends Neurosci*, 22(9):391–397.

Dobelle, W. H. (2000). Artificial vision for the blind by connecting a television camera to the visual cortex. *ASAIO J*, 46(1):3–9.

Dormn, G. and Prestwich, G. D. (2000). Using photolabile ligands in drug discovery and development. *Trends Biotechnol*, 18(2):64–77.

Dowell, R. C., Martin, L. F., Clark, G. M., and Brown, A. M. (1985). Results of a preliminary clinical trial on a multiple channel cochlear prosthesis. *Ann Otol Rhinol Laryngol*, 94(3):244–250.

Dymond, A. M., Kaechele, L. E., Jurist, J. M., and Crandall, P. H. (1970). Brain tissue reaction to some chronically implanted metals. *J Neurosurg*, 33(5):574–580.

Edell, D. J., Toi, V. V., McNeil, V. M., and Clark, L. D. (1992). Factors influencing the biocompatibility of insertable silicon microshafts in cerebral cortex. *IEEE Trans Biomed Eng*, 39(6):635–643.

Faissner, A., Kruse, J., Goridis, C., Bock, E., and Schachner, M. (1984). The neural cell adhesion molecule l1 is distinct from the n-cam related group of surface antigens bsp-2 and d2. *EMBO J*, 3(4):733–737.

Feng, W., Zhu, S., Ishihara, K., and Brash, J. L. (2005). Adsorption of fibrinogen and lysozyme on silicon grafted with poly(2-methacryloyloxyethyl phosphorylcholine) via surface-initiated atom transfer radical polymerization. *Langmuir*, 21(13):5980–5987.

Ferguson, S. M., Eskenazi, D., Ishikawa, M., Wanat, M. J., Phillips, P. E. M., Dong, Y., Roth, B. L., and Neumaier, J. F. (2011). Transient neuronal inhibition reveals opposing roles of indirect and direct pathways in sensitization. *Nat Neurosci*, 14(1):22–24.

Fetz, E. E. and Finocchio, D. V. (1975). Correlations between activity of motor cortex cells and arm muscles during operantly conditioned response patterns. *Exp Brain Res*, 23(3):217–240.

Field-Fote, E. C. (2001). Combined use of body weight support, functional electric stimulation, and treadmill training to improve walking ability in individuals with chronic incomplete spinal cord injury. *Arch Phys Med Rehabil*, 82(6):818–824.

Filin, V. A. and Kosichkin, D. I. (1970). [discriminatory ability of the skin of the fingers during the use of vibrotactile signals for information transmission to the blind]. *Nov Med Priborostr*, 3:74–77.

Fisher, G., Sayre, G., and Bickford, R. (1961). *Electrical stimulation of the brain.*, chapter Histological changes in the cat's brain after introduction of metallic and plastic-coated wire., pages 55–9. Austin: University of Texas Press.

Flagel, S. B., Clark, J. J., Robinson, T. E., Mayo, L., Czuj, A., Willuhn, I., Akers, C. A., Clinton, S. M., Phillips, P. E. M., and Akil, H. (2011). A selective role for dopamine in stimulus-reward learning. *Nature*, 469(7328):53–57.

Foley, C. P., Neeves, K. B., Saltzman, W. M., and Olbricht, W. L. (2006). Bioerodible scaffolds for implantable microfluidic probes in convection enchanced neural drug delivery. In *AIChE Annual Meeting*, San Francisco, CA.

Frey, O., Holtzman, T., McNamara, R. M., Theobald, D. E. H., van der Wal, P. D., de Rooij, N. F., Dalley, J. W., and Koudelka-Hep, M. (2010a). Enzyme-based choline and l-glutamate biosensor electrodes on silicon microprobe arrays. *Biosens Bioelectron*, 26(2):477–484.

Frey, O., Talaei, S., van der Wal, P. D., Koudelka-Hep, M., and de Rooij, N. F. (2010b). Continuous-flow multi-analyte biosensor cartridge with controllable linear response range. *Lab Chip*, 10(17):2226–2234.

Frey, O., van der Wal, P., de Rooij, N., and Koudelka-Hep, M. (2007). Development and characterization of choline and l-glutamate biosensor integrated on silicon microprobes for in-vivo monitoring. *Conf Proc IEEE Eng Med Biol Soc*, 2007:6040–6043.

Fromherz and Stett (1995). Silicon-neuron junction: Capacitive stimulation of an individual neuron on a silicon chip. *Phys Rev Lett*, 75(8):1670–1673.

Gabay, T., Ben-David, M., Kalifa, I., Sorkin, R., Abrams, Z. R., Ben-Jacob, E., and Hanein, Y. (2007). Electro-chemical and biological properties of carbon nanotube based multi-electrode arrays. *Nanotechnology*, 18(3):035201.

Gage, G. J., Ludwig, K. A., Otto, K. J., Ionides, E. L., and Kipke, D. R. (2005). Naive coadaptive cortical control. *J Neural Eng*, 2(2):52–63.

Garguilo, M. G., Huynh, N., Proctor, A., and Michael, A. C. (1993). Amperometric sensors for peroxide, choline, and acetylcholine based on electron transfer between horseradish peroxidase and a redox polymer. *Anal Chem*, 65(5):523–528.

Georgopoulos, A. P., Schwartz, A. B., and Kettner, R. E. (1986). Neuronal population coding of movement direction. *Science*, 233(4771):1416–1419.

Gilletti, A. and Muthuswamy, J. (2006). Brain micromotion around implants in the rodent somatosensory cortex. *J Neural Eng*, 3(3):189–195.

Giovanni, S. D., Movsesyan, V., Ahmed, F., Cernak, I., Schinelli, S., Stoica, B., and Faden, A. I. (2005). Cell cycle inhibition provides neuroprotection and reduces glial proliferation and scar formation after traumatic brain injury. *Proc Natl Acad Sci U S A*, 102(23):8333–8338.

Goda, T., Konno, T., Takai, M., and Ishihara, K. (2007). Photoinduced phospholipid polymer grafting on parylene film: advanced lubrication and antibiofouling properties. *Colloids Surf B Biointerfaces*, 54(1):67–73.

Golde, S., Coles, A., Lindquist, J. A., and Compston, A. (2003). Decreased inos synthesis mediates dexamethasone-induced protection of neurons from inflammatory injury in vitro. *Eur J Neurosci*, 18(9):2527–2537.

Goldstein, S. R. and Salcman, M. (1973). Mechanical factors in the design of chronic recording intracortical microelectrodes. *IEEE Trans Biomed Eng*, 20(4):260–269.

Gonzalez-Perez, O., Quiones-Hinojosa, A., and Garcia-Verdugo, J. M. (2010). Immunological control of adult neural stem cells. *J Stem Cells*, 5(1):23–31.

Grand, L., Wittner, L., Herwik, S., Gthelid, E., Ruther, P., Oscarsson, S., Neves, H., Dombovri, B., Csercsa, R., Karmos, G., and Ulbert, I. (2010). Short and long term biocompatibility of neuroprobes silicon probes. *J Neurosci Methods*, 189(2):216–229.

Groothuis, D. R., Ward, S., Schlageter, K. E., Itskovich, A. C., Schwerin, S. C., Allen, C. V., Dills, C., and Levy, R. M. (1998). Changes in blood-brain barrier permeability associated with insertion of brain cannulas and microdialysis probes. *Brain Res*, 803(1-2):218–230.

Grupioni, A. A. F., Arashiro, E., and Lassali, T. A. F. (2002). Voltammetric characterization of an iridium oxide-based system: the pseudocapacitive nature of the ir0.3mn0.7o2 electrode. *Electrochimica Acta*, 48(4):407–418.

Guyton, D. L. and Hambrecht, F. T. (1973). Capacitor electrode stimulates nerve or muscle without oxidation-reduction reactions. *Science*, 181(94):74–76.

Hallab, N. J., Bundy, K. J., O'Connor, K., Moses, R. L., and Jacobs, J. J. (2001). Evaluation of metallic and polymeric biomaterial surface energy and surface roughness characteristics for directed cell adhesion. *Tissue Eng*, 7(1):55–71.

Hambrecht, F. T. (1989). Functional electrical stimulation: an overview. *Pacing Clin Electrophysiol*, 12(5):840–843.

Hanly, J. G., Fisk, J. D., and Eastwood, B. (1994). Brain reactive autoantibodies and cognitive impairment in systemic lupus erythematosus. *Lupus*, 3(3):193–199.

Harris, J. M. (1992). *Poly(Ethylene Glycol) Chemistry: Biotechnical and Biomedical Applications*. Plenum Press, New York, USA.

He, W. and Bellamkonda, R. V. (2005). Nanoscale neuro-integrative coatings for neural implants. *Biomaterials*, 26(16):2983–2990.

Henze, D. A., Borhegyi, Z., Csicsvari, J., Mamiya, A., Harris, K. D., and Buzski, G. (2000). Intracellular features predicted by extracellular recordings in the hippocampus in vivo. *J Neurophysiol*, 84(1):390–400.

Herrwerth, S., Eck, W., Reinhardt, S., and Grunze, M. (2003). Factors that determine the protein resistance of oligoether self-assembled monolayers –internal hydrophilicity, terminal hydrophilicity, and lateral packing density. *J Am Chem Soc*, 125(31):9359–9366.

Hetke, J. and Anderson, D. (2002). *Handbook of Neuroprosthetic Methods.*, chapter Chapter 7: Silicon microelectrodes for extracellular recording. CRC Press, Boca Raton, FL.

Histed, M. H., Bonin, V., and Reid, R. C. (2009). Direct activation of sparse, distributed populations of cortical neurons by electrical microstimulation. *Neuron*, 63(4):508–522.

Hong, K., Nishiyama, M., Henley, J., Tessier-Lavigne, M., and Poo, M. (2000). Calcium signalling in the guidance of nerve growth by netrin-1. *Nature*, 403(6765):93–98.

Hoogerwerf, A. C. and Wise, K. D. (1994). A three-dimensional microelectrode array for chronic neural recording. *IEEE Trans Biomed Eng*, 41(12):1136–1146.

Horbett, T. A. and Brash, J. L., editors (1995). *Proteins at Interfaces II Fundamentals and Applications*, volume 602 of *ACS Symposium Series*. American Chemical Society, Washington D.C.

House, P. A., MacDonald, J. D., Tresco, P. A., and Normann, R. A. (2006). Acute microelectrode array implantation into human neocortex: preliminary technique and histological considerations. *Neurosurg Focus*, 20(5):E4.

Hu, Y., Mitchell, K. M., Albahadily, F. N., Michaelis, E. K., and Wilson, G. S. (1994). Direct measurement of glutamate release in the brain using a dual enzyme-based electrochemical sensor. *Brain Res*, 659(1-2):117–125.

Hugel, H., Ellershaw, J., and Gambles, M. (2006). Respiratory tract secretions in the dying patient: a comparison between glycopyrronium and hyoscine hydrobromide. *J Palliat Med*, 9(2):279–284.

Hui-Chou, H. G., Hashemi, S. S., Hoke, A., and Dellon, A. L. (2011). Clinical implications of peripheral myelin protein 22 for nerve compression and neural regeneration: a review. *J Reconstr Microsurg*, 27(1):67–74.

Ide, H. and Obata, S. (1975). [vibrotactile stimulation for a reading aid for the blind]. *Iyodenshi To Seitai Kogaku*, 13(5):282–286.

Im, M., Cho, I.-J., Wise, K. D., and Yoon, E. (2011). Neural probes integrated with optical mixer/splitter waveguides and multiple stimulation sites. In *IEEE MEMS*, pages 1051–1054, Cancun, Mexico.

Inoue, Y., Watanabe, J., and Ishihara, K. (2004). Dynamic motion of phosphorylcholine groups at the surface of poly(2-methacryloyloxyethyl phosphorylcholine-random-2,2,2-trifluoroethyl methacrylate). *J Colloid Interface Sci*, 274(2):465–471.

Isaksson, J., Kjll, P., Nilsson, D., Robinson, N. D., Berggren, M., and Richter-Dahlfors, A. (2007). Electronic control of ca2+ signalling in neuronal cells using an organic electronic ion pump. *Nat Mater*, 6(9):673–679.

Ishihara, K., Oshida, H., Endo, Y., Ueda, T., Watanabe, A., and Nakabayashi, N. (1992). Hemocompatibility of human whole blood on polymers with a phospholipid polar group and its mechanism. *J Biomed Mater Res*, 26(12):1543–1552.

Ivens, S., Kaufer, D., Flores, L. P., Bechmann, I., Zumsteg, D., Tomkins, O., Seiffert, E., Heinemann, U., and Friedman, A. (2007). Tgf-beta receptor-mediated albumin uptake into astrocytes is involved in neocortical epileptogenesis. *Brain*, 130(Pt 2):535–547.

James, C. D., Spence, A. J. H., Dowell-Mesfin, N. M., Hussain, R. J., Smith, K. L., Craighead, H. G., Isaacson, M. S., Shain, W., and Turner, J. N. (2004). Extracellular recordings from patterned neuronal networks using planar microelectrode arrays. *IEEE Trans Biomed Eng*, 51(9):1640–1648.

Jan, E., Hendricks, J. L., Husaini, V., Richardson-Burns, S. M., Sereno, A., Martin, D. C., and Kotov, N. A. (2009). Layered carbon nanotube-polyelectrolyte electrodes outperform traditional neural interface materials. *Nano Lett*, 9(12):4012–4018.

Jaroch, D. B., Ward, M. P., Chow, E. Y., Rickus, J. L., and Irazoqui, P. P. (2009). Magnetic insertion system for flexible electrode implantation. *J Neurosci Methods*, 183(2):213–222.

Jiang, X. W., Chen, H. Y., Galvan, G., Yoshida, M., and Lahann, J. (2008). Vapor-based initiator coatings for atom transfer radical polymerization. *Advanced Functional Materials*, 18(1):27–35.

Johnson, K. L., Kendall, K., and Roberts, A. D. (1971). Surface energy and the contact of elastic solids. *Proceedings of the Royal Society of London. Series A, Mathematical and Physical Sciences*, 324(1558):301–313.

Johnson, M. D., Kao, O. E., and Kipke, D. R. (2007). Spatiotemporal ph dynamics following insertion of neural microelectrode arrays. *J Neurosci Methods*, 160(2):276–287.

Johnson, M. D., Langhals, N. B., and Kipke, D. R. (2006). Neural interface dynamics following insertion of hydrous iridium oxide microelectrode arrays. *Conf Proc IEEE Eng Med Biol Soc*, 1:3178–3181.

Johnson, M. D., Otto, K. J., and Kipke, D. R. (2005). Repeated voltage biasing improves unit recordings by reducing resistive tissue impedances. 13(2):160–165.

Kane, R. S., Deschatelets, P., and Whitesides, G. M. (2003). Kosmotropes form the basis of protein-resistant surfaces. *Langmuir*, 19(6):2388–2391.

Kaper, M., Meinicke, P., Grossekathoefer, U., Lingner, T., and Ritter, H. (2004). Bci competition 2003–data set iib: support vector machines for the p300 speller paradigm. *IEEE Trans Biomed Eng*, 51(6):1073–1076.

Kargo, W. J. and Nitz, D. A. (2003). Early skill learning is expressed through selection and tuning of cortically represented muscle synergies. *J Neurosci*, 23(35):11255–11269.

Keefer, E. W., Botterman, B. R., Romero, M. I., Rossi, A. F., and Gross, G. W. (2008). Carbon nanotube coating improves neuronal recordings. *Nat Nanotechnol*, 3(7):434–439.

Kempski, O. (2001). Cerebral edema. *Semin Nephrol*, 21(3):303–307.

Kennedy, P. R. (1989). The cone electrode: a long-term electrode that records from neurites grown onto its recording surface. *J Neurosci Methods*, 29(3):181–193.

Kennedy, P. R., Mirra, S. S., and Bakay, R. A. (1992). The cone electrode: ultrastructural studies following long-term recording in rat and monkey cortex. *Neurosci Lett*, 142(1):89–94.

Khan, A. S. Michael, A. C. (2003). Invasive consequences of using micro-electrodes and microdialysis probes in the brain. *Trac-Trends in Analytical Chemistry*, 22(9):503–508.

Kim, D.-H., Abidian, M., and Martin, D. C. (2004a). Conducting polymers grown in hydrogel scaffolds coated on neural prosthetic devices. *J Biomed Mater Res A*, 71(4):577–585.

Kim, D.-H. and Martin, D. C. (2006). Sustained release of dexamethasone from hydrophilic matrices using plga nanoparticles for neural drug delivery. *Biomaterials*, 27(15):3031–3037.

Kim, D.-H., Viventi, J., Amsden, J. J., Xiao, J., Vigeland, L., Kim, Y.-S., Blanco, J. A., Panilaitis, B., Frechette, E. S., Contreras, D., Kaplan, D. L., Omenetto, F. G., Huang, Y., Hwang, K.-C., Zakin, M. R., Litt, B., and Rogers, J. A. (2010). Dissolvable films of silk fibroin for ultrathin conformal bio-integrated electronics. *Nat Mater*, 9(6):511–517.

Kim, H. K., Biggs, S. J., Schloerb, D. W., Carmena, J. M., Lebedev, M. A., Nicolelis, M. A. L., and Srinivasan, M. A. (2006). Continuous shared control for stabilizing reaching and grasping with brain-machine interfaces. *IEEE Trans Biomed Eng*, 53(6):1164–1173.

Kim, Y.-T., Hitchcock, R. W., Bridge, M. J., and Tresco, P. A. (2004b). Chronic response of adult rat brain tissue to implants anchored to the skull. *Biomaterials*, 25(12):2229–2237.

Kimelberg, H. K. (1995). Current concepts of brain edema. review of laboratory investigations. *J Neurosurg*, 83(6):1051–1059.

Kipke, D. R., Shain, W., Buzski, G., Fetz, E., Henderson, J. M., Hetke, J. F., and Schalk, G. (2008). Advanced neurotechnologies for chronic neural interfaces: new horizons and clinical opportunities. *J Neurosci*, 28(46):11830–11838.

Klatzo, I. (1967). Presidental address. neuropathological aspects of brain edema. *J Neuropathol Exp Neurol*, 26(1):1–14.

Korsching, S. and Thoenen, H. (1983). Nerve growth factor in sympathetic ganglia and corresponding target organs of the rat: correlation with density of sympathetic innervation. *Proc Natl Acad Sci U S A*, 80(11):3513–3516.

Kozai, T. D. Y. and Kipke, D. R. (2009). Insertion shuttle with carboxyl terminated self-assembled monolayer coatings for implanting flexible polymer neural probes in the brain. *J Neurosci Methods*, 184(2):199–205.

Kozai, T. D. Y., Marzullo, T. C., Hooi, F., Langhals, N. B., Majewska, A. K., Brown, E. B., and Kipke, D. R. (2010). Reduction of neurovascular damage resulting from microelectrode insertion into the cerebral cortex using in vivo two-photon mapping. *J Neural Eng*, 7(4):046011.

Kuida, K., Haydar, T. F., Kuan, C. Y., Gu, Y., Taya, C., Karasuyama, H., Su, M. S., Rakic, P., and Flavell, R. A. (1998). Reduced apoptosis and cytochrome c-mediated caspase activation in mice lacking caspase 9. *Cell*, 94(3):325–337.

Kuida, K., Lippke, J. A., Ku, G., Harding, M. W., Livingston, D. J., Su, M. S., and Flavell, R. A. (1995). Altered cytokine export and apoptosis in mice deficient in interleukin-1 beta converting enzyme. *Science*, 267(5206):2000–2003.

Kulagina, N. V. and Michael, A. C. (2003). Monitoring hydrogen peroxide in the extracellular space of the brain with amperometric microsensors. *Anal Chem*, 75(18):4875–4881.

Kwok, J. C. F., Afshari, F., Garca-Alas, G., and Fawcett, J. W. (2008). Proteoglycans in the central nervous system: plasticity, regeneration and their stimulation with chondroitinase abc. *Restor Neurol Neurosci*, 26(2-3):131–145.

Lahann, J., Choi, I. S., Lee, J., Jenson, K. F., and Langer, R. (2001). A new method toward microengineered surfaces based on reactive coating. *Angewandte Chemie-International Edition*, 40(17):3166–9.

Langer, R. (2000). Biomaterials in drug delivery and tissue engineering: one laboratory's experience. *Acc Chem Res*, 33(2):94–101.

LaPlaca, M. C., Cullen, D. K., McLoughlin, J. J., and Cargill, R. S. (2005). High rate shear strain of three-dimensional neural cell cultures: a new in vitro traumatic brain injury model. *J Biomech*, 38(5):1093–1105.

Lebedev, M. A. and Nicolelis, M. A. L. (2006). Brain-machine interfaces: past, present and future. *Trends Neurosci*, 29(9):536–546.

Lee, H., Bellamkonda, R. V., Sun, W., and Levenston, M. E. (2005). Biomechanical analysis of silicon microelectrode-induced strain in the brain. *J Neural Eng*, 2(4):81–89.

Lee, K. K., He, J. P., Singh, A., Massia, S., Ehteshami, G., Kim, B., and Raupp, G. (2004). Polyimide-based intracortical neural implant with improved structural stiffness. *Journal of Micromechanics and Microengineering*, 14(1):32–37.

Lehmkuhle, M. J., Mayes, S. M., and Kipke, D. R. (2010). Unilateral neuromodulation of the ventromedial hypothalamus of the rat through deep brain stimulation. *J Neural Eng*, 7(3):036006.

Leuthardt, E. C., Freudenberg, Z., Bundy, D., and Roland, J. (2009). Microscale recording from human motor cortex: implications for minimally invasive electrocorticographic brain-computer interfaces. *Neurosurg Focus*, 27(1):E10.

Leuthardt, E. C., Schalk, G., Wolpaw, J. R., Ojemann, J. G., and Moran, D. W. (2004). A brain-computer interface using electrocorticographic signals in humans. *J Neural Eng*, 1(2):63–71.

Liao, W., Randall, B. A., Alba, N. A., and Cui, X. T. (2008). Conducting polymer-based impedimetric aptamer biosensor for in situ detection. *Anal Bioanal Chem*, 392(5):861–864.

Lindholm, D. (1994). Role of neurotrophins in preventing glutamate induced neuronal cell death. *J Neurol*, 242(1 Suppl 1):S16–S18.

Liu, X., McCreery, D. B., Bullara, L. A., and Agnew, W. F. (2006). Evaluation of the stability of intracortical microelectrode arrays. *IEEE Trans Neural Syst Rehabil Eng*, 14(1):91–100.

Liu, X., McCreery, D. B., Carter, R. R., Bullara, L. A., Yuen, T. G., and Agnew, W. F. (1999). Stability of the interface between neural tissue and chronically implanted intracortical microelectrodes. *IEEE Trans Rehabil Eng*, 7(3):315–326.

Lohof, A. M., Quillan, M., Dan, Y., and Poo, M. M. (1992). Asymmetric modulation of cytosolic camp activity induces growth cone turning. *J Neurosci*, 12(4):1253–1261.

Love, J. C., Estroff, L. A., Kriebel, J. K., Nuzzo, R. G., and Whitesides, G. M. (2005). Self-assembled monolayers of thiolates on metals as a form of nanotechnology. *Chem Rev*, 105(4):1103–1169.

Ludwig, K. A., Langhals, N. B., Joseph, M. D., Richardson-Burns, S. M., Hendricks, J. L., and Kipke, D. R. (2011). Poly(3,4-ethylenedioxythiophene) (pedot) polymer coatings facilitate smaller neural recording electrodes. *J Neural Eng*, 8(1):014001.

Ludwig, K. A., Uram, J. D., Yang, J., Martin, D. C., and Kipke, D. R. (2006). Chronic neural recordings using silicon microelectrode arrays electrochemically deposited with a poly(3,4-ethylenedioxythiophene) (pedot) film. *J Neural Eng*, 3(1):59–70.

Luo, X. and Cui, X. T. (2009). Sponge-like nanostructured conducting polymers for electrically controlled drug release. *Electrochem commun*, 11(10):1956.

Ma, H., Hyun, J., Stiller, P., and Chilkoti, A. (2004). non-fouling oligo(ethylene glycol)- functionalized polymer brushes synthesized by surface-initiated atom transfer radical polymerization. *Advanced Materials*, 16(4):338–341.

Macias, M. Y., Battocletti, J. H., Sutton, C. H., Pintar, F. A., and Maiman, D. J. (2000). Directed and enhanced neurite growth with pulsed magnetic field stimulation. *Bioelectromagnetics*, 21(4):272–286.

Majji, A. B., Humayun, M. S., Weiland, J. D., Suzuki, S., D'Anna, S. A., and de Juan, E. (1999). Long-term histological and electrophysiological results of an inactive epiretinal electrode array implantation in dogs. *Invest Ophthalmol Vis Sci*, 40(9):2073–2081.

Marchase, R. B., Barbera, A. J., and Roth, S. (1975). A molecular approach to retinotectal specificity. *Ciba Found Symp*, 0(29):315–341.

Marmarou, A. (1994). Traumatic brain edema: an overview. *Acta Neurochir Suppl (Wien)*, 60:421–424.

Massia, S. P., Holecko, M. M., and Ehteshami, G. R. (2004). In vitro assessment of bioactive coatings for neural implant applications. *J Biomed Mater Res A*, 68(1):177–186.

Mayberg, H. S. (2009). Targeted electrode-based modulation of neural circuits for depression. *J Clin Invest*, 119(4):717–725.

Mayberg, H. S., Lozano, A. M., Voon, V., McNeely, H. E., Seminowicz, D., Hamani, C., Schwalb, J. M., and Kennedy, S. H. (2005). Deep brain stimulation for treatment-resistant depression. *Neuron*, 45(5):651–660.

Mayer, M., Terrettaz, S., Giovangrandi, L., Stora, T., and Vogel, H. (2004). *Biosensors*, volume 268 of *Practical Approach Series*, chapter Chapter 8: Functional analysis of ion channels: Planar patch clamp and impedance spectroscopy of tethered limid membranes. Oxford University Press, Oxford, UK, 2nd ed. edition.

McCaig, C. D., Rajnicek, A. M., Song, B., and Zhao, M. (2002). Has electrical growth cone guidance found its potential? *Trends Neurosci*, 25(7):354–359.

McConnell, G. C., Rees, H. D., Levey, A. I., Gutekunst, C.-A., Gross, R. E., and Bellamkonda, R. V. (2009). Implanted neural electrodes cause chronic, local inflammation that is correlated with local neurodegeneration. *J Neural Eng*, 6(5):056003.

McCreery, D., Lossinsky, A., Pikov, V., and Liu, X. (2006). Microelectrode array for chronic deep-brain microstimulation and recording. *IEEE Trans Biomed Eng*, 53(4):726–737.

McCreery, D. B., Agnew, W. F., Yuen, T. G., and Bullara, L. (1990). Charge density and charge per phase as cofactors in neural injury induced by electrical stimulation. *IEEE Trans Biomed Eng*, 37(10):996–1001.

McCreery, D. B., Agnew, W. F., Yuen, T. G., and Bullara, L. A. (1988). Comparison of neural damage induced by electrical stimulation with faradaic and capacitor electrodes. *Ann Biomed Eng*, 16(5):463–481.

Mcfarlane, J. S. and Tabor, D. (1950). Adhesion of solids and the effect of surface films. *Proceedings of the Royal Society of London Series a-Mathematical and Physical Sciences*, 202(1069):224–243.

McMahon, C. P., Rocchitta, G., Serra, P. A., Kirwan, S. M., Lowry, J. P., and O'Neill, R. D. (2006). The efficiency of immobilised glutamate oxidase decreases with surface enzyme loading: an electrostatic effect, and reversal by a polycation significantly enhances biosensor sensitivity. *Analyst*, 131(1):68–72.

McNaughton, B. L., O'Keefe, J., and Barnes, C. A. (1983). The stereotrode: a new technique for simultaneous isolation of several single units in the central nervous system from multiple unit records. *J Neurosci Methods*, 8(4):391–397.

Merletti, R., Acimovic, R., Grobelnik, S., and Cvilak, G. (1975). Electrophysiological orthosis for the upper extremity in hemiplegia: feasibility study. *Arch Phys Med Rehabil*, 56(12):507–513.

Merrill, D. R., Bikson, M., and Jefferys, J. G. R. (2005). Electrical stimulation of excitable tissue: design of efficacious and safe protocols. *J Neurosci Methods*, 141(2):171–198.

Merrill, D. R. and Tresco, P. A. (2005). Impedance characterization of microarray recording electrodes in vitro. 52(11):1960–1965.

Metz, S., Bertsch, A., Bertrand, D., and Renaud, P. (2004). Flexible polyimide probes with microelectrodes and embedded microfluidic channels for simultaneous drug delivery and multichannel monitoring of bioelectric activity. *Biosens Bioelectron*, 19(10):1309–1318.

Miller, G. (2006). Optogenetics. shining new light on neural circuits. *Science*, 314(5806):1674–1676.

Ming, G., Henley, J., Tessier-Lavigne, M., Song, H., and Poo, M. (2001). Electrical activity modulates growth cone guidance by diffusible factors. *Neuron*, 29(2):441–452.

Moon, A. and Drubin, D. G. (1995). The adf/cofilin proteins: stimulus-responsive modulators of actin dynamics. *Mol Biol Cell*, 6(11):1423–1431.

Morrison, B., Meaney, D. F., and McIntosh, T. K. (1998). Mechanical characterization of an in vitro device designed to quantitatively injure living brain tissue. *Ann Biomed Eng*, 26(3):381–390.

Morrison, M. E. and Mason, C. A. (1998). Granule neuron regulation of purkinje cell development: striking a balance between neurotrophin and glutamate signaling. *J Neurosci*, 18(10):3563–3573.

Motta, P. S. and Judy, J. W. (2005). Multielectrode microprobes for deep-brain stimulation fabricated with a customizable 3-d electroplating process. *IEEE Trans Biomed Eng*, 52(5):923–933.

Moxon, K. A., Leiser, S. C., Gerhardt, G. A., Barbee, K. A., and Chapin, J. K. (2004). Ceramic-based multisite electrode arrays for chronic single-neuron recording. 51(4):647–656.

Mrksich, M., Dike, L. E., Tien, J., Ingber, D. E., and Whitesides, G. M. (1997). Using microcontact printing to pattern the attachment of mammalian cells to self-assembled monolayers of alkanethiolates on transparent films of gold and silver. *Exp Cell Res*, 235(2):305–313.

Mrksich, M. and Whitesides, G. M. (1997). *Poly(ethylene glycol)*, volume 680 of *ACS Symposium Series*, chapter Ch 23: Using Self-Assembled Monolayers that Present Oligo(ethylene glycol) Groups to Control the Interactions of Proteins with Surfaces, pages 361–373. American Chemical Society, Washington DC.

Muir, G. D. and Steeves, J. D. (1997). Sensorimotor stimulation to improve locomotor recovery after spinal cord injury. *Trends Neurosci*, 20(2):72–77.

Musallam, S., Bak, M. J., Troyk, P. R., and Andersen, R. A. (2007). A floating metal microelectrode array for chronic implantation. *J Neurosci Methods*, 160(1):122–127.

Nadal, A., Fuentes, E., Pastor, J., and McNaughton, P. A. (1995). Plasma albumin is a potent trigger of calcium signals and dna synthesis in astrocytes. *Proc Natl Acad Sci U S A*, 92(5):1426–1430.

Nadal, A., Sul, J. Y., Valdeolmillos, M., and McNaughton, P. A. (1998). Albumin elicits calcium signals from astrocytes in brain slices from neonatal rat cortex. *J Physiol*, 509 (Pt 3):711–716.

Nandivada, H., Jiang, X., and Lahann, J. (2007). Click chemistry: Versatility and control in the hands of materials scientists. *Advanced Materials*, 19(17):2197–2208.

Neary, J. T., Kang, Y., Willoughby, K. A., and Ellis, E. F. (2003). Activation of extracellular signal-regulated kinase by stretch-induced injury in astrocytes involves extracellular atp and p2 purinergic receptors. *J Neurosci*, 23(6):2348–2356.

Neves, H. P. and Ruther, P. (2007). The neuroprobes project. *Conf Proc IEEE Eng Med Biol Soc*, 2007:6443–6445.

Nicolelis, M. A. L., Dimitrov, D., Carmena, J. M., Crist, R., Lehew, G., Kralik, J. D., and Wise, S. P. (2003). Chronic, multisite, multielectrode recordings in macaque monkeys. *Proc Natl Acad Sci U S A*, 100(19):11041–11046.

Niparko, J. K., Altschuler, R. A., Xue, X. L., Wiler, J. A., and Anderson, D. J. (1989). Surgical implantation and biocompatibility of central nervous system auditory prostheses. *Ann Otol Rhinol Laryngol*, 98(12 Pt 1):965–970.

Nordhausen, C. T., Maynard, E. M., and Normann, R. A. (1996). Single unit recording capabilities of a 100 microelectrode array. *Brain Res*, 726(1-2):129–140.

O'Brien, D. P., Nichols, T. R., and Allen, M. G. (2001). Flexible microelectrode arrays with integrated insertion devices. In *Proc. 14th IEEE Int. Conf. Micro Electro Mechanical Systems MEMS 2001*, pages 216–219.

O'brien, F. and Azrin, N. H. (1970). Behavioral engineering: control of posture by informational feedback. *J Appl Behav Anal*, 3(4):235–240.

Parrot, S., Bert, L., Mouly-Badina, L., Sauvinet, V., Colussi-Mas, J., Lambs-Seas, L., Robert, F., Bouilloux, J.-P., Suaud-Chagny, M.-F., Denoroy, L., and Renaud, B. (2003). Microdialysis monitoring of catecholamines and excitatory amino acids in the rat and mouse brain: recent developments based on capillary electrophoresis with laser-induced fluorescence detection–a mini-review. *Cell Mol Neurobiol*, 23(4-5):793–804.

Patterson, P. E. and Katz, J. A. (1992). Design and evaluation of a sensory feedback system that provides grasping pressure in a myoelectric hand. *J Rehabil Res Dev*, 29(1):1–8.

Peckham, P. H. (1992). Opportunities and challenges for the clinical utilization of functional electrical stimulation. *Assist Technol*, 4(1):46–48.

Pei, X., Leuthardt, E. C., Gaona, C. M., Brunner, P., Wolpaw, J. R., and Schalk, G. (2011). Spatiotemporal dynamics of electrocorticographic high gamma activity during overt and covert word repetition. *Neuroimage*, 54(4):2960–2972.

Pellinen, D., Moon, T., Vetter, R., Miriani, R., and Kipke, D. (2005). Multifunctional flexible parylene-based intracortical microelectrodes. *Conf Proc IEEE Eng Med Biol Soc*, 5:5272–5275.

Pertsin, A. J., Hayashi, T., and Grunze, M. (2002). Grand canonical monte carlo simulations of the hydration interaction between oligo(ethylene glycol)-terminated alkanethiol self-assembled monolayers. *J. Phys. Chem. B*, 106(47):12274–81.

Pierce, A. L., Sommakia, S., Rickus, J. L., and Otto, K. J. (2009). Thin-film silica sol-gel coatings for neural microelectrodes. *J Neurosci Methods*, 180(1):106–110.

Polikov, V. S., Tresco, P. A., and Reichert, W. M. (2005). Response of brain tissue to chronically implanted neural electrodes. *J Neurosci Methods*, 148(1):1–18.

Pomerleau, F., Day, B. K., Huettl, P., Burmeister, J. J., and Gerhardt, G. A. (2003). Real time in vivo measures of l-glutamate in the rat central nervous system using ceramic-based multisite microelectrode arrays. *Ann N Y Acad Sci*, 1003:454–457.

Poser, C. M., Paty, D. W., Scheinberg, L., McDonald, W. I., Davis, F. A., Ebers, G. C., Johnson, K. P., Sibley, W. A., Silberberg, D. H., and Tourtellotte, W. W. (1983). New diagnostic criteria for multiple sclerosis: guidelines for research protocols. *Ann Neurol*, 13(3):227–231.

Protas, E. J., Holmes, S. A., Qureshy, H., Johnson, A., Lee, D., and Sherwood, A. M. (2001). Supported treadmill ambulation training after spinal cord injury: a pilot study. *Arch Phys Med Rehabil*, 82(6):825–831.

Purcell, E. K., Seymour, J. P., Yandamuri, S., and Kipke, D. R. (2009a). In vivo evaluation of a neural stem cell-seeded prosthesis. *J Neural Eng*, 6(2):026005.

Purcell, E. K., Singh, A., and Kipke, D. R. (2009b). Alginate composition effects on a neural stem cell-seeded scaffold. *Tissue Eng Part C Methods*, 15(4):541–550.

Purcell, E. K., Thompson, D. E., Ludwig, K. A., and Kipke, D. R. (2009c). Flavopiridol reduces the impedance of neural prostheses in vivo without affecting recording quality. *J Neurosci Methods*, 183(2):149–157.

Qin, S., van der Zeyden, M., Oldenziel, W. H., Cremers, T. I. F. H., and Westerink, B. H. C. (2008). Microsensors for in vivo measurement of glutamate in brain tissue. *Sensors*, 8(11):6860–6884.

Rand, D. and Woods, R. (1971). The nature of adsorbed oxygen on rhodium, palladium and gold electrodes. *Journal of Electroanalytical Chemistry and Interfacial Electrochemistry*, 31(1):29–38.

Rathnasingham, R., Kipke, D. R., Bledsoe, S. C., J., and McLaren, J. D. (2004). Characterization of implantable microfabricated fluid delivery devices. 51(1):138–145.

Ratner, B. D. and Bryant, S. J. (2004). Biomaterials: where we have been and where we are going. *Annu Rev Biomed Eng*, 6:41–75.

Reading, M. A., editor (1975). *Interfacial electrochemistry: an experimental approach.* Addison-Wesley.

Rennaker, R. L., Ruyle, A. M., Street, S. E., and Sloan, A. M. (2005). An economical multi-channel cortical electrode array for extended periods of recording during behavior. *J Neurosci Methods*, 142(1):97–105.

Reswick, J. B. (1976). Functional electrical stimulation–neural prosthesis for the disabled. *Bull Prosthet Res*, (10-25):1–4.

Retterer, S. T., Smith, K. L., Bjornsson, C. S., Turner, J. N., Isaacson, M. S., and Shain, W. (2008). Constant pressure fluid infusion into rat neocortex from implantable microfluidic devices. *J Neural Eng*, 5(4):385–391.

Robinson, D. A. (1968). The electrical properties of metal microelectrodes. 56(6):1065–1071.

Robinson, D. L., Hermans, A., Seipel, A. T., and Wightman, R. M. (2008). Monitoring rapid chemical communication in the brain. *Chem Rev*, 108(7):2554–2584.

Robinson, K. R. and McCaig, C. (1980). Electrical fields, calcium gradients, and cell growth. *Ann N Y Acad Sci*, 339:132–138.

Roderick, H. L. and Bootman, M. D. (2006). New ca2+ indicator has freedom to express. *Chem Biol*, 13(5):463–464.

Rodger, D. C., Fong, A. J., Li, W., Ameri, H., Ahuja, A. K., Gutierrez, C., Lavrov, I., Zhong, H., Menon, P. R., Meng, E., Burdick, J. W., Roy, R. R., Edgerton, V. R., Weiland, J. D., Humayun, M. S., and Taia, Y.-C. (2008). Flexible parylene-based multielectrode array technology for high-density neural stimulation and recording. *Sensors and Actuators B: Chemical*, 132(2):449–460.

Rohatgi, P., Langhals, N. B., Kipke, D. R., and Patil, P. G. (2009). In vivo performance of a microelectrode neural probe with integrated drug delivery. *Neurosurg Focus*, 27(1):E8.

Roitbak, T. and Sykov, E. (1999). Diffusion barriers evoked in the rat cortex by reactive astrogliosis. *Glia*, 28(1):40–48.

Rose, T. L., Kelliher, E. M., and Robblee, L. S. (1985). Assessment of capacitor electrodes for intracortical neural stimulation. *J Neurosci Methods*, 12(3):181–193.

Rousche, P. J. and Normann, R. A. (1998). Chronic recording capability of the utah intracortical electrode array in cat sensory cortex. *J Neurosci Methods*, 82(1):1–15.

Rousche, P. J., Pellinen, D. S., Pivin, D. P., Williams, J. C., Vetter, R. J., and Kipke, D. R. (2001). Flexible polyimide-based intracortical electrode arrays with bioactive capability. *IEEE Trans Biomed Eng*, 48(3):361–371.

Ryan, M. R., Lowry, J. P., and O'Neill, R. D. (1997). Biosensor for neurotransmitter l-glutamic acid designed for efficient use of l-glutamate oxidase and effective rejection of interference. *Analyst*, 122(11):1419–1424.

Ryhnen, J., Kallioinen, M., Tuukkanen, J., Junila, J., Niemel, E., Sandvik, P., and Serlo, W. (1998). In vivo biocompatibility evaluation of nickel-titanium shape memory metal alloy: muscle and perineural tissue responses and encapsule membrane thickness. *J Biomed Mater Res*, 41(3):481–488.

Sani, S., Jobe, K., Smith, A., Kordower, J. H., and Bakay, R. A. E. (2007). Deep brain stimulation for treatment of obesity in rats. *J Neurosurg*, 107(4):809–813.

Santini, J. T., Cima, M. J., and Langer, R. (1999). A controlled-release microchip. *Nature*, 397(6717):335–338.

Satish, L., Gandhi, D., and Rousche, P. J. (2004). Preliminary study of neurite outgrowth within polyimide microtubes. *Conf Proc IEEE Eng Med Biol Soc*, 6:4306–4309.

Saul, J. M., Annapragada, A., Natarajan, J. V., and Bellamkonda, R. V. (2003). Controlled targeting of liposomal doxorubicin via the folate receptor in vitro. *J Control Release*, 92(1-2):49–67.

Sawyer, P. and Srinivasan, S. (1974). *Medical engineering*, pages 1099–110. Chicago: Year Bood Medical Publishers.

Schalk, G., McFarland, D. J., Hinterberger, T., Birbaumer, N., and Wolpaw, J. R. (2004). Bci2000: a general-purpose brain-computer interface (bci) system. *IEEE Trans Biomed Eng*, 51(6):1034–1043.

Schmidt, S., Horch, K., and Normann, R. (1993). Biocompatibility of silicon-based electrode arrays implanted in feline cortical tissue. *J Biomed Mater Res*, 27(11):1393–1399.

Schoen, I. and Fromherz, P. (2008). Extracellular stimulation of mammalian neurons through repetitive activation of na+ channels by weak capacitive currents on a silicon chip. *J Neurophysiol*, 100(1):346–357.

Schubert, D., LaCorbiere, M., Whitlock, C., and Stallcup, W. (1978). Alterations in the surface properties of cells responsive to nerve growth factor. *Nature*, 273(5665):718–723.

Schultz, A. E., Marasco, P. D., and Kuiken, T. A. (2009). Vibrotactile detection thresholds for chest skin of amputees following targeted reinnervation surgery. *Brain Res*, 1251:121–129.

Schuvailo, O. N., Dzyadevych, S. V., El'skaya, A. V., Gautier-Sauvign, S., Csregi, E., Cespuglio, R., and Soldatkin, A. P. (2005). Carbon fibre-based microbiosensors for in vivo measurements of acetylcholine and choline. *Biosens Bioelectron*, 21(1):87–94.

Schuvalio, O. M., Soldatkin, O. O., Lefebre, A., Cespuglio, R., and Soldatkin, A. P. (2006). Highly selective microbiosensor for in vivo measurement of glucose, lactate, and glutamate. *Analytica Chimica Acta*, 573-574:110–116.

Schwartz, A. B. (2004). Cortical neural prosthetics. *Annu Rev Neurosci*, 27:487–507.

Schwartz, A. B., Cui, X. T., Weber, D. J., and Moran, D. W. (2006). Brain-controlled interfaces: movement restoration with neural prosthetics. *Neuron*, 52(1):205–220.

Schwartz, A. B. and Moran, D. W. (1999). Motor cortical activity during drawing movements: population representation during lemniscate tracing. *J Neurophysiol*, 82(5):2705–2718.

Schwartz, A. B. and Moran, D. W. (2000). Arm trajectory and representation of movement processing in motor cortical activity. *Eur J Neurosci*, 12(6):1851–1856.

Schwendel, D., Hayashi, T., Dahint, R., Pertsin, A., Grunze, M., and andF. Schreiber, R. S. (2003). Interaction of water with self-assembled monolayers: Neutron reflectivity measurements of the water density in the interface region. *Langmuir*, 19(6):2284–2293.

Seymour, J. P. and Kipke, D. R. (2006). Fabrication of polymer neural probes with sub-cellular features for reduced tissue encapsulation. *Conf Proc IEEE Eng Med Biol Soc*, 1:4606–4609.

Seymour, J. P. and Kipke, D. R. (2007). Neural probe design for reduced tissue encapsulation in cns. *Biomaterials*, 28(25):3594–3607.

Shackman, H. M., Shou, M., Cellar, N. A., Watson, C. J., and Kennedy, R. T. (2007). Microdialysis coupled on-line to capillary liquid chromatography with tandem mass spectrometry for monitoring acetylcholine in vivo. *J Neurosci Methods*, 159(1):86–92.

Shain, W., Spataro, L., Dilgen, J., Haverstick, K., Retterer, S., Isaacson, M., Saltzman, M., and Turner, J. N. (2003). Controlling cellular reactive responses around neural prosthetic devices using peripheral and local intervention strategies. *IEEE Trans Neural Syst Rehabil Eng*, 11(2):186–188.

Shanbhag, A. S., Jacobs, J. J., Black, J., Galante, J. O., and Glant, T. T. (1994). Macrophage/particle interactions: effect of size, composition and surface area. *J Biomed Mater Res*, 28(1):81–90.

Shannon, R. V. (1992). A model of safe levels for electrical stimulation. *IEEE Trans Biomed Eng*, 39(4):424–426.

Shi, R. and Borgens, R. B. (1995). Three-dimensional gradients of voltage during development of the nervous system as invisible coordinates for the establishment of embryonic pattern. *Dev Dyn*, 202(2):101–114.

Sienko, K. H., Vichare, V. V., Balkwill, M. D., and Wall, C. (2010). Assessment of vibrotactile feedback on postural stability during pseudorandom multidirectional platform motion. *IEEE Trans Biomed Eng*, 57(4):944–952.

Simon, D. T., Kurup, S., Larsson, K. C., Hori, R., Tybrandt, K., Goiny, M., Jager, E. W. H., Berggren, M., Canlon, B., and Richter-Dahlfors, A. (2009). Organic electronics for precise delivery of neurotransmitters to modulate mammalian sensory function. *Nat Mater*, 8(9):742–746.

Sommakia, S., Rickus, J. L., and Otto, K. J. (2009). Effects of adsorbed proteins, an antifouling agent and long-duration dc voltage pulses on the impedance of silicon-based neural microelectrodes. *Conf Proc IEEE Eng Med Biol Soc*, 2009:7139–7142.

Spataro, L., Dilgen, J., Retterer, S., Spence, A. J., Isaacson, M., Turner, J. N., and Shain, W. (2005). Dexamethasone treatment reduces astroglia responses to inserted neuroprosthetic devices in rat neocortex. *Exp Neurol*, 194(2):289–300.

Stauffer, W. R. and Cui, X. T. (2006). Polypyrrole doped with 2 peptide sequences from laminin. *Biomaterials*, 27(11):2405–2413.

Stensaas, S. S. and Stensaas, L. J. (1976). The reaction of the cerebral cortex to chronically implanted plastic needles. *Acta Neuropathol*, 35(3):187–203.

Stieglitz, T., Schuettler, M., and Koch, K. P. (2005). Implantable biomedical microsystems for neural prostheses. *IEEE Eng Med Biol Mag*, 24(5):58–65.

Strumwasser, F. (1958). Long-term recording' from single neurons in brain of unrestrained mammals. *Science*, 127(3296):469–470.

Subbaroyan, J. (2007). *Quantification of Micromotion Induced Injury Response in Intracortical implants through modeling and in vivo experiments*. PhD thesis, University of Michigan, Ann Arbor, Mi.

Subbaroyan, J., Martin, D. C., and Kipke, D. R. (2005). A finite-element model of the mechanical effects of implantable microelectrodes in the cerebral cortex. *J Neural Eng*, 2(4):103–113.

Suner, S., Fellows, M. R., Vargas-Irwin, C., Nakata, G. K., and Donoghue, J. P. (2005). Reliability of signals from a chronically implanted, silicon-based electrode array in non-human primate primary motor cortex. 13(4):524–541.

Suzuki, T., Mabuchi, K., and Takeuchi, S. (2003). A 3d flexible parylene probe array for multichannel neural recording. In *Proc. First Int Neural Engineering IEEE EMBS Conf*, pages 154–156.

Suzuki, T., Ziegler, D., Mabuchi, K., and Takeuchi, S. (2004). Flexible neural probes with microfluidic channels for stable interface with the nervous system. In *Proc. 26th Annual Int. Conf. of the IEEE Engineering in Medicine and Biology Society IEMBS '04*, volume 2, pages 4057–4058.

Szarowski, D. H., Andersen, M. D., Retterer, S., Spence, A. J., Isaacson, M., Craighead, H. G., Turner, J. N., and Shain, W. (2003). Brain responses to micro-machined silicon devices. *Brain Res*, 983(1-2):23–35.

Takeuchi, S., Yoshida, Y., Ziegler, D., Mabuchi, K., and Suzuki, T. (2004). Parylene flexible neural probe with micro fluidic channel. In *Proc. 17th IEEE Int Micro Electro Mechanical Systems Conf. . (MEMS)*, pages 208–211.

Takeuchi, S., Ziegler, D., Yoshida, Y., Mabuchi, K., and Suzuki, T. (2005). Parylene flexible neural probes integrated with microfluidic channels. *Lab Chip*, 5(5):519–523.

Taylor, D. M., Tillery, S. I. H., and Schwartz, A. B. (2002). Direct cortical control of 3d neuroprosthetic devices. *Science*, 296(5574):1829–1832.

Thomas, M. V. (1977). Microelectrode amplifier with improved method of input-capacitance neutralisation. *Med Biol Eng Comput*, 15(4):450–454.

Toda, H., Suzuki, T., Sawahata, H., Majima, K., Kamitani, Y., and Hasegawa, I. (2011). Simultaneous recording of ecog and intracortical neuronal activity using a flexible multichannel electrode-mesh in visual cortex. *Neuroimage*, 54(1):203–12.

Townsend, G., Peloquin, P., Kloosterman, F., Hetke, J. F., and Leung, L. S. (2002). Recording and marking with silicon multichannel electrodes. *Brain Res Brain Res Protoc*, 9(2):122–129.

Turner, J. N., Shain, W., Szarowski, D. H., Andersen, M., Martins, S., Isaacson, M., and Craighead, H. (1999). Cerebral astrocyte response to micromachined silicon implants. *Exp Neurol*, 156(1):33–49.

Ueda, T., Oshida, H., Kurita, K., Ishihara, K., and Nakabayashi, N. (1992). Preparation of 2-methacryloyloxyethyl phosphorylcholine copolymers with alkyl methacrylates and their blood compatibility. *Polymer Journal*, 24(11):1259–69.

Ulijn, R. V. (2006). Enzyme-responsive materials: a new class of smart biomaterials. *Journal of Materials Chemistry*, 16(23):2217–2225.

Velliste, M., Perel, S., Spalding, M. C., Whitford, A. S., and Schwartz, A. B. (2008). Cortical control of a prosthetic arm for self-feeding. *Nature*, 453(7198):1098–1101.

Venugopalan, S. (1994). Kinetics of hydrogen-evolution reaction on lead and lead-alloy electrodes in sulfuric-acid electrolyte with phosphoric-acid and antimony additives. *Journal of Power Sources*, 48(3):371–384.

Verdaguer, E., Jimnez, A., Canudas, A. M., Jord, E. G., Sureda, F. X., Palls, M., and Camins, A. (2004). Inhibition of cell cycle pathway by flavopiridol promotes survival of cerebellar granule cells after an excitotoxic treatment. *J Pharmacol Exp Ther*, 308(2):609–616.

Wadhwa, R., Lagenaur, C. F., and Cui, X. T. (2006). Electrochemically controlled release of dexamethasone from conducting polymer polypyrrole coated electrode. *J Control Release*, 110(3):531–541.

Wang, R., Kreuzer, H. J., and Grunze, M. (1997). Molecular conformation and solvation of oligo(ethylene glycol)-terminated self-assembled monolayers and their resistance to protein adsorption. *J. Phys. Chem. B*, 101(47):9767–9773.

Ward, M. P., Rajdev, P., Ellison, C., and Irazoqui, P. P. (2009). Toward a comparison of microelectrodes for acute and chronic recordings. *Brain Res*, 1282:183–200.

Weber, N., Bolikal, D., Bourke, S. L., and Kohn, J. (2004). Small changes in the polymer structure influence the adsorption behavior of fibrinogen on polymer surfaces: validation of a new rapid screening technique. *J Biomed Mater Res A*, 68(3):496–503.

Weinberg, M. S., Wall, C., Robertsson, J., O'Neil, E., Sienko, K., and Fields, R. (2006). Tilt determination in mems inertial vestibular prosthesis. *J Biomech Eng*, 128(6):943–956.

Wessberg, J., Stambaugh, C. R., Kralik, J. D., Beck, P. D., Laubach, M., Chapin, J. K., Kim, J., Biggs, S. J., Srinivasan, M. A., and Nicolelis, M. A. (2000). Real-time prediction of hand trajectory by ensembles of cortical neurons in primates. *Nature*, 408(6810):361–365.

Wilks, S. J., Richardson-Burns, S. M., Hendricks, J. L., Martin, D. C., and Otto, K. J. (2009). Poly(3,4-ethylenedioxythiophene) as a micro-neural interface material for electrostimulation. *Front Neuroengineering*, 2:7.

Williams, J. C., Hippensteel, J. A., Dilgen, J., Shain, W., and Kipke, D. R. (2007). Complex impedance spectroscopy for monitoring tissue responses to inserted neural implants. *J Neural Eng*, 4(4):410–423.

Williams, J. C., Holecko, M. M., Massia, S. P., Rousche, P., and Kipke, D. R. (2005). Multi-site incorporation of bioactive matrices into mems-based neural probes. *J Neural Eng*, 2(4):L23–L28.

Williams, J. C., Rennaker, R. L., and Kipke, D. R. (1999). Long-term neural recording characteristics of wire microelectrode arrays implanted in cerebral cortex. *Brain Res Brain Res Protoc*, 4(3):303–313.

Wilson, G. S. and Gifford, R. (2005). Biosensors for real-time in vivo measurements. *Biosens Bioelectron*, 20(12):2388–2403.

Wilson, H. A., Winfield, J. B., Lahita, R. G., and Koffler, D. (1979). Association of igg anti-brain antibodies with central nervous system dysfunction in systemic lupus erythematosus. *Arthritis Rheum*, 22(5):458–462.

Winslow, B. D., Christensen, M. B., Yang, W.-K., Solzbacher, F., and Tresco, P. A. (2010). A comparison of the tissue response to chronically implanted parylene-c-coated and uncoated planar silicon microelectrode arrays in rat cortex. *Biomaterials*, 31(35):9163–9172.

Wise, K. D., Anderson, D. J., Hetke, J. F., Kipke, D. R., and Najafi, K. (2004). Wireless implantable microsystems: High-density electronic interfaces to the nervous system. In *Proceedings of the Ieee*, volume 92, pages 76–97.

Wood, M. D. and Willits, R. K. (2009). Applied electric field enhances drg neurite growth: influence of stimulation media, surface coating and growth supplements. *J Neural Eng*, 6(4):046003.

Wu, Y., Zheng, Q., Du, J., Song, Y., Wu, B., and Guo, X. (2006). Self-assembled ikvav peptide nanofibers promote adherence of pc12 cells. *J Huazhong Univ Sci Technolog Med Sci*, 26(5):594–596.

Xin, Q. and Wightman, R. M. (1997). Enzyme modified amperometric sensors for choline and acetylcholine with tetrathiafulvalene tetracyanoquinodimethane as the electron-transfer mediator. *Analytica Chimica Acta*, 341(1):43–51.

Yanagisawa, T., Hirata, M., Saitoh, Y., Kato, A., Shibuya, D., Kamitani, Y., and Yoshimine, T. (2009). Neural decoding using gyral and intrasulcal electrocorticograms. *Neuroimage*, 45(4):1099–1106.

Yin, J., Sakamoto, K., Zhang, H., Ito, Z., Imagama, S., Kishida, S., Natori, T., Sawada, M., Matsuyama, Y., and Kadomatsu, K. (2009). Transforming growth factor-?1 upregulates keratan sulfate and chondroitin sulfate biosynthesis in microglias after brain injury. *Bran Research*, 1263:10–22.

Yoshida, S. Kanno, H. W. T. (1995). Glutamate sensors carrying glutamate oxidase/peroxidase bienzyme system on tin oxide electrode. *Analytical Sciences*, 11(2):251–256.

Young, L. R., Hecht, H., Lyne, L. E., Sienko, K. H., Cheung, C. C., and Kavelaars, J. (2001). Artificial gravity: head movements during short-radius centrifugation. *Acta Astronaut*, 49(3-10):215–226.

Young, L. R., Sienko, K. H., Lyne, L. E., Hecht, H., and Natapoff, A. (2003). Adaptation of the vestibulo-ocular reflex, subjective tilt, and motion sickness to head movements during short-radius centrifugation. *J Vestib Res*, 13(2-3):65–77.

Yu, Z., McKnight, T. E., Ericson, M. N., Melechko, A. V., Simpson, M. L., and Morrison, B. (2007). Vertically aligned carbon nanofiber arrays record electrophysiological signals from hippocampal slices. *Nano Lett*, 7(8):2188–2195.

Yuen, T. G., Agnew, W. F., Bullara, L. A., Jacques, S., and McCreery, D. B. (1981). Histological evaluation of neural damage from electrical stimulation: considerations for the selection of parameters for clinical application. *Neurosurgery*, 9(3):292–299.

Zhang, F., Gradinaru, V., Adamantidis, A. R., Durand, R., Airan, R. D., de Lecea, L., and Deisseroth, K. (2010). Optogenetic interrogation of neural circuits: technology for probing mammalian brain structures. *Nat Protoc*, 5(3):439–456.

Zhang, Z., Zhang, M., Chen, S., Horbett, T. A., Ratner, B. D., and Jiang, S. (2008). Blood compatibility of surfaces with superlow protein adsorption. *Biomaterials*, 29(32):4285–4291.

Zhong, Y. and Bellamkonda, R. V. (2005). Controlled release of anti-inflammatory agent alpha-msh from neural implants. *J Control Release*, 106(3):309–318.

Zhong, Y. and Bellamkonda, R. V. (2007). Dexamethasone-coated neural probes elicit attenuated inflammatory response and neuronal loss compared to uncoated neural probes. *Brain Res*, 1148:15–27.

Zhong, Y., Yu, X., Gilbert, R., and Bellamkonda, R. V. (2001). Stabilizing electrode-host interfaces: a tissue engineering approach. *J Rehabil Res Dev*, 38(6):627–632.

Zhou, J., Tam, T. K., Pita, M., Ornatska, M., Minko, S., and Katz, E. (2009). Bioelectrocatalytic system coupled with enzyme-based biocomputing ensembles performing boolean logic operations: approaching "smart" physiologically controlled biointerfaces. *ACS Appl Mater Interfaces*, 1(1):144–149.

Zorzos, A. N., Boyden, E. S., and Fonstad, C. G. (2010). Multiwaveguide implantable probe for light delivery to sets of distributed brain targets. *Opt Lett*, 35(24):4133–4135.

Zuleta, M. (2005). *Electrochemical and Ion Transport Characterization of a Nanoporous Carbon Derived from SiC*. PhD thesis, KTH-Royal Institute of Technology.

CHAPTER II

Insertion shuttle with carboxyl terminated self-assembled monolayer coatings for implanting flexible polymer neural probes in the brain

Abstract

Penetrating microscale microelectrodes made from flexible polymers tend to bend or deflect and may fail to reach their target location. The development of flexible neural probes requires methods for reliable and controlled insertion into the brain. Previous approaches for implanting flexible probes into the cortex required modifications that negate the flexibility, limit the functionality, or restrict the design of the probe. This study investigated the use of an electronegative self-assembled monolayer (SAM) as a coating on a stiff insertion shuttle to carry a polymer probe into the cerebral cortex, and then the detachment of the shuttle from the probe by altering the shuttle's hydrophobicity. Polydimethylsiloxane (PDMS) and polyimide probes were inserted into an agarose *in vitro* brain model using silicon insertion shuttles. The silicon shuttles were coated with a carboxyl terminal SAM. The precision of insertion using the shuttle was measured by the percentage displacement of the probe upon shuttle removal after the probe was fully inserted. The average relative displacement of polyimide probes inserted with SAM-coated shuttles was (1.0±0.66)% of the total insertion depth compared to (26.5±3.7)% for uncoated silicon shuttles. The aver-

age relative displacement of PDMS probes was (2.1±1.1)% of the insertion depth compared to 100% (complete removal) for uncoated silicon shuttles. SAM-coated shuttles were further validated through their use to reliably insert PDMS probes in the cerebral cortex of rodents. This study found that SAM-coated silicon shuttles are a viable method for accurately and precisely inserting flexible neural probes in the brain.

Index Terms- Microelectrode, Surgical technique, Cortex, Implant.

2.1 Introduction

There is an ongoing need for higher fidelity and longer lasting implantable microscale neural interfaces for recording and stimulation both in scientific and emerging clinical applications (Brown et al., 1998; Fetz and Finocchio, 1975; Gage et al., 2005; Georgopoulos et al., 1986; Kargo and Nitz, 2003; Kipke et al., 2008; Nicolelis et al., 2003; Schwartz and Moran, 2000; Taylor et al., 2002). Multiple groups have reported wire-, silicon-, and polymer-based implantable neural probe technologies at various stages of development that are advancing neural interface capabilities across many dimensions, including channel count, site and substrate materials, and ability to precisely target locations in neocortex, deep brain, and spinal cord (Bartels et al., 2008; Hetke and Anderson, 2002; McCreery et al., 2006; McNaughton et al., 1983; Motta and Judy, 2005; Musallam et al., 2007; Neves and Ruther, 2007; Nicolelis et al., 2003; Nordhausen et al., 1996; Rennaker et al., 2005; Schwartz, 2004; Wise et al., 2004). For chronically implanted probes, one challenge is to improve and/or control the degree to which the probe integrates with the surrounding tissue to meet particular performance requirements, such as high signal-to-noise ra-

tio and long-term stability (Liu et al., 2006; Nicolelis et al., 2003; Polikov et al., 2005; Rousche and Normann, 1998; Schwartz et al., 2006; Williams et al., 1999). Computer models and experimental studies of the probe-tissue interface suggest that flexible and soft probes that approach the brain's bulk material characteristics may help to minimize micromotion between the probe and surrounding tissue (Biran et al., 2005; Cheung et al., 2007; Gilletti and Muthuswamy, 2006; Kim et al., 2004; LaPlaca et al., 2005; Lee et al., 2005; Neary et al., 2003; Subbaroyan et al., 2005). To this end, biocompatible polymers such as polyimide, Parylene-C, and PDMS have been employed for flexible probes, although they have not been extensively tested for long term stability for neural recordings (Rousche et al., 2001; Weiland et al., 2005). Additionally, advanced types of probe architectures with subcellular sized features have been shown to elicit smaller reactive tissue responses (Metz et al., 2004; Rousche et al., 2001; Seymour and Kipke, 2007). Both mechanisms may facilitate improved long-term tissue integration, and thus long-term function of the device.

However, there is an interesting conflict between a probe's flexibility, softness, and feature size that are hypothesized to be important for long-term tissue integration and the largely opposite mechanical characteristics that are thought to be important for reliable and minimally damaging insertion in the brain. The viscoelastic and inhomogeneous properties of the brain make the mechanics of probe insertion a complex process involving device size, sharpness, stiffness, and the target area of the brain. There is not a consensus on optimal insertion techniques, although it is a function of many parameters. Empirical evidence suggests that stiff, sharp, and straight probes should be inserted relatively fast, but under control for a minimally damaging insertion (Bjornsson et al., 2006; Edell et al., 1992; Johnson et al., 2007).

In particular, thin-film, microscale polymer probes that have desirable flexibility for long-term implantation tend to buckle before penetrating the pia mater or deflect while being directed to the target area. Existing methods to suitably strengthen polymer probes for insertion restrict the design of the probe, limit its functionality, or negate its flexibility. One approach is to integrate a rigid insertion device during fabrication (O'Brien et al., 2001), however this technique restricts probe design and presents challenges in precise implantations. Another approach is to coat a flexible or small probe with stiff biodegradable polymers or crystals (Foley et al., 2006; Suzuki et al., 2003), but these present significant challenges to achieve the appropriate stiffness, reproducibility, and sharpness in a small conformal coating. An alternative approach is to create channels in the substrate which can be filled with stiff biodegradable polymers or crystals (Takeuchi et al., 2004). These electrode designs require a larger fluid channel to fill with biodegradable material to reach a critical stiffness for insertion. This larger channel then results in a larger implanted footprint, potentially creating more damage. Other methods include a polymer substrate integrated with a stiff silicon backbone (Lee et al., 2004), but this negates the flexibility of the polymer substrate.

Our development strategy is to find ways to uncouple the requirements of a long-term implanted probe from the requirements required for minimally damaging insertion. Our approach involves an assembly having a soft, flexible, small implantable probe and a separate thin stiff, sharp, straight insertion shuttle that carries the probe into the brain and is then removed. However, polymer probes stick to metallic and silicon surfaces through hydrophobic interactions, causing a polymer probe to be carried out of the brain when the insertion shuttle is removed. Our innovative approach is to use a highly hydrophilic, electronegative, self-assembled monolayer (SAM) coat-

ing on the shuttle. When the assembly is in the brain, the hydrophilic-coated shuttle attracts water molecules to the probe-shuttle surface causing the polymer probe to separate from the shuttle. A study that shows that 'stab wounds' from silicon microelectrodes do not cause noticeable neuronal loss (Biran et al., 2005), suggests that the incremental damage associated with the shuttle would be expected to have negligible negative effects to the tissue. This two-component approach decouples the biocompatibility, flexibility, and neural integration requirements of probes from the contradictory mechanical and handling requirements for reliably inserting the probe into the brain.

In this study, we developed a novel carboxylic acid terminal SAM coating for the insertion shuttle and then validated the insertion shuttle polymer probe system through *in vitro* and *in vivo* testing. 11-mercaptoundecanoic acid has been used for various SAM applications for *in vitro* cell cultures and *in vivo* and has indications of good biocompatibility (Huang et al., 2008; Lan et al., 2005; Romanova et al., 2006; Tidwell et al., 1997; Xiao et al., 2007), particularly for short term applications. We quantified the accuracy and precision of insertion of polymer probes using SAM-coated shuttles into a gel model of the brain and also into rat cortex. We found the SAM-coated shuttle to be an effective and reliable insertion tool for polymer probes that is validated for further development.

2.2 Methods

2.2.1 Probe insertion shuttles

The probe insertion shuttles were conventional, "Michigan"-style thin-film silicon-substrate neural probes (Drake et al., 1988; Hetke and Anderson, 2002) modified to have a SAM surface to enable release of polymer probes. These shuttles had one penetrating shank 15 μm thick, 1cm long, and 400 μm wide gradually tapering to

the tip. Each shuttle was mounted onto a blank printed circuit board (PCB) and attached to a bare silicon wafer using Kapton tape. The flat surface of the silicon shuttles and wafer were then coated together with 100 Å titanium, followed by 1000 Å gold via resistive evaporation. The Kapton tape was removed, and then the gold coated shuttles and wafer were immersed together in 1 mM ethanolic solution of 11-Mercaptoundecanoic Acid for 48 hours. They were then rinsed twice in ethanol for 5 min, followed by a 0.1-M HCl rinse, and then a de-ionized (DI) water rinse. The SAM-coated shuttles and wafer were then stored in ethanol for up to one week before use. A 1 cm x 1 cm SAM-coated wafer fragment was inspected and compared to a 1 cm x 1 cm gold coated wafer using infrared spectroscopy on a Magna 550 spectrometer (Nicolete) to confirm that the SAM was present on the gold surface. Figure 2.1 shows two representative IR spectra of the uncoated and SAM coated silicon fragments. The spectrum of the SAM coated shuttle has three peaks characteristic of the SAM: two peaks at wavenumbers 2919 cm^{-1} and 2851 cm^{-1} related to the hydrocarbon backbone of 11-Mercaptoundecanoic Acid and a peak at 1714 cm^{-1} indicating the carboxyl group.

2.2.2 Flexible neural probes

Two types of flexible polymer probes were used. The first type was a thin-film polyimide-substrate probe obtained from NeuroNexus Technologies, Inc. (Ann Arbor, Michigan, USA). These probes had a single penetrating shank 12.5 μm thick, 196 μm wide and 1.2 cm long with a pointed tip. The probes also had 12 exposed metal electrode sites and buried thin-film metal traces that were not used in this study.

The second type was a PDMS-substrate probe made in our laboratory. The fabrication process started with deposition of a 1 μm thick sacrificial aluminum

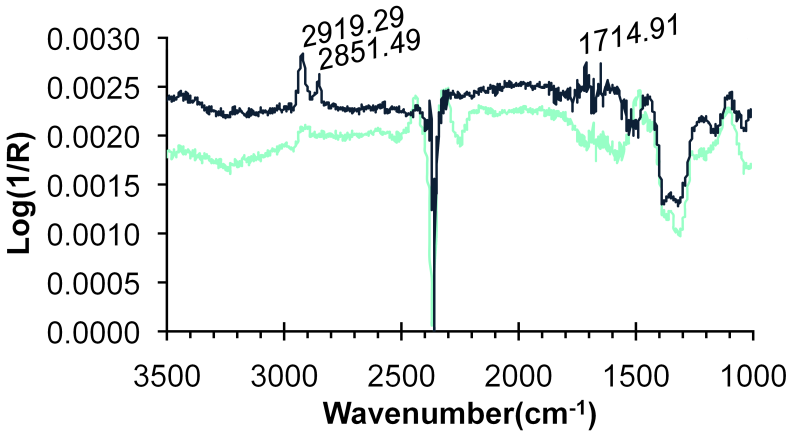

Figure 2.1: IR Spectroscopy: Gray; control Si wafer coated with 100 Å Ti and 1000 Å Au. Black; Si wafer coated with 100 Å Ti, 1000 Å Au, and 11-Mercaptoundecanoic Acid. Three peaks are seen at wavenumbers 2919 cm^{-1}, 2851 cm^{-1}, 1714 cm^{-1}. Peaks indicate that 11-Mercaptoundecanoic Acid was present on the wafer and the shuttle.

layer through e-beam evaporation (Denton Vacuum) onto a silicon wafer. This was followed by spin coating of an epoxy based, negative photoresist SU-8 2075 to a thickness of 100 μm. The photoresist layer was patterned in UV light. These probes were patterned to be 200 μm wide and 1.5 cm long with a pointed tip. The patterned SU-8 layer served as a mold for the PDMS.

PDMS (Sylgard 184, Dow Corning) was prepared by mixing pre-polymer and curing agent in a 10:1 ratio. The mixture was degassed in a vacuum chamber to remove bubbles and spun coated onto the silicon wafer. Excess PDMS was removed using a clean blade. The PDMS was cured at 150°C for 12 hours, followed by residual PDMS removal through etching with CF4:O2 (3:1) plasma for three to five minutes. The sacrificial aluminum layer was removed through etching with potassium hydroxide (KOH) solution. The individual PDMS probes were then manually removed from the wafer using microforceps. The released probes were rinsed in ethanol, DI water, and dried in air.

2.2.3 Insertion technique and quantification

Individual polymer probes of either type were placed by hand onto the SAM-coated surface of the insertion shuttle using microforceps 2-5 minutes prior to insertion. The probe was placed such that it did not extend past the tip of the insertion shuttle and its edges rested within the edges of the shuttle (Fig. 2.2A, Fig. 2.3). When necessary, a droplet of 70% ethanol was temporarily placed onto the SAM-coated surface of the shuttle to help positioning of the polymer probe onto the shuttle, and then the shuttle assembly was dried in air. This assembly was then manually positioned and inserted using microforceps into either a gel model of the brain or *in vivo* rat brain. After the assembly was inserted, the polymer probe was peeled from the insertion shuttle to the surface of the gel or brain as shown in Figure 2.2B. A drop of artificial cerebrospinal fluid (ACSF) (Harvard Apparatus) was used to help detach the polymer probe from the insertion shuttle as illustrated in Figure 2.2C. To ensure that the probe and shuttle are detached, additional droplets of ACSF may be applied until a meniscus can be observed between the probe and the shuttle or until the craniotomy is filled. After the polymer probe detached from the shuttle, the shuttle was manually grasped using microforceps and slowly removed from the gel or brain.

Probe insertions using both types of polymer probes were quantified using a gel model of the bulk mechanical characteristics of the cortex under controlled conditions. The transparent gel model consisted of 250 ml 0.5% agarose in phosphate buffered saline (PBS) with a thin layer of PBS on the surface of the agarose (Chen et al., 2002, 2004; Theer et al., 2003). Agarose of this concentration has similar elastic and shear moduli as brain tissue, (Barrangou et al., 2006; Gefen et al., 2003; Hamhaber et al., 2003; Normand et al., 2000; Prange and Margulies, 2002;

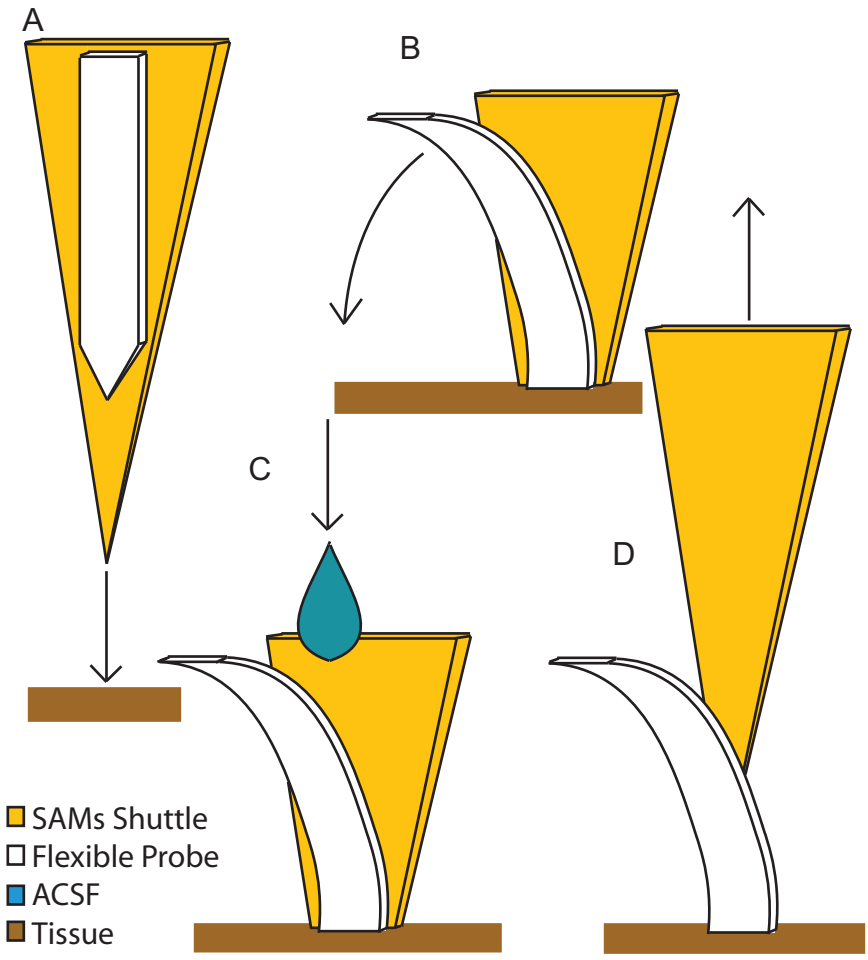

Figure 2.2: A) The flexible probe and SAM-coated insertion shuttle were inserted together with forceps. B) The polymer probe was then peeled from the top of the insertion shuttle to the base of the tissue surface. C) A drop of ACSF was used to help separate the polymer from the insertion shuttle. D) The insertion shuttle was then slowly explanted using forceps.

Thibault and Margulies, 1998) while allowing visualization of probes within the gel. Blue dye or red dye was used to contrast the clear PDMS probes from the gel for imaging purposes. Each shuttle-probe assembly was inserted into the agarose using the previously described technique. High resolution digital images were then obtained of the assembly and/or the released probe in the gel model using a fixed-position camera (Fujifilm FinePix S2 Pro with a Sigma Ex 105 mm 1:2.8 D Macro Lens at full zoom) a known distance from the model. The resolution of each image was calculated by dividing the known width of the probe in microns by the measured width of the probe from the images in pixels. The average resolution of each image was 5.3 μm/pixel. Probe penetration distance was measured immediately after insertion with the shuttle in place and again following the removal of the shuttle. The accuracy of implantation was evaluated by calculating the absolute displacement magnitude of the probe tip from probe insertion to shuttle removal. Precision was measured from the standard error. Statistical significance was calculated using a T-test.

Additionally, PDMS probes were manually inserted into rat cerebral cortex to validate the insertion technique in a typical experimental preparation. Adult male Sprague-Dawley rats (Charles River Laboratories) weighing 300-350 g were prepared for cortical implants using previously established methods (Ludwig et al., 2006; Vetter et al., 2004). The animal was anesthetized with a mixture of 50 mg/mL ketamine, 5 mg/mL xylazine, and 1 mg/mL of acepromazine administered intraperitoneally with an initial dosage of 0.125 mL/100 g of body weight and regular updates of ketamine. The depth of anesthesia was regulated by monitoring heart rate and blood oxygen saturation. The animal was placed into a stereotaxic frame and a 3 mm by 3 mm craniotomy was made over the primary motor cortex in each hemisphere.

The dura was incised and resected. Sterile saline was used to keep the brain surface moist throughout the procedure.

Controlled probe implantations involved lowering a polymer probe inserted shuttle through the craniotomy and into brain tissue. The shuttle and polymer probe were held across the PCB with a micro-alligator clip (BU-34C, Mueller Electric Company, Cleveland, OH). A piezoelectric actuator (M-230.25, Physik Instrumente, Karlsruhe, Germany) mounted to the stereotaxic frame guided insertions by means of a dc-motor controller (C-890.PS, Physik Instrumente). The insertion tool system had a maximum velocity of 1.2 mm/s with a spatial range of 25 mm with a resolution of 4.6 nm monitored by Hall effect transducers. During the first insertion trial, the shuttle was positioned until the tip of the shuttle touched the surface of the brain and then advanced at various speeds of 1mm/s, 50μm/s, 5 μm/s, and 1 μm/s for 5 mm such that the polymer probe penetrated the tissue 2-3 mm. Subsequently, arrays were inserted into brain tissue 5 times at each speed with horizontal separations of at least 400-500 μm. All procedures complied with the United States Department of Agriculture guidelines for the care and use of laboratory animals and were approved by the University of Michigan Committee on Use and Care of Animals.

2.3 Results

2.3.1 Characterization of insertion shuttle using gel models

Polymer probes were placed onto the insertion shuttle (Fig. 2.3) and inserted into separate gel tissue phantoms. Immediately after insertion with the shuttle still in place, the polymer probe penetration distance was measured. A second measurement was taken following the removal of the shuttle. Displacement of ten polyimide probes using ten SAM-coated insertion shuttles was significantly less than that of non-SAM-coated shuttles ($p<0.0001$) (Fig. 2.4A&B, Table 2.1). The average relative probe

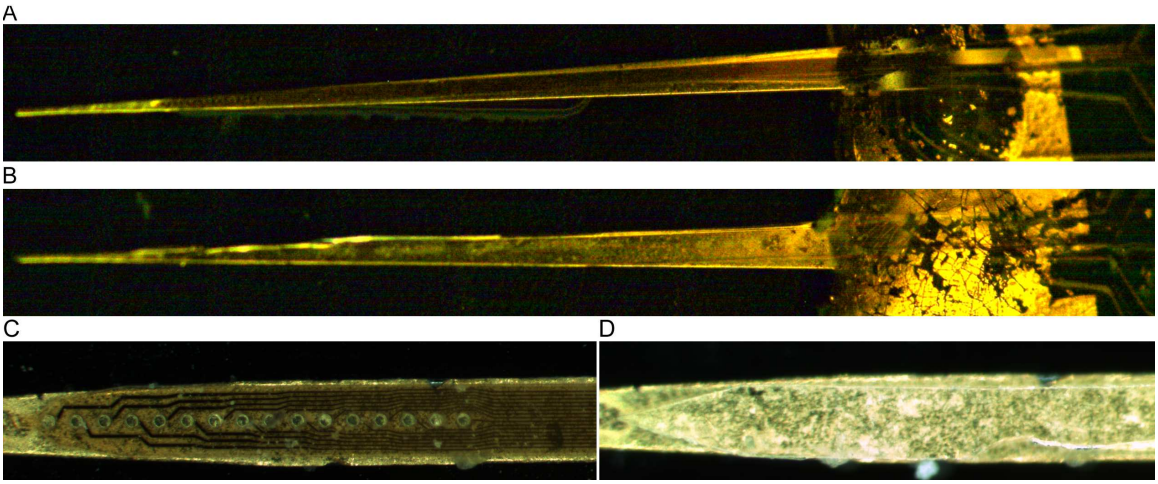

Figure 2.3: Polymer probes prepared on SAM-coated insertion shuttle. A) 196 μm wide polyimide probe. B) 200 μm wide PDMS probe. C) Tip of polyimide probe on the shuttle. D) Tip of clear PDMS probe on the shuttle, the clear PDMS probe can be identified by its white outline.

displacement was (1.0±0.66)% (mean ± standard error) of the insertion distance or 85 ± 55 μm displacement for an average target depth of t_{target} = 8,830 μm insertion. On average, the net final position of the polymer probes after the shuttle removal was t_{target} + 23 μm. For ten polyimide probes inserted into separate gel models using ten insertion shuttles without SAM coating (Fig. 2.4A&B, Table 2.1), the average relative displacement was (26.5 ± 3.7)% of the insertion distance or 2365 ± 334 μm displacement for an average t_{target} = 8,830 μm insertion. On average the net final position was t_{target} + 2365 μm.

Additionally, when reusing a single SAM-coated shuttle, displacement of ten polyimide probes was significantly less than that of non-SAM-coated shuttles ($p<0.0001$) (Table 2.1). The average relative probe displacement was (3.3±1.5)% of the implantation distance or 300 ± 135 μm displacement for an average t_{target} = 8,270 μm insertion. On average the final position was t_{target} + 57 μm. After the first insertion, there was an increase in displacement. However, displacement remained steady for the remaining nine insertions. While it is possible to reuse a SAM-coated shuttle, a

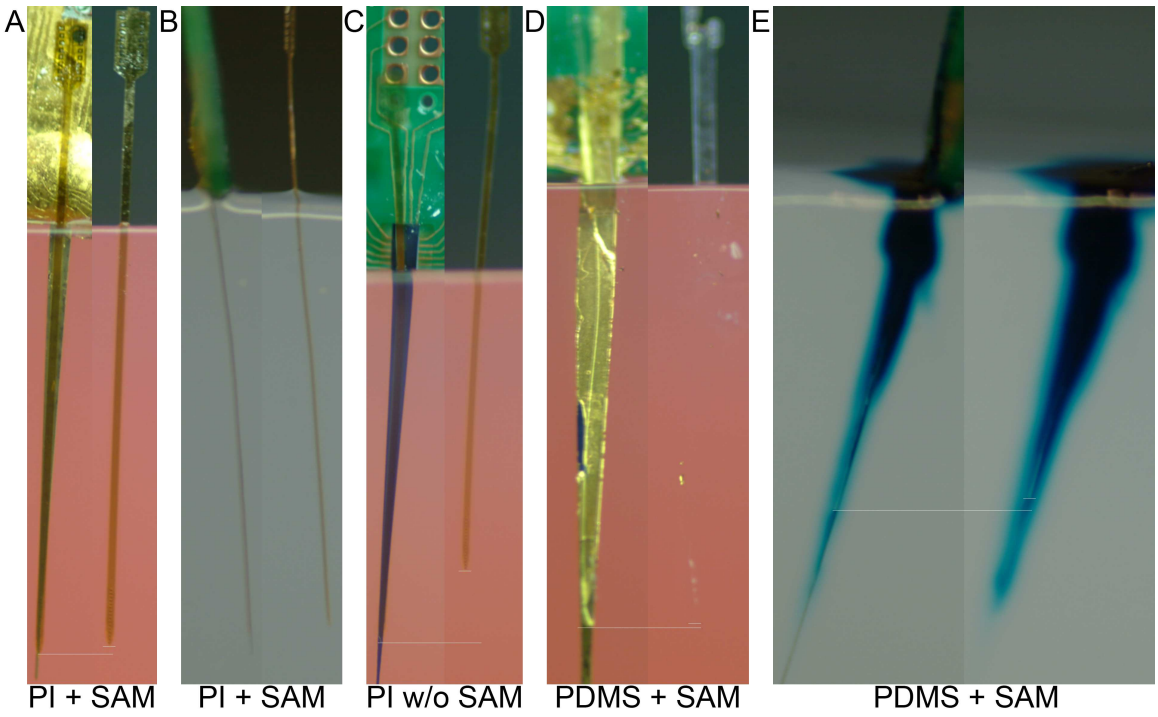

Figure 2.4: Polymer probes prepared on SAM-coated insertion shuttle. A) 196 μm wide polyimide probe. B) 200 μm wide PDMS probe. C) Tip of polyimide probe on the shuttle. D) Tip of clear PDMS probe on the shuttle, the clear PDMS probe can be identified by its white outline.

freshly coated shuttle evokes less than one-half the displacement of a used shuttle.

Displacement of ten PDMS probes using ten SAM-coated insertion shuttles was significantly less than that of non-SAM-coated shuttles ($p<0.0001$) (Fig. 2.4D-E, Table 2.1). The average relative probe displacement was (2.1±1.1)% of the implantation distance or 167 ± 79 μm displacement for an average t_{target} = 8,280 μm insertion. On average, the net final position was t_{target} + 71 μm. For ten PDMS probes inserted using ten insertion shuttles without SAM coating, all ten probes were completely explanted for an average t_{target} = 8,130 μm implantation.

2.3.2 *In vivo* validation of insertion shuttle

SAM-coated insertion shuttles were validated for inserting flexible polymer probes into the brain. Six PDMS probes were successfully implanted into the motor cortex of

Table 2.1: Displacement of shuttle inserted polymer probes in tissue phantom during shuttle removal.

Probe	Shuttle Coating	Avg Implant Distance (μm)	Avg % Displacement±S.E.	Avg μm Displacement±S.E.	N
Polyimide	SAM	8830	1.0±0.7	85±55	10
Polyimide	SAM(Repeat)*	8270	3.3±1.5	299±135	10
PDMS	SAM	8280	2.1±1.1	167±79	10
Polyimide	No Coating	8830	26.5±3.7	2365±334	10
PDMS	No Coating	8130	100.0±0.0	8130±N/A	10

*Probes were implanted consecutively with a single shuttle

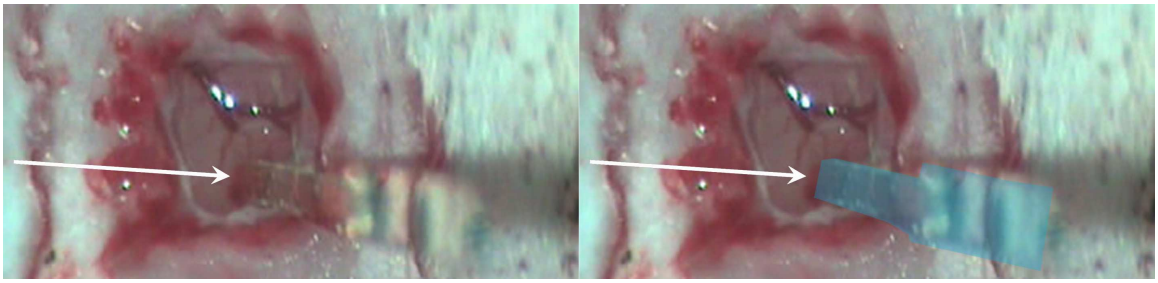

Figure 2.5: A craniotomy was made over the motor cortex. Dura was cut and folded back. A clear PDMS probe was inserted into the rat motor cortex using the insertion shuttle. Right; PDMS probe was released from the shuttle and then the shuttle was removed leaving the PDMS probe only. Arrow indicates the point of insertion. Left; shading highlights the location of the clear PDMS probe.

three male, adult rats using SAM-coated insertion shuttles (Fig. 2.5). Removal of the SAM-coated insertion shuttle did not cause visible displacement of the PDMS probes, while removal of the non-coated insertion shuttle caused complete removal of the PDMS probes. PDMS probes could not be inserted into cortex without the insertion shuttle because of their flexibility. When using a controlled insertion technique with a stereotaxic frame guided piezoelectric actuator, polymer probes were successfully inserted each trial at 1mm/s, 50 μm/s, 5 μm/s, and 1 μm/s.

2.4 Discussion

2.4.1 Probe insertion and displacement

This is the first time SAM modification of a silicon insertion shuttle has been demonstrated to enable flexible polymer devices to enter soft tissue with subsequent

removal of the shuttle resulting in negligible displacement of the polymer device. We hypothesize that the polymer probe is held to the surface of the insertion shuttle through electrostatic interactions, therefore it is important that the probe lies flat on the shuttle. Polyimide probes showed improved reliability and controllability of insertion when coupled with the SAM modified shuttle. The PDMS probes were too flexible to enter the cerebral cortex alone. The SAM modified shuttle enabled implantation of PDMS probes and subsequent removal of the shuttle.

Occasionally the PDMS probe would slide along the insertion shuttle during insertion into agarose. Ensuring the PDMS probe and shuttle were dry, gripping closer to the bottom of the PCB with forceps, and inserting in a straight controlled fashion assured successful implantation of the PDMS probe. Mounting a shorter silicon shuttle substrate onto the PCB or mounting the polymer probe tip closer to the base of the shuttle can achieve similar results without directly gripping the silicon substrate with forceps. Once the tip of the polymer probe was inserted into the tissue or tissue phantom, the probe would not separate until it was released with a drop of saline, even with manual insertions ($\sim$1mm/s). A controlled insertion technique can enable slower insertions. Additionally, a precise parallel alignment of the probe was not necessary along the axis of the shuttle so long as the polymer probe lay within the edges of the shuttle. If the probe laid outside of the edges of the shuttle, particularly near the tip, there is a chance that the polymer probe can get caught on the tissue during insertion, particularly for PDMS probes. Therefore, the shuttle should be at least as wide as the polymer probe. While a shuttle with the same size as a flexible probe will reduce the initial insertion footprint, it may increase difficulty in probe alignment.

2.4.2 Release mechanism model

Solid materials such as polymers and silicon adhere to each other in an aqueous environment due to surface energies (Johnson et al., 1971). In the presence of a thin aqueous meniscus, two hydrophobic substrates in contact, such as glass and metal, demonstrate strong adhesive forces (Mcfarlane and Tabor, 1950). It is further understood that this adhesive force is formed by a convex-shaped menisci which creates a lower pressure inside the meniscus resulting in an intrinsic attractive force, and during separation the viscosity of the liquid causes an additional attractive force (Cai and Bhushan, 2008a,b). In the case of a polymer probe and silicon shuttle in the brain, this thin aqueous meniscus is formed at the triple junction between polymer, silicon, and extracellular fluid.

For hydrophilic surfaces, meniscus forces have been well characterized (Cai and Bhushan, 2008a). A concave-shaped meniscus is formed driving the liquid between the two surfaces in a phenomena described as capillary action, which leads to a separation of the two surfaces in an aqueous solution. Therefore, separation can be achieved by converting one of the hydrophobic surfaces (the shuttle) to a highly hydrophilic surface with a coating such that the meniscus force along the new hydrophilic surface overcomes the meniscus force along the hydrophobic probe surface. 11-mercaptoundecanoic acid coated surfaces become highly electronegative and hydrophilic (Yan et al., 1997), and can be used to coat the shuttle for this purpose.

Finally, the polymer probe seems to rarely separate during insertion into hydrated tissue. The surface tension and atomic level roughness on the surface of the polymer probe and shuttle junction may prevent fluid in the tissue from separating the bundle during implantation (Denkov et al., 1999; Grassi et al., 2006). This may be why it is necessary to peel the polymer probe from the SAM-coated shuttle at the back

end and then add a droplet of ACSF to separate the shuttle from the probe after implantation.

2.4.3 Future Directions

The insertion shuttle could be modified to be narrower and thicker to improve handling and decrease the chance of fracture within the tissue. 15 μm thick shuttles are unable to penetrate the dura, however, 50 μm thick silicon shuttles or 40 μm thick C1095 spring steel shuttles can penetrate the dura, and may enable flexible polymer probe insertions through the dura as well as improve ease of use. Insertion shuttles also could be made from stiffer materials such as titanium or tungsten for insertion of probes into sub-cortical structures. However, a larger shuttle would evoke greater tissue damage during insertion. This damage may be minimal in chronic implantations since the shuttle is immediately removed similar to a stab wound (Biran et al., 2005). Additionally, sustained tissue responses have been shown to be similar for two different style probes with an order of magnitude different cross-sectional area (Szarowski et al., 2003), which suggests that a slightly larger shuttle may not create a noticeable difference in tissue response. However, the specific relationship between shuttle size and stab wound on chronic tissue response has not been determined. Channels or grooves on the surface of the insertion shuttle could improve separation of the PDMS probe from the insertion shuttle. Additionally, the shape of the shuttle tip could be optimized to reduce mechanical trauma to the tissue during insertion. Incorporating this shuttle approach for controlled insertion techniques with motorized insertions may lead to minimally damaging insertions (Bjornsson et al., 2006; Johnson et al., 2007). Future investigations also include examining adhesion forces between the polymer probe and shuttle before and after release.

Many polymers are currently available for the fabrication of microelectrodes.

These polymers have unique characteristics such as flexibility, structural stability, electrical properties, surface chemistry, and biocompatibility. Flexible microelectrode technologies have been underdeveloped in part because investigators lack a precise and efficient method to implant and validate these flexible microelectrodes *in vivo*. The ability to quickly and precisely implant polymer probes into the cortex will promote future polymer microelectrode development. Furthermore, microelectrode geometries (Szarowski et al., 2003), tip shapes, and insertion speeds influence mechanical and chemical strain on the tissue (Bjornsson et al., 2006; Johnson et al., 2007). Uncoupling the biocompatibility and neural integration requirements of probes from the mechanical and handling requirements for reliably inserting the probe into the brain can allow a new degree of freedom to explore flexible microelectrode designs. Microelectrode tip shape, anchor, stiffness, size, and surface chemistry can be designed for biocompatibility independent of the requirements to minimize insertion trauma. This can in turn open opportunities for innovative microelectrode designs that focus solely on improving the chronic device-tissue interface.

2.5 Acknowledgements

The author thanks Jeyakumar Subbaroyan for his help in the clean room and for performing the surgeries. This research is supported by Center for Neural Communication Technology, a P41 Resource Center funded by the National Institute of Biomedical Imaging and Bioengineering (NIBIB, P41 EB002030) and supported by the National Institutes of Health (NIH).

2.6 References

Barrangou, L. M., Drake, M., Daubert, C. R., and Foegeding, E. A. (2006). Textural properties of agarose gels. ii. relationships between rheological properties and sensory texture. *Food Hydrocolloids*, 20(2-3):196 – 203. 7th International Hydrocolloids Conference.

Bartels, J., Andreasen, D., Ehirim, P., Mao, H., Seibert, S., Wright, E. J., and Kennedy, P. (2008). Neurotrophic electrode: Method of assembly and implantation into human motor speech cortex. *Journal of Neuroscience Methods*, 174(2):168 – 176.

Biran, R., Martin, D. C., and Tresco, P. A. (2005). Neuronal cell loss accompanies the brain tissue response to chronically implanted silicon microelectrode arrays. *Experimental Neurology*, 195(1):115 – 126.

Bjornsson, C. S., Oh, S. J., Al-Kofahi, Y. A., Lim, Y. J., Smith, K. L., Turner, J. N., De, S., Roysam, B., Shain, W., and Kim, S. J. (2006). Effects of insertion conditions on tissue strain and vascular damage during neuroprosthetic device insertion. *J Neural Eng*, 3(3):196–207.

Brown, E. N., Frank, L. M., Tang, D., Quirk, M. C., and Wilson, M. A. (1998). A statistical paradigm for neural spike train decoding applied to position prediction from ensemble firing patterns of rat hippocampal place cells. *J Neurosci*, 18(18):7411–7425.

Cai, S. and Bhushan, B. (2008a). Meniscus and viscous forces during separation of hydrophilic and hydrophobic surfaces with liquid-mediated contacts. *Materials Science and Engineering: R: Reports*, 61(1-6):78 – 106.

Cai, S. and Bhushan, B. (2008b). Viscous force during tangential separation of meniscus bridges. *Philosophical Magazine*, 88:449–461.

Chen, Z.-J., Broaddus, W. C., Viswanathan, R. R., Raghavan, R., and Gillies, G. T. (2002). Intraparenchymal drug delivery via positive-pressure infusion: experimental and modeling studies of poroelasticity in brain phantom gels. *IEEE Trans Biomed Eng*, 49(2):85–96.

Chen, Z.-J., Gillies, G. T., Broaddus, W. C., Prabhu, S. S., Fillmore, H., Mitchell, R. M., Corwin, F. D., and Fatouros, P. P. (2004). A realistic brain tissue phantom for intraparenchymal infusion studies. *J Neurosurg*, 101(2):314–322.

Cheung, K. C., Renaud, P., Tanila, H., and Djupsund, K. (2007). Flexible polyimide microelectrode array for in vivo recordings and current source density analysis. *Biosens Bioelectron*, 22(8):1783–1790.

Denkov, N. D., Cooper, P., and Martin, J.-Y. (1999). Mechanisms of action of mixed solid-liquid antifoams. 1. dynamics of foam film rupture. *Langmuir*, 15(24):8514–8529.

Drake, K. L., Wise, K. D., Farraye, J., Anderson, D. J., and BeMent, S. L. (1988). Performance of planar multisite microprobes in recording extracellular single-unit intracortical activity. *IEEE Trans Biomed Eng*, 35(9):719–732.

Edell, D. J., Toi, V. V., McNeil, V. M., and Clark, L. D. (1992). Factors influencing the biocompatibility of insertable silicon microshafts in cerebral cortex. *IEEE Trans Biomed Eng*, 39(6):635–643.

Fetz, E. E. and Finocchio, D. V. (1975). Correlations between activity of motor cortex cells and arm muscles during operantly conditioned response patterns. *Exp Brain Res*, 23(3):217–240.

Foley, C. P., Neeves, K. B., Saltzman, W. M., and Olbricht, W. L. (2006). Bioerodible scaffolds for implantable microfluidic probes in convection enchanced neural drug delivery. In *AIChE Annual Meeting*, San Francisco, CA.

Gage, G. J., Ludwig, K. A., Otto, K. J., Ionides, E. L., and Kipke, D. R. (2005). Naive coadaptive cortical control. *J Neural Eng*, 2(2):52–63.

Gefen, A., Gefen, N., Zhu, Q., Raghupathi, R., and Margulies, S. S. (2003). Age-dependent changes in material properties of the brain and braincase of the rat. *J Neurotrauma*, 20(11):1163–1177.

Georgopoulos, A. P., Schwartz, A. B., and Kettner, R. E. (1986). Neuronal population coding of movement direction. *Science*, 233(4771):1416–1419.

Gilletti, A. and Muthuswamy, J. (2006). Brain micromotion around implants in the rodent somatosensory cortex. *J Neural Eng*, 3(3):189–195.

Grassi, M., Cox, B., and Zhang, X. (2006). Simulation of pin-reinforced single-lap composite joints. *Composites Science and Technology*, 66(11-12):1623 – 1638.

Hamhaber, U., Grieshaber, F. A., Nagel, J. H., and Klose, U. (2003). Comparison of quantitative shear wave mr-elastography with mechanical compression tests. *Magn Reson Med*, 49(1):71–77.

Hetke, J. and Anderson, D. (2002). *Handbook of Neuroprosthetic Methods.*, chapter Chapter 7: Silicon microelectrodes for extracellular recording. CRC Press, Boca Raton, FL.

Huang, X.-L., Zhang, B., Ren, L., Ye, S.-F., Sun, L.-P., Zhang, Q.-Q., Tan, M.-C., and Chow, G.-M. (2008). In vivo toxic studies and biodistribution of near infrared sensitive au-au(2)s nanoparticles as potential drug delivery carriers. *J Mater Sci Mater Med*, 19(7):2581–2588.

Johnson, K. L., Kendall, K., and Roberts, A. D. (1971). Surface energy and the contact of elastic solids. *Proceedings of the Royal Society of London. Series A, Mathematical and Physical Sciences*, 324(1558):301–313.

Johnson, M. D., Kao, O. E., and Kipke, D. R. (2007). Spatiotemporal ph dynamics following insertion of neural microelectrode arrays. *J Neurosci Methods*, 160(2):276–287.

Kargo, W. J. and Nitz, D. A. (2003). Early skill learning is expressed through selection and tuning of cortically represented muscle synergies. *J Neurosci*, 23(35):11255–11269.

Kim, Y.-T., Hitchcock, R. W., Bridge, M. J., and Tresco, P. A. (2004). Chronic response of adult rat brain tissue to implants anchored to the skull. *Biomaterials*, 25(12):2229–2237.

Kipke, D. R., Shain, W., Buzski, G., Fetz, E., Henderson, J. M., Hetke, J. F., and Schalk, G. (2008). Advanced neurotechnologies for chronic neural interfaces: new horizons and clinical opportunities. *J Neurosci*, 28(46):11830–11838.

Lan, S., Veiseh, M., and Zhang, M. (2005). Surface modification of silicon and gold-patterned silicon surfaces for improved biocompatibility and cell patterning selectivity. *Biosens Bioelectron*, 20(9):1697–1708.

LaPlaca, M. C., Cullen, D. K., McLoughlin, J. J., and Cargill, R. S. (2005). High rate shear strain of three-dimensional neural cell cultures: a new in vitro traumatic brain injury model. *J Biomech*, 38(5):1093–1105.

Lee, H., Bellamkonda, R. V., Sun, W., and Levenston, M. E. (2005). Biomechanical analysis of silicon microelectrode-induced strain in the brain. *J Neural Eng*, 2(4):81–89.

Lee, K. K., He, J. P., Singh, A., Massia, S., Ehteshami, G., Kim, B., and Raupp, G. (2004). Polyimide-based intracortical neural implant with improved structural stiffness. *Journal of Micromechanics and Microengineering*, 14(1):32–37.

Liu, X., McCreery, D. B., Bullara, L. A., and Agnew, W. F. (2006). Evaluation of the stability of intracortical microelectrode arrays. *IEEE Trans Neural Syst Rehabil Eng*, 14(1):91–100.

Ludwig, K. A., Uram, J. D., Yang, J., Martin, D. C., and Kipke, D. R. (2006). Chronic neural recordings using silicon microelectrode arrays electrochemically deposited with a poly(3,4-ethylenedioxythiophene) (pedot) film. *J Neural Eng*, 3(1):59–70.

McCreery, D., Lossinsky, A., Pikov, V., and Liu, X. (2006). Microelectrode array for chronic deep-brain microstimulation and recording. *IEEE Trans Biomed Eng*, 53(4):726–737.

Mcfarlane, J. S. and Tabor, D. (1950). Adhesion of solids and the effect of surface films. *Proceedings of the Royal Society of London Series a-Mathematical and Physical Sciences*, 202(1069):224–243.

McNaughton, B. L., O'Keefe, J., and Barnes, C. A. (1983). The stereotrode: a new technique for simultaneous isolation of several single units in the central nervous system from multiple unit records. *J Neurosci Methods*, 8(4):391–397.

Metz, S., Bertsch, A., Bertrand, D., and Renaud, P. (2004). Flexible polyimide probes with microelectrodes and embedded microfluidic channels for simultaneous drug delivery and multichannel monitoring of bioelectric activity. *Biosens Bioelectron*, 19(10):1309–1318.

Motta, P. S. and Judy, J. W. (2005). Multielectrode microprobes for deep-brain stimulation fabricated with a customizable 3-d electroplating process. *IEEE Trans Biomed Eng*, 52(5):923–933.

Musallam, S., Bak, M. J., Troyk, P. R., and Andersen, R. A. (2007). A floating metal microelectrode array for chronic implantation. *J Neurosci Methods*, 160(1):122–127.

Neary, J. T., Kang, Y., Willoughby, K. A., and Ellis, E. F. (2003). Activation of extracellular signal-regulated kinase by stretch-induced injury in astrocytes involves extracellular atp and p2 purinergic receptors. *J Neurosci*, 23(6):2348–2356.

Neves, H. P. and Ruther, P. (2007). The neuroprobes project. *Conf Proc IEEE Eng Med Biol Soc*, 2007:6443–6445.

Nicolelis, M. A. L., Dimitrov, D., Carmena, J. M., Crist, R., Lehew, G., Kralik, J. D., and Wise, S. P. (2003). Chronic, multisite, multielectrode recordings in macaque monkeys. *Proc Natl Acad Sci U S A*, 100(19):11041–11046.

Nordhausen, C. T., Maynard, E. M., and Normann, R. A. (1996). Single unit recording capabilities of a 100 microelectrode array. *Brain Res*, 726(1-2):129–140.

Normand, V., Lootens, D. L., Amici, E., Plucknett, K. P., and Aymard, P. (2000). New insight into agarose gel mechanical properties. *Biomacromolecules*, 1(4):730–738.

O'Brien, D. P., Nichols, T. R., and Allen, M. G. (2001). Flexible microelectrode arrays with integrated insertion devices. In *Proc. 14th IEEE Int. Conf. Micro Electro Mechanical Systems MEMS 2001*, pages 216–219.

Polikov, V. S., Tresco, P. A., and Reichert, W. M. (2005). Response of brain tissue to chronically implanted neural electrodes. *J Neurosci Methods*, 148(1):1–18.

Prange, M. T. and Margulies, S. S. (2002). Regional, directional, and age-dependent properties of the brain undergoing large deformation. *J Biomech Eng*, 124(2):244–252.

Rennaker, R. L., Ruyle, A. M., Street, S. E., and Sloan, A. M. (2005). An economical multichannel cortical electrode array for extended periods of recording during behavior. *J Neurosci Methods*, 142(1):97–105.

Romanova, E. V., Oxley, S. P., Rubakhin, S. S., Bohn, P. W., and Sweedler, J. V. (2006). Self-assembled monolayers of alkanethiols on gold modulate electrophysiological parameters and cellular morphology of cultured neurons. *Biomaterials*, 27(8):1665–1669.

Rousche, P. J. and Normann, R. A. (1998). Chronic recording capability of the utah intracortical electrode array in cat sensory cortex. *J Neurosci Methods*, 82(1):1–15.

Rousche, P. J., Pellinen, D. S., Pivin, D. P., Williams, J. C., Vetter, R. J., and Kipke, D. R. (2001). Flexible polyimide-based intracortical electrode arrays with bioactive capability. *IEEE Trans Biomed Eng*, 48(3):361–371.

Schwartz, A. B. (2004). Cortical neural prosthetics. *Annu Rev Neurosci*, 27:487–507.

Schwartz, A. B., Cui, X. T., Weber, D. J., and Moran, D. W. (2006). Brain-controlled interfaces: movement restoration with neural prosthetics. *Neuron*, 52(1):205–220.

Schwartz, A. B. and Moran, D. W. (2000). Arm trajectory and representation of movement processing in motor cortical activity. *Eur J Neurosci*, 12(6):1851–1856.

Seymour, J. P. and Kipke, D. R. (2007). Neural probe design for reduced tissue encapsulation in cns. *Biomaterials*, 28(25):3594–3607.

Subbaroyan, J., Martin, D. C., and Kipke, D. R. (2005). A finite-element model of the mechanical effects of implantable microelectrodes in the cerebral cortex. *J Neural Eng*, 2(4):103–113.

Suzuki, T., Mabuchi, K., and Takeuchi, S. (2003). A 3d flexible parylene probe array for multichannel neural recording. In *Proc. First Int Neural Engineering IEEE EMBS Conf*, pages 154–156.

Szarowski, D. H., Andersen, M. D., Retterer, S., Spence, A. J., Isaacson, M., Craighead, H. G., Turner, J. N., and Shain, W. (2003). Brain responses to micro-machined silicon devices. *Brain Res*, 983(1-2):23–35.

Takeuchi, S., Yoshida, Y., Ziegler, D., Mabuchi, K., and Suzuki, T. (2004). Parylene flexible neural probe with micro fluidic channel. In *Proc. 17th IEEE Int Micro Electro Mechanical Systems Conf. . (MEMS)*, pages 208–211.

Taylor, D. M., Tillery, S. I. H., and Schwartz, A. B. (2002). Direct cortical control of 3d neuroprosthetic devices. *Science*, 296(5574):1829–1832.

Theer, P., Hasan, M. T., and Denk, W. (2003). Two-photon imaging to a depth of 1000 microm in living brains by use of a ti:al2o3 regenerative amplifier. *Opt Lett*, 28(12):1022–1024.

Thibault, K. L. and Margulies, S. S. (1998). Age-dependent material properties of the porcine cerebrum: effect on pediatric inertial head injury criteria. *J Biomech*, 31(12):1119–1126.

Tidwell, C. D., Ertel, S. I., Ratner, B. D., Tarasevich, B. J., Atre, S., and Allara, D. L. (1997). Endothelial cell growth and protein adsorption on terminally functionalized, self-assembled monolayers of alkanethiolates on gold. *Langmuir*, 13(13):3404–3413.

Vetter, R. J., Williams, J. C., Hetke, J. F., Nunamaker, E. A., and Kipke, D. R. (2004). Chronic neural recording using silicon-substrate microelectrode arrays implanted in cerebral cortex. *IEEE Trans Biomed Eng*, 51(6):896–904.

Weiland, J., Fink, W., Humayun, M., Liu, W., Rodger, D., Tai, Y.-C., and Tarbell, M. (2005). Progress towards a high-resolution retinal prosthesis. *Conf Proc IEEE Eng Med Biol Soc*, 7:7373–7375.

Williams, J. C., Rennaker, R. L., and Kipke, D. R. (1999). Long-term neural recording characteristics of wire microelectrode arrays implanted in cerebral cortex. *Brain Res Brain Res Protoc*, 4(3):303–313.

Wise, K. D., Anderson, D. J., Hetke, J. F., Kipke, D. R., and Najafi, K. (2004). Wireless implantable microsystems: High-density electronic interfaces to the nervous system. In *Proceedings of the Ieee*, volume 92, pages 76–97.

Xiao, Y., Guo, C., Li, C. M., Li, Y., Zhang, J., Xue, R., and Zhang, S. (2007). Highly sensitive and selective method to detect dopamine in the presence of ascorbic acid by a new polymeric composite film. *Anal Biochem*, 371(2):229–237.

Yan, L., Marzolin, C., Terfort, A., and Whitesides, G. M. (1997). Formation and reaction of interchain carboxylic anhydride groups on self-assembled monolayers on gold. *Langmuir*, 13(25):6704–6712.

CHAPTER III

Reduction of neurovascular damage resulting from microelectrode insertion into cerebral cortex using *in vivo* two-photon mapping

Abstract

Penetrating neural probe technologies allow investigators to record electrical signals in the brain. Implantation of probes causes acute tissue damage, partially due to vasculature disruption during probe implantation. This trauma can cause abnormal electrophysiological responses, temporary increases in neurotransmitter levels, and perpetuate chronic immune responses. A significant challenge for investigators is examining neurovascular features below the surface of the brain *in vivo*. The objective of this study was to investigate localized bleeding resulting from inserting microscale neural probes into cortex using two-photon microscopy (TPM) and to explore an approach to minimize blood vessel disruption through insertion methods and probe design. 3D TPM images of cortical neurovasculature were obtained from mice and used to select preferred insertion positions for probe insertion to reduce neurovasculature damage. There was an 82.8±14.3% reduction in neurovascular damage for probes inserted in regions devoid of major (> 5 μm) sub-surface vessels. Also, the deviation of surface vessels from the vector normal to the surface as a function of depth and vessel diameter was measured and characterized. 68% of the major ves-

sels were found to deviate less than 49 μm from their surface origin up to a depth of 500 μm. Inserting probes more than 49 μm from major surface vessels can reduce chances of severing major sub-surface neurovasculature without using TPM.

Index Terms- Implant, Surgery, Trauma, Blood Brain Barrier, Neural Probe, Neurovasculature, Brain Injury.

3.1 Introduction

High fidelity, permanent, implantable microscale neural interface devices are enabling components for a broad class of scientific and emerging clinical applications. The capability of monitoring specific neuronal ensembles using these probes for long periods of time with great precision would be a powerful tool in neuroscience research for linking low-level neuronal circuits to high-level brain function, such as learning, memory, and perception. In clinical areas, it would enable the development of closed-loop neurostimulation and neuroprosthetic systems using multichannel unit activity or local field potentials. A growing body of work provides evidence that long-term neuro-implants for spike recording are feasible (Kipke et al., 2008; Schmidt et al., 1976). This work can be summarized through four overall findings: (1) one can typically record useful spike activity from cortex and deeper structures for more than six months using any of the several types of implantable microelectrode probes; (2) the recording quality is typically adequate, but not outstanding, over this time period; (3) the quality of recordings eventually degrade to the point where they are of limited or no use, and (4) the unresolved engineering issue is to increase the quality, stability, and longevity of recordings using implantable microelectrode probes. While progress is being made to improve implantable probes and to better understand the associated reactive tissue responses, the complex relationships between structure and

function in chronic neural interfaces are not well understood.

The present study is focused on the initial localized disruption of the blood brain barrier (BBB) and bleeding resulting from inserting a microscale neural probe into cerebral cortex. This is important because acute tissue damage leads to the release of erythrocytes, clotting factors, and inflammatory factors from disrupted blood vessels which facilitate recruitment of activated microglia and a broad region of astrocyte activation around the inserted probe (Schwartz et al., 2006; Szarowski et al., 2003; Turner et al., 1999; Grill et al., 2009). During insertion, the highly regulated blood brain barrier is compromised leading to plasma protein release into the surrounding parenchyma, resulting in adsorption onto the electrode, increased concentrations of extracellular serum proteins, ions, and other solutes, and deposition of plasma into the neuropil (Groothuis et al., 1998; Kimelberg, 1995). Acutely, this damage can be observed as irregularities in neuronal spike activity (Johnson et al., 2006), elevated levels of extracellular neurotransmitters (Camp and Robinson, 1992; Goldsmith et al., 1995; Holson et al., 1998) and a net increase in extracellular water content (Betz et al., 1989; Klatzo, 1967; Unterberg et al., 2004). This vasogenic edema leads to increased brain tissue volume and intracranial pressure (Barzo et al., 1997) often associated with their impact on tissue damage (Dixon et al., 1991; McIntosh et al., 1996) and clinical outcome (Narayan et al., 2002). For example, albumin, the most abundant protein in blood plasma (Shen et al., 2004), is responsible, in part, for inducing glial cell activation and proliferation (Nadal et al., 1998, 1995). Although stab wound studies show limited chronic tissue damage (McConnell et al., 2009; Biran et al., 2005), plasma protein adsorption onto the electrode may perpetuate the tissue response in chronically implanted electrodes. Furthermore, disrupting major arterioles during probe insertion can cause additional neuronal damage, by

means of ischemia, through loss of perfusion to the tissue below the disrupted region, which is typically where the recording sites are located (Nishimura et al., 2007; Zhang et al., 2005).

Investigation of initial localized bleeding resulting from neural probe insertion is also important because there is experimental evidence that it can be affected through electrode design and surgical technique. For example, electrode shape and insertion speed have been related to tissue damage (Johnson et al., 2007; Bjornsson et al., 2006; Edell et al., 1992). Details of probe insertion may also impact chemical trauma in tissue (Johnson et al., 2007), as the implantation of probes punctures and tears neural vasculature (House et al., 2006; Bjornsson et al., 2006). These types of high-resolution investigations of neurovasculature currently use post-mortem histology or ex vivo brain tissue slice preparations. In both cases, the brain tissue under study must be excised from the native environment and extensively processed, which limits the degree to which temporal effects (both immediate and chronic) of probe insertion can be investigated.

In vivo two-photon microscopy (TPM) provides an innovative approach to studying the localized, microscale tissue effects of neural probe insertion and implantation. TPM is experiencing significant growth in biomedical research (Zipfel et al., 2003; Svoboda and Yasuda, 2006; Dunn and Sutton, 2008; Lowery et al., 2009; Majewska et al., 2000a; Chauhan et al., 2009) because it allows detailed observation of deeper tissue structures beyond the range of confocal microscopy (Helmchen and Denk, 2005). Specifically, TPM has been used to create 2D and 3D models of vasculature associated with tumor growth (Abdul-Karim et al., 2003; Tyrrell et al., 2005). Our interest is to use *in vivo* TPM to generate 3D maps of the vasculature in small regions of cortex in the live mouse in order to investigate tissue

damage associated with inserting neural probes.

The objective of this study was to investigate localized bleeding resulting from inserting microscale neural probes into cortex and to explore an approach to minimize blood vessel disruption through insertion methods and probe design. We used *in vivo* two-photon microscopy in mouse cortex to characterize neurovascular architecture to a depth of 500 μm from the cortical surface. We examined neurovasculature maps prior to probe insertion and then used these vascular maps to select preferred insertion positions and trajectories to reduce localized neurovasculature damage. We show that the details of insertion location and trajectory do affect initial neurovascular damage. Additionally, we found that large penetrating vessels do not penetrate into cortex exactly perpendicularly from the surface, but deviate slightly from the normal axis in a statistically predictable manner. This results in the possibility of probes disrupting major neurovasculature below the cortical surface upon insertion even when they are positioned to avoid surface blood vessels. These results are important for providing experimental data for the rational design of improved probes and surgical techniques to minimize localized bleeding, and as such, increase the likelihood of improved long-term function.

3.2 Methods

3.2.1 Surgery

All animal techniques were developed and practiced in accordance with the policies of the University Committee on Animal Resources at the University of Rochester. Five adult male CD1 mice 38-44g (Jackson Labs, Bar Harbor, ME) were anesthetized intraperitoneally with 90 mg Ketamine hydrochloride and 9 mg Xylazine (Hospira, Lake Forest, IL) per kg body weight.

After removal of the skin and connective tissue on the surface of the skull, the skull

was glued to a metal plate that was then fastened into a metal base that connected directly into the microscope stage for imaging. The skull was thinned using a high-speed dental drill (Fine Science Tools, Foster City, CA) and removed with forceps to create a 2 mm by 3 mm craniotomy between lambda and bregma lateral to midline. The skull was periodically bathed in saline to ensure that the underlying cortex did not experience thermal damage from drilling. Because mouse dura (few cell layers thick, $<<$ 80 μm) is substantially thinner than rat dura ($\sim$ 80 μm), it was left intact to prevent the brain from expanding due to excessive hydration (Maikos et al., 2008). During imaging, anesthesia was maintained with periodic injections of Ketamine/Xylazine. Occasionally, removing the skull cap resulted in bleeding from the dura or cortex. Once bleeding subsided, the mice were injected with 0.5 mL of 5 mg/mL FITC-albumin retro-orbitally.

3.2.2 Two-photon neurovascular mapping and insertion

A custom two-photon laser scanning microscope (Majewska et al., 2000b) was used for *in vivo* imaging. The microscope consisted of a modified Fluoview confocal scan head (Olympus Optical) and a Ti:S laser providing 100 fs pulses at 80 MHz at a wavelength of 920 nm (Mai Tai; Spectra-Physics, Menlo Park, CA). Fluorescence was detected using non-descanned photomultiplier tubes (HC125-02; Hamamatsu, Shizouka, Japan) in whole-field detection mode. The craniotomy over the exposed cortex was initially identified under a dissection scope, and a detailed neurovasculature map was created using a 20x, 0.95 numerical aperture lens (IR2; Olympus Optical). Images were acquired using Olympus Fluoview software. Z stacks taken 5 μm apart from the pia to a depth of 500 μm below the surface were acquired immediately before and immediately after electrode explantation. A 3D neurovascular map was reconstructed from the image stack and two probe insertion regions

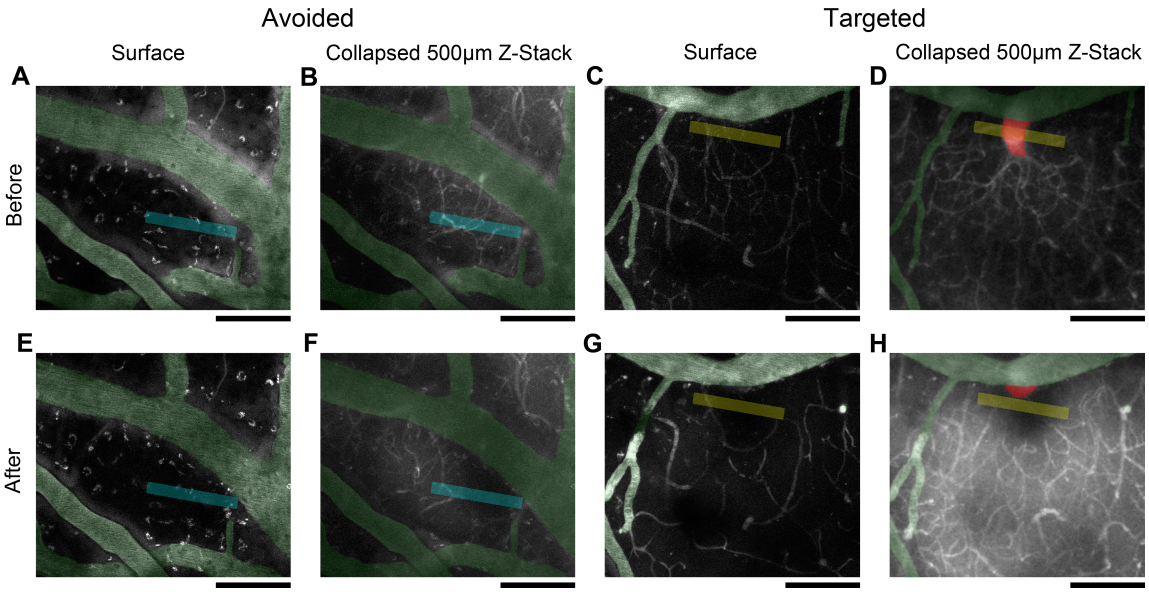

Figure 3.1: Two-photon imaging of cortical vasculature in a single mouse before probe insertion (A),(B),(C),(D) and after probe insertion, 30 min incubation, and probe explantation (E),(F),(G),(H). Capillaries (<5 μm diameter) are indicated as white. Major vessels (>5 μm diameter) are highlighted; surface vessels (green) and vessels below the pia (red). (A),(C),(E),(G): Image of the surface vasculature. (B),(D),(F),(H): Collapsed image of neurovasculature 0-500 μm for (A),(C),(E),(G), respectively. Blue indicates probe insertion sites for avoiding major vessels and only disrupting capillaries. Yellow indicates probe insertion sites for disrupting a major blood vessel not visible from the surface. Red blood cells can be visualized by dark regions in collapsed images. Scale bar indicates 100 μm.

were selected for each animal: 1) a region containing a large diving blood vessel not visible from the surface, 2) a region devoid of any major blood vessels containing minimal blood capillaries (Figure 3.1&3.2). These regions were ∼200 to 1000 μm apart and were co-registered using major surface vessel landmarks. Two different single tapered penetrating shank 15 μm thick, 3 mm long Michigan-style micromachined silicon probes with a base width of 123 μm (A1x16 3mm100-177, NeuroNexus Technologies, Inc., Ann Arbor MI), provided by the University of Michigan, Center for Neural Communication Technology (CNCT), were inserted into these regions using a stereotaxic micropositioner at a manual speed of ∼1-1.5 mm/s (hand-dialed) under visual guidance using an Olympus SZ61 microscope on a ∼30° angled tilt mount. Minimal dimpling was observed. Because the center-to-center spacing of the electrodes sites are known to be 100 μm, the depth of insertion was confirmed by counting the number of exposed electrode sites on the probe using the tilted surgical microscope. In each trial, the order of electrode implantation was randomized. The second device insertion was completed within forty five seconds of the first device being implanted. Probes were left in place for 30 minutes, then removed in the order that they were implanted. Immediately after probe removal, Z stacks were again taken 5 μm apart for up to 500 μm below the surface (Figure 3.1&3.2). If excessive surface bleeding was observed following imaging, the coagulated blood was gently swabbed off and the brain surface was imaged again. This was possible without causing additional bleeding because the dura was left intact.

3.2.3 Data analysis

In each animal, prior to insertion, the depth at which the projected probe track would sever the major vessel was noted through examination of the image stacks. This depth was then also used for the control insertion comparison in which the

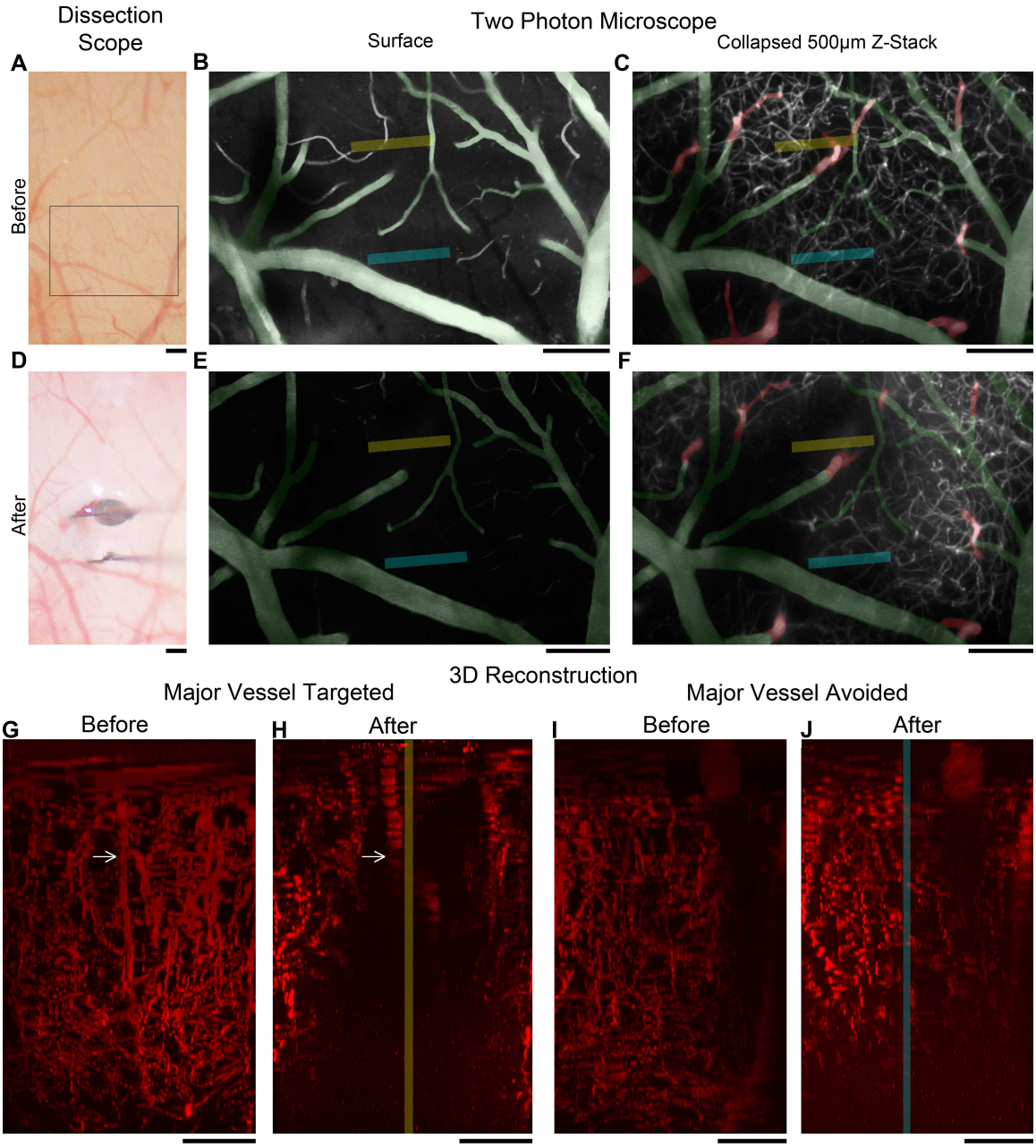

Figure 3.2: Imaging of cortical vasculature in a single mouse before probe insertion (A), (B), (C), (G), (I) and after insertion (D), 30 min incubation, and probe explantation (E), (F), (H), (J). Blue indicates probe insertion sites for avoiding major vessels and only disrupting capillaries. Yellow indicates probe insertion sites for disrupting a major blood vessel not visible from the surface. (B), (C), (E), (F); Capillaries (<5 μm diameter) are indicated as white. Major vessels (>5μm diameter) are highlighted; surface vessels (green) and vessels below the pia (red). (A), (B), (D), (E): Image of the surface vasculature. (C), (F): Collapsed image of neurovasculature 0-500 μm for (B), (E), respectively. (G)-(J); 3D reconstruction of vasculature in IMARIS (Bitplane, Saint Paul, MN) to a depth into the image of 180 μm surrounding the probe. Dark regions devoid of capillaries indicate bleeding or loss of perfusion from neurovascular damage. Scale bars indicate 100 μm. Note the loss of signal when vasculature was avoided (J) is reduced compared to when major vasculature was targeted (H). White arrows indicate the targeted major vessel.

electrode did not target a major vessel. Following the experiments, the image slice at the noted depth prior to the probe insertion and after probe removal was then compared side by side for both the targeted and avoided insertions (Figure 3.3A, B). TPM can only image the shadows where blood cells suppressed fluorescent signal, therefore the area of neurovascular damage was measured through marking the depth in which the projected probe track would have severed the major vessel, instead of calculating the volume of the damage. Area of neurovascular damage was measured and calculated in ImageJ (NIH) using the 'Measure' functions by a blind observer by circling dark regions using the 'Freehand Selection' tool where blood cells either due to bleeding or loss of perfusion suppressed fluorescent signals from capillaries that were visible prior to insertion (Figure 3.3) (Kleinfeld et al., 1998). This area in each animal was then compared between when major vessels were avoided and when major vessels were targeted (Figure 3.5). Percentages were calculated by "damage area for major vessel avoided insertion" / "damage area for major vessel targeted insertion" for each animal at the same depth. In all cases, the damaged areas between the two probe insertion sites at the noted depth did not overlap. We also measured bleeding at the surface of the brain after electrode explantation using a similar blind scoring method on the most dorsal image slice in the stack (Figure 3.5). A paired 2-tailed t-test comparison was used to determine statistical significance at $p < 0.05$. Data are presented as mean ± standard deviation.

3.2.4 Neurovascular characterization

In an effort to estimate the necessary insertion distance from surface vessels to statistically decrease the chance of disrupting major penetrating vessels during probe insertion, the penetrating neurovasculature was studied through two-photon imaging. Blood vessels were identified from collected images under digital zoom (600%)

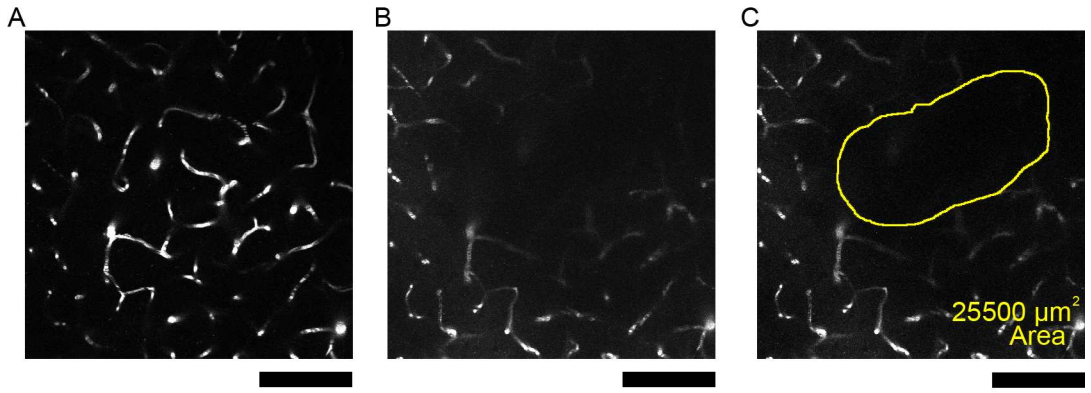

Figure 3.3: Two-photon imaging of cortical vasculature at a depth in which the targeted probe would have disrupted the major vessel in a mouse before probe insertion (A) and after probe insertion, 30 min incubation, and probe explantation (B). Neurovascular damage was visualized by dark regions, where previously blood vessels could be seen. (C), Same image as (B), but dark regions where blood cells suppress fluorescent signals have been circled by a blind observer. Scale bars indicate 100 μm.

using ImageJ. Surface vessels were first noted in superficial slices and traced onto subsequent deeper image slices. To determine average vessel deviation from normal relative to the surface, vessels up to 400-500 μm below the surface were studied. Vessels with diameter of less than 5 μm were considered capillaries (Chaigneau et al., 2003). If the surface of the brain was slightly tilted during imaging, the measurements were geometrically adjusted as needed. Tilt angles were calculated using the Pythagorean Theorem by noting the depth at which the surface of the brain came into focus in each corner of the image, and width and height of each image. In this experimental setup, the view angle alignment has an error up to 0.22°.

Major surface vessels extend into the brain tissue, usually at an angle from the vector normal (defined as the z axis) to the brain surface (defined as the x-y plane). To quantify the position of these vessels in the x-y plane, the "deviation radius" was defined as the distance from the edge of a major surface vessel in the x-y plane that each major penetrating vessel occupied (Figure 3.4). This was measured as the maximum distance between the penetrating vessel wall and the nearest surface vessel

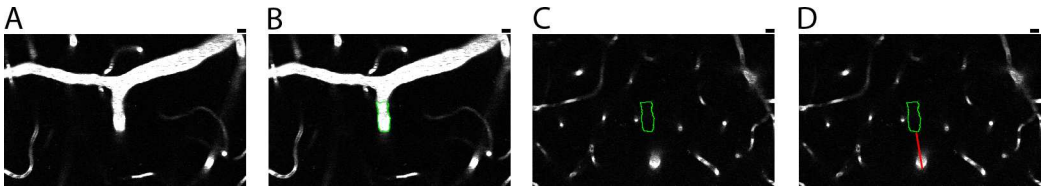

Figure 3.4: Measuring the "deviation radius" of major neurovasculature using TPM. (A) Neurovasculature at the surface of the brain. (B). Relevant major surface vessels were traced (green), and (C), traced onto subsequent deeper image slices (250 μm). (D) Deviation radius (red) was measured as the maximum distance between the penetrating vessel wall and the nearest surface vessel wall. Scale bars indicate 10 μm.

wall which was traced in the complete xyz image stack. For each selected vessel in each image slice, the deviation radius and vessel diameter were recorded.

3.3 Results

3.3.1 Probe insertion targeting or avoiding neurovasculature

Probe insertion location was examined using TPM to determine the effects of targeting or avoiding major penetrating vessels on neurovascular damage. Hemorrhaging at the surface of the brain was highly variable. The time course of bleeding could not be examined due to blood cells' intrinsic property to suppress two photon induced fluorescent signals. Images were used to quantify the area of loss of fluorescent signal from neurovascular damage caused by probe insertion. The results indicate that neurovascular damage and bleeding can be reduced by inserting the probe to avoid major penetrating blood vessels that are not visible on the surface. On average (N=5), neurovascular damage area was reduced by 82.8±14.3% ($p = 0.049$) in deep cortical areas when avoiding major vessels compared to targeting major vessels. This corresponds to a neurovascular damage area that is about 17% that of the damage area when a major vessel was targeted. At the surface of the brain, the neurovascular damage area was reduced by 73.7±20.3% ($p = 0.22$) when major vessels were avoided relative to when vessels were targeted. This corresponds to a

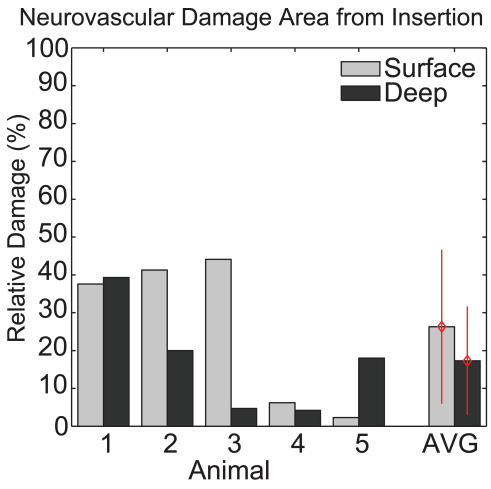

Figure 3.5: Relative size of neurovascular damage measured using *in vivo* two-photon imaging from when probe insertion disrupted only capillaries normalized to when insertion targeted a major blood vessel in the same animal 30 min after insertion. Light: Hemorrhaging at the surface was reduced on average 73% ($p = 0.22$) when avoiding major vessels. Dark: Neurovascular damage at the vessel disruption depth, 80-255 μm below the tissue surface, was reduced on average 82.8% ($p = 0.049$). Red bars indicate standard deviation.

damage area that is about 26% of the area when a major vessel is targeted (Figure 3.5).

3.3.2 Neurovascular characterization

Blood vessel deviation

The "deviation radius" was defined as the distance of the penetrating vessel at a given depth from the edge of a major surface vessel (defined as > 5 μm) in the x-y plane and measured as the distance between the furthest penetrating vessel wall to the nearest surface vessel wall traced throughout the complete xyz image stack. The deviation radius as a function of depth for each major vessel was plotted together relative to their respective surface origin (Figure 3.6A). Surface neurovasculature tended to lie horizontally along the surface plane (Figure 3.1 and 3.2). However, major vessels just below the surface of the brain tended to be vertically aligned with limited horizontal displacement. The average slope of the deviation radius was

0.102 μm/μm with respect to depth. Major blood vessels were binned according to their maximum horizontal displacement from the vertical plane perpendicular to the surface or vessel deviation radius (Figure 3.6B). The average maximum deviation radius from a vessel's surface origin was 39.3±24.3 μm at 500 μm depth.

Blood vessel diameter

Maximum deviation radius was also compared to the respective surface vessel diameter to determine if the diameter of the originating surface vessel influences the maximal deviation radius (Figure 3.6C). An $R^2 < 0.001$ showed a lack of correlation between deviation distance and vessel diameter. Major vessel diameter was also compared as a function of depth to determine if the diameter of penetrating blood vessels decreases greatly with depth (Figure 3.7A,B). If so, disrupting a major vessel deeper in the cortex may result in less neurovascular damage. However, while a general trend can be observed where vessel diameter decreases as a function of depth (0.0149 μm lateral per micron depth, $R^2 = 0.454$), the diameter only decreases 15 nm per μm depth. Additionally, neurovascular models can be developed from these observations to optimize neural probe insertion targets with respect to minimizing blood brain barrier disruption.

3.4 Discussion

3.4.1 Two-photon neurovascular mapping and insertion

All types of implantable neural probes for recording exhibit variability and limited reliability with respect to long-term recording performance and tissue responses. In this study, we examined one possible component of this variability: immediate neurovascular damage from bleeding or loss of perfusion as a function of probe insertion relative to surface and penetrating blood vessels. Inasmuch as capillary disruption

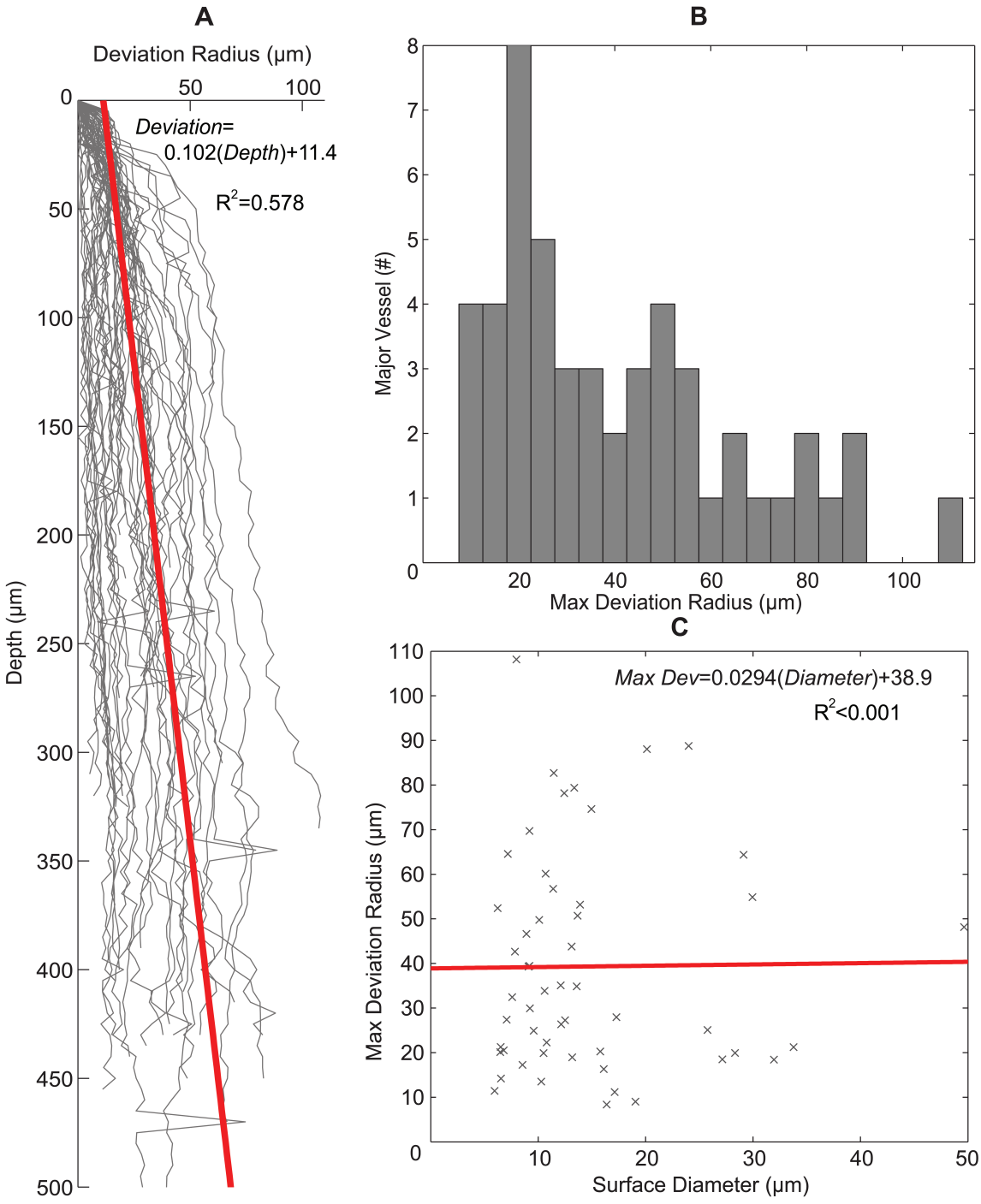

Figure 3.6: Neurovascular Characterization. (A) Traces of vessel deviation from its surface origin as a function of depth. Red trend line represents average slope. (B) Histogram plot of major blood vessels' maximal deviation from their surface origin. (C) Surface vessel diameter is examined against maximum deviation radius from its surface origin. Trend line shows poor correlation between surface vessel diameter and deviation.

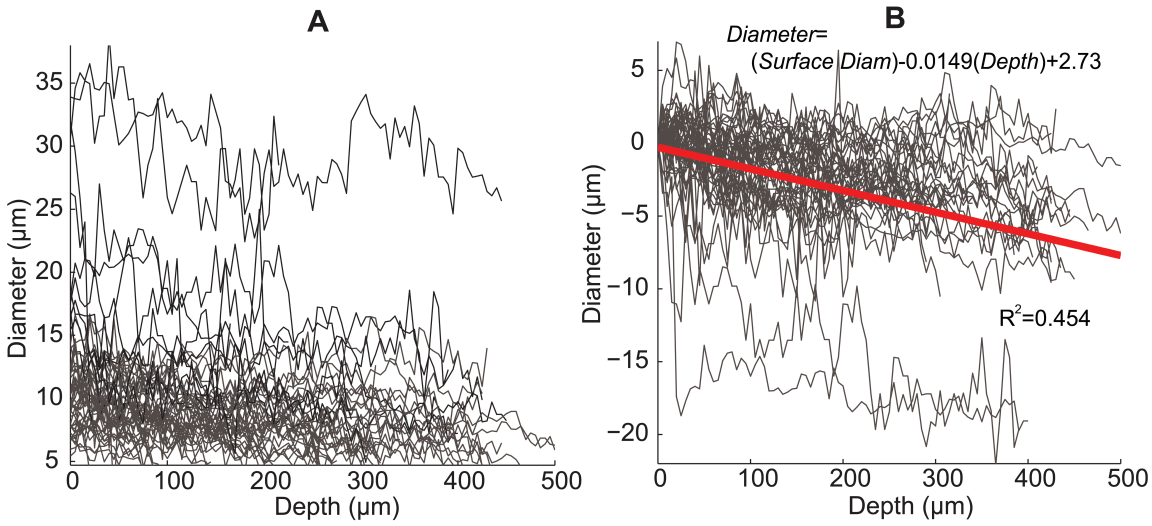

Figure 3.7: Neurovascular characterization of non-capillary vessel diameters (>5 μm diameter). (A) Traces are colored according to their starting diameter; 5-15 μm (grey), >15 μm (black). (B) Traces offset to a common origin showing a general decreasing trend of vessel diameter as a function of depth.

causes less local neurovascular damage in the region around the probe than severing a major blood vessel, we used two-photon imaging to investigate approaches to minimize vessel damage through precisely positioning and insertion of the probe relative to relatively large blood vessels. Specifically, we found that by using a tilted stereo microscope and micro-manipulator it is possible to bias probe insertions to avoid (or alternatively, to target) penetrating major vessels. While this study was not intended to directly link chronic recording performance to initial neurovascular damage, it is the first study to demonstrate that it is possible to vary the degree of local neurovascular damage by strategically selecting the probe insertion location. Moreover, this study suggests that not controlling the insertion location of each penetrating probe shank is very likely to result in a range of neurovascular damage around the individual shanks. It provides a solid step forward towards understanding the relationships between probe design, neurovascular damage, and functional performance.

At the depth in which the probe disrupted major penetrating vessels, the average

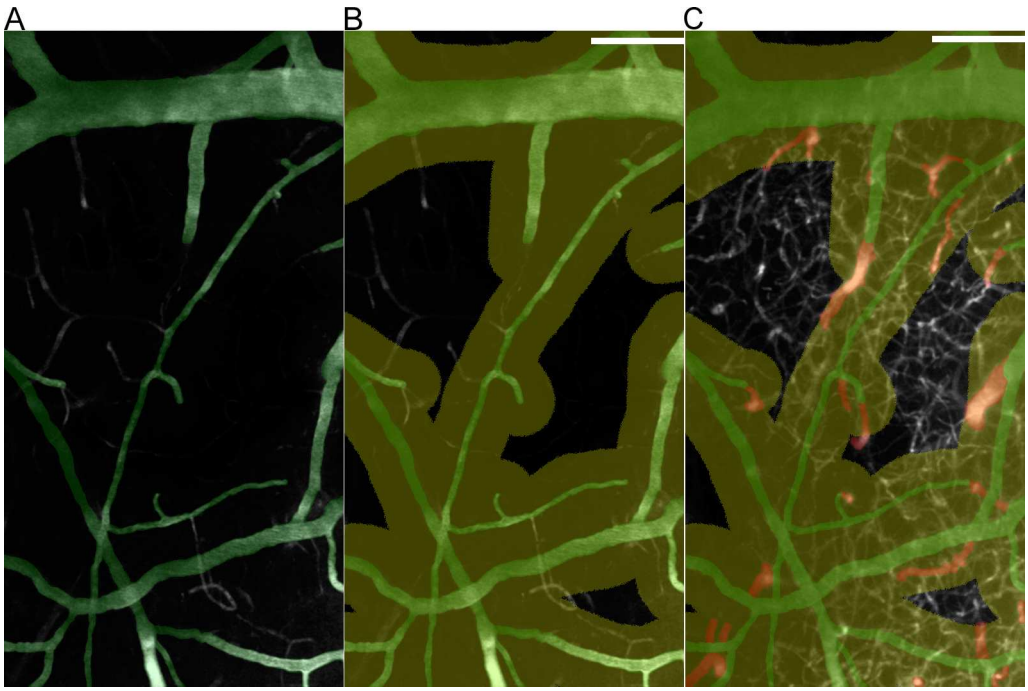

Figure 3.8: Two photon image of the vasculature of mouse cortex. Major vessels (>5 μm diameter) are highlighted: surface vessels (green) and diving vessels (red). Capillaries (<5 μm diameter) are represented in white. (A) Surface image of mouse cortex. (B) Surface image with a 49 μm 'No Implant' region highlighted in yellow. Outline indicates range of 68% confidence interval for vessel deviation. (C) Collapsed image of labeled vessels to a depth of 500 μm shown with the same outline.

damage area observed was 57,000 μm^2, compared to an average damage area of 9,300 μm^2 at the same depth when major penetrating vessels were avoided. Interestingly, hemorrhaging on the surface is not indicative of overall bleeding within the extent of the cortex as it appeared to be highly variable and did not show statistically significant changes between the two implantation sites ($p = 0.22$). This may be due to multiple causes, including hydration level as well as size and depth of the major vessel that was disrupted. Thus, surface bleeding does not appear to be a reliable indication of cortical damage sustained during electrode implantation.

3.4.2 Neurovascular characterization

This is the first time the neurovascular pattern has been characterized in the cortex for the purpose of neural probe insertion. Previous studies in many mammals, including mice and humans, found that large intracortical vessels penetrate perpendicularly from the cortical surface and extend deep into cortical layers and even into white matter (Helmchen and Kleinfeld, 2008; Duvernoy et al., 1981; Bolan et al., 2006; Dorr et al., 2007; Nishimura et al., 2007). For this reason, the standard practice for probe and microelectrode insertion is to only avoid severing surface vessels during insertion. However, this study shows that large penetrating vessels do not penetrate into cortex exactly perpendicularly, but deviate slightly from the normal axis. Therefore, probe insertions can disrupt major neurovasculature below the surface of the cortex even when the surface vessels are not penetrated. We found that non-capillary blood vessels tended to deviate at an average of 7.0 from normal relative to the cortical surface. Sixty-eight percent of the major blood vessels remained within 49 μm of the normal axis to the surface for the first $\sim$500 μm in depth, and 95% of the vessels remained within 97 μm of normal. This experimental setup had an angle alignment error of 0.2°, which is small relative to the practical limitations of manually aligning probes to be perpendicular to the surface of the brain with a micropositoner. Neurovascular deviation also was not found to be related to the vessel diameter, but vessel diameter generally does appear to gradually decrease as a function of depth.

Going beyond the use of two-photon microscopy, these findings suggest a set of neurosurgery guidelines to improve probe insertion outcomes relative to local neurovascular damage. Since 68% of the major (non-capillary) vessels remain within a 48.6 μm radius from their surface origin along the normal axis, avoiding insertion

within about 49 μm from any surface vessel will significantly decrease the chance of disrupting the penetrating segment of the vessel during insertion. To demonstrate this approach, an additional cortical TPM image was obtained in one case (Figure 3.8). Surface vessels were outlined for 49 μm from the vessel wall to mark a 'no implant' zone. A collapsed 500 μm image of outlined blood vessels demonstrates the effectiveness of this technique to reduce the probability of disrupting a major blood vessel during insertion, showing that major blood vessels are not targeted within this zone even deep inside the brain.

Using currently available multiphoton microscopes, combined with the limited concentrations of fluorescent dyes that can be achieved within the vasculature, the depth of penetration for imaging subsurface vessels was limited to about 500 μm. For this reason, a mouse model was used in this study over rats or higher mammals because the cortex is proportionally thinner in mice. For example, in mouse cortex, cell bodies of layer V neurons are located only 700-800 μm below the surface of the cortex (Levene et al., 2004). This results in more complete imaging of the entire neurovasculature within the mouse cortex, whereas in larger mammals, deeper output layers of cortex would be unlikely to fall within the potential imaging depth. The 'no implant' zones we report for the mouse may have to be updated and scaled appropriately for optimal electrode insertion and electrode design in humans. Penetrating cortical vessels in humans typically have a diameter of 40 μm or less in diameter which is similar to measurements in cats and dogs (Duvernoy et al., 1981), and is similar to the mouse penetrating cortical vessels observed in this study. However, the depth of human cortex ($\sim$2 mm)(Lauwers et al., 2008) is different from the depth of mouse cortex (900 μm)(Zhang and Sejnowski, 2000), which may affect the 49 μm 'no implant zone' we reported here on the mouse model. Additionally, the

size of the animal may also influence the degree to which the brain moves due to blood pulsation and breathing affects this 'no implant zone'. To date, mouse cerebral vasculature studies have focused on the circle of Willis, and detailed studies examining mouse cortical vasculature are still necessary in order to compare it to human cortical vasculature (Dorr et al., 2007).

3.4.3 Future direction

Complete cortical neurovascular mapping and histology

Even though this study only examined a 500 μm depth from the cortical surface, new studies are underway using similar dye injection techniques combined with advanced postmortem histological techniques, to map and characterize the entire neurovasculature in the brain (Tsai et al., 2009). Findings from these studies may indicate whether examining the first 500 μm would provide enough information to substantially reduce the risk of damage for deeper insertions. Additionally, further histology is necessary to piece together accurate shape and volume of bleeding in the cortex, since TPM can only image the optical shadows where blood cells suppressed fluorescent signal. Histological analysis would also provide a more accurate and complete understanding, as well as determine the accuracy of TPM imaging when there is blood on or near the surface of the brain. Furthermore, blood plasma and its components, such as blood cells and FITC-albumin, can be smeared during probe insertion or can diffuse away from the rupture site. Because their antagonistic effects on the CNS tissue are well documented in the literature as described in the introduction, future studies should focused on the presence and location of non-perfusing blood cells and plasma molecules in the assessment of neurovascular damage in the cortex. It is possible that the blood vessels are disrupted from tearing during electrode insertion as well as rupturing from compression. Further investigation *in vivo*

will be necessary to determine their exact contribution. Finally, discrete end point chronic histology will provide a more accurate depiction of bleeding damage by limiting secondary damage caused by explantation. This will also enable combining chronic electrophysiological recording to histological analysis.

Blood brain barrier disruption and long-term neural implant

In this study, we have validated that TPM can be used to map the neurovasculature in a live animal preparation in order to determine preferred locations for inserting neural probes to limit vascular damage. We have also shown that it is possible to systematically target and avoid subsurface vasculature in order to control the degree of neurovascular damage from device implantation. The ability to specifically target large subsurface blood vessels, while not desirable for creating a chronic, reliable interface, enables the ability to control the experimental test space and will allow researchers to better design future experiments to understand the effects of blood brain barrier disruption and the related blood products on the electrode-tissue interface.

While this study does not directly link neurovascular damage to electrode function, it does enable and motivate subsequent experiments to determine if reducing acute vascular disruption can reduce variability in long-term recording capabilities and tissue reaction. Even among the same microelectrode array, recording sites can fail as early as several weeks or last as long as a few years. Further understanding of this variability in long-term recording capabilities may improve the efficacy of implanted neural microelectrode sites and provide insight on the molecular level into developing strategies to further prolonging long-term recording capabilities. Since increased tissue trauma and vascular disruption most likely create an increase in the encapsulation of the implanted device, this sheath around the electrode site could

result in an increase in the impedance of the site with consequent increases in thermal noise and decreases in signal due to shunt loss pathways. Additionally, vascular disruption can also cause neuronal loss though ischemia to tissue downstream of the disrupted vessel, causing extended neural loss around other recording sites that may have avoided major vascular disruption (Nishimura et al., 2007). By minimizing trauma that occurs during electrode implantation, we expect that these negative effects can be minimized and the consequential variability reduced, resulting in a more stable and efficacious electrode-tissue interface to improve the number of effective recording sites and increase the average recording site lifetime of chronically implanted electrode arrays.

Furthermore, by using advanced TPM techniques, it is possible to study how neurovascular damage affects encapsulation and how encapsulation grows around an electrode track. Chronic TPM studies may reveal where encapsulation originates: at the probe tip, the probe base (pia), at the largest severed blood vessel, near all severed blood vessels, and/or from nearby large uncut leaking blood vessels suffering from chronic violation, such as micromotion. It may also reveal the time course for encapsulation and answer how long encapsulation takes to grow around the entirety of the electrode shaft. Findings from these continuation studies can help investigators focus and test their intervention strategies to further improve chronic recordings.

Implications on neural probe designs

This study also has broad implications for probe design. If we assume an association between vascular disruption and long-term recording capabilities, these results imply that anti-biofouling coatings will be an important part of chronic implantable microelectrodes. Additionally, chronic microelectrodes should be designed to have a small footprint and perhaps be made of a flexible substrate suitable for navigating

between or around major penetrating blood vessels. Alternatively, chronic probes designed to have small flexible shanks and tips designed to deflect off diving vessels may allow probes to bend to follow a vessel into the cortex rather than penetrate the vessel. This study suggests that the use of multi-shank electrodes could increase the random chance of having at least some shanks implanted outside 'no implant' zones. However, it also increases the odds that some shanks will not be well positioned. If any shank disrupts a major arteriole during probe insertion, it can cause additional broad range of neuronal damage, by means of ischemia, through loss of perfusion to tissue downstream of the disrupted vessel, causing extended neural loss (Nishimura et al., 2007) and affecting other recording sites. On the other hand, single shank multi-site microelectrodes allow easier navigation of neurovasculature, but it limits the horizontal region in which one can record from the cortex. An alternative design may be a multi-shank microelectrode in which each shank can be individually positioned. Additionally, it may be possible to develop insertion assist devices that perfectly align stereotaxic frames for perpendicular insertions into the surface of the brain by finely controlling the x and y rotational axes. Alternatively, it may be possible to generate and align, perhaps automatically or by generating input coordinates, stereotaxic micropositioners for an optimal angled insertion that will run parallel to a penetrating major vessel. The tradeoff is complexity and surgical time unless an automated system can be developed.

If vascular disruption turns out to not be correlated with long-term recording capabilities, it would allow investigators to focus on other aspects of chronic probe design such as growth factor coatings (Azemi et al., 2008), stem cell seeding (Purcell et al., 2009), drug delivery (Rohatgi et al., 2009), advanced probe architectures (Seymour and Kipke, 2007), and flexibility (Kozai and Kipke, 2009;

Subbaroyan et al., 2005; Lee et al., 2005). The final probe design that addresses the chronic interface problem is likely to be a fine-tuned combination of these many parameters. However, further investigation of vascular disruption to long-term recording capabilities will allow investigators to prioritize or eliminate these parameters in future probe designs.

3.5 Conclusion

This study explores the cortical neurovasculature in order to allow for the ability to decrease localized vascular damage from probe insertions. While neurovascular damage can be easily increased by administering drugs like heparin, using a larger device, or applying horizontal movement during and after probe insertion, this approach to electrode insertion does the opposite and provides a method to reduce bleeding, ischemia, and blood brain barrier leakage. Avoiding neurovasculature may have additional benefits for neural implants since neuronal nuclei statistically lie further away from vessels than would be expected from a random spatial distribution (Tsai et al., 2009). Therefore, by avoiding subsurface neurovasculature near electrode recording sites, there is an increase likelihood of being closer to neuronal nuclei. However, a better understanding of patterns of vascular deviation as vessels leave the surface to extend into the parenchyma will allow neurosurgeons to not only optimize their implant locations for cortical prostheses in order to obtain better long-term efficacy, but potentially help to minimize adverse side effects due to cortical vascular disruption and bleeding resulting from trauma of deep brain electrode implantation.

3.6 Acknowledgement

The authors would like to thank Badri Roysam for helpful project discussions, Anna Devor for helpful two-photon vascular imaging discussions, and Paras Patel for assistance characterizing neurovasculature. This research is supported by Center for Neural Communication Technology, a P41 Resource Center funded by the National Institute of Biomedical Imaging and Bioengineering (NIBIB, P41 EB002030) and supported by the National Institutes of Health (NEI; EY019277), Burroughs Wellcome Fund Career Award in the Biomedical sciences, Fellowship from the Alfred P Sloan Foundation, the Whitehall Foundation, Department of Defense Era of Hope Scholar Award, and Pew Scholar in the Biomedical Sciences Award.

3.7 References

Abdul-Karim, M.-A., Al-Kofahi, K., Brown, E. B., Jain, R. K., and Roysam, B. (2003). Automated tracing and change analysis of angiogenic vasculature from in vivo multiphoton confocal image time series. *Microvasc Res*, 66(2):113–125.

Azemi, E., Stauffer, W. R., Gostock, M. S., Lagenaur, C. F., and Cui, X. T. (2008). Surface immobilization of neural adhesion molecule l1 for improving the biocompatibility of chronic neural probes: In vitro characterization. *Acta Biomater*, 4(5):1208–1217.

Barzo, P., Marmarou, A., Fatouros, P., Hayasaki, K., and Corwin, F. (1997). Contribution of vasogenic and cellular edema to traumatic brain swelling measured by diffusion-weighted imaging. *J Neurosurg*, 87(6):900–907.

Betz, A. L., Iannotti, F., and Hoff, J. T. (1989). Brain edema: a classification based on blood-brain barrier integrity. *Cerebrovasc Brain Metab Rev*, 1(2):133–154.

Biran, R., Martin, D. C., and Tresco, P. A. (2005). Neuronal cell loss accompanies the brain tissue response to chronically implanted silicon microelectrode arrays. *Experimental Neurology*, 195(1):115 – 126.

Bjornsson, C. S., Oh, S. J., Al-Kofahi, Y. A., Lim, Y. J., Smith, K. L., Turner, J. N., De, S., Roysam, B., Shain, W., and Kim, S. J. (2006). Effects of insertion conditions on tissue strain and vascular damage during neuroprosthetic device insertion. *J Neural Eng*, 3(3):196–207.

Bolan, P. J., Yacoub, E., Garwood, M., Ugurbil, K., and Harel, N. (2006). In vivo micro-mri of intracortical neurovasculature. *Neuroimage*, 32(1):62–69.

Camp, D. M. and Robinson, T. E. (1992). On the use of multiple probe insertions at the same site for repeated intracerebral microdialysis experiments in the nigrostriatal dopamine system of rats. *J Neurochem*, 58(5):1706–1715.

Chaigneau, E., Oheim, M., Audinat, E., and Charpak, S. (2003). Two-photon imaging of capillary blood flow in olfactory bulb glomeruli. *Proc Natl Acad Sci U S A*, 100(22):13081–13086.

Chauhan, V. P., Lanning, R. M., Diop-Frimpong, B., Mok, W., Brown, E. B., Padera, T. P., Boucher, Y., and Jain, R. K. (2009). Multiscale measurements distinguish cellular and interstitial hindrances to diffusion in vivo. *Biophys J*, 97(1):330–336.

Dixon, C. E., Clifton, G. L., Lighthall, J. W., Yaghmai, A. A., and Hayes, R. L. (1991). A controlled cortical impact model of traumatic brain injury in the rat. *J Neurosci Methods*, 39(3):253–262.

Dorr, A., Sled, J. G., and Kabani, N. (2007). Three-dimensional cerebral vasculature of the cba mouse brain: a magnetic resonance imaging and micro computed tomography study. *Neuroimage*, 35(4):1409–1423.

Dunn, K. W. and Sutton, T. A. (2008). Functional studies in living animals using multiphoton microscopy. *ILAR J*, 49(1):66–77.

Duvernoy, H. M., Delon, S., and Vannson, J. L. (1981). Cortical blood vessels of the human brain. *Brain Res Bull*, 7(5):519–579.

Edell, D. J., Toi, V. V., McNeil, V. M., and Clark, L. D. (1992). Factors influencing the biocompatibility of insertable silicon microshafts in cerebral cortex. *IEEE Trans Biomed Eng*, 39(6):635–643.

Goldsmith, J. D., Kujawa, S. G., McLaren, J. D., and Bledsoe, S. C. (1995). In vivo release of neuroactive amino acids from the inferior colliculus of the guinea pig using brain microdialysis. *Hear Res*, 83(1-2):80–88.

Grill, W. M., Norman, S. E., and Bellamkonda, R. V. (2009). Implanted neural interfaces: biochallenges and engineered solutions. *Annu Rev Biomed Eng*, 11:1–24.

Groothuis, D. R., Ward, S., Schlageter, K. E., Itskovich, A. C., Schwerin, S. C., Allen, C. V., Dills, C., and Levy, R. M. (1998). Changes in blood-brain barrier permeability associated with insertion of brain cannulas and microdialysis probes. *Brain Res*, 803(1-2):218–230.

Helmchen, F. and Denk, W. (2005). Deep tissue two-photon microscopy. *Nat Methods*, 2(12):932–940.

Helmchen, F. and Kleinfeld, D. (2008). Chapter 10. in vivo measurements of blood flow and glial cell function with two-photon laser-scanning microscopy. *Methods Enzymol*, 444:231–254.

Holson, R. R., Gazzara, R. A., and Gough, B. (1998). Declines in stimulated striatal dopamine release over the first 32 h following microdialysis probe insertion: generalization across releasing mechanisms. *Brain Res*, 808(2):182–189.

House, P. A., MacDonald, J. D., Tresco, P. A., and Normann, R. A. (2006). Acute microelectrode array implantation into human neocortex: preliminary technique and histological considerations. *Neurosurg Focus*, 20(5):E4.

Johnson, M. D., Kao, O. E., and Kipke, D. R. (2007). Spatiotemporal ph dynamics following insertion of neural microelectrode arrays. *J Neurosci Methods*, 160(2):276–287.

Johnson, M. D., Langhals, N. B., and Kipke, D. R. (2006). Neural interface dynamics following insertion of hydrous iridium oxide microelectrode arrays. *Conf Proc IEEE Eng Med Biol Soc*, 1:3178–3181.

Kimelberg, H. K. (1995). Current concepts of brain edema. review of laboratory investigations. *J Neurosurg*, 83(6):1051–1059.

Kipke, D. R., Shain, W., Buzski, G., Fetz, E., Henderson, J. M., Hetke, J. F., and Schalk, G. (2008). Advanced neurotechnologies for chronic neural interfaces: new horizons and clinical opportunities. *J Neurosci*, 28(46):11830–11838.

Klatzo, I. (1967). Presidental address. neuropathological aspects of brain edema. *J Neuropathol Exp Neurol*, 26(1):1–14.

Kleinfeld, D., Mitra, P. P., Helmchen, F., and Denk, W. (1998). Fluctuations and stimulus-induced changes in blood flow observed in individual capillaries in layers 2 through 4 of rat neocortex. *Proc Natl Acad Sci U S A*, 95(26):15741–15746.

Kozai, T. D. Y. and Kipke, D. R. (2009). Insertion shuttle with carboxyl terminated self-assembled monolayer coatings for implanting flexible polymer neural probes in the brain. *J Neurosci Methods*, 184(2):199–205.

Lauwers, F., Cassot, F., Lauwers-Cances, V., Puwanarajah, P., and Duvernoy, H. (2008). Morphometry of the human cerebral cortex microcirculation: general characteristics and space-related profiles. *Neuroimage*, 39(3):936–948.

Lee, H., Bellamkonda, R. V., Sun, W., and Levenston, M. E. (2005). Biomechanical analysis of silicon microelectrode-induced strain in the brain. *J Neural Eng*, 2(4):81–89.

Levene, M. J., Dombeck, D. A., Kasischke, K. A., Molloy, R. P., and Webb, W. W. (2004). In vivo multiphoton microscopy of deep brain tissue. *J Neurophysiol*, 91(4):1908–1912.

Lowery, R. L., Zhang, Y., Kelly, E. A., Lamantia, C. E., Harvey, B. K., and Majewska, A. K. (2009). Rapid, long-term labeling of cells in the developing and adult rodent visual cortex using double-stranded adeno-associated viral vectors. *Dev Neurobiol*, 69(10):674–688.

Maikos, J. T., Elias, R. A. I., and Shreiber, D. I. (2008). Mechanical properties of dura mater from the rat brain and spinal cord. *J Neurotrauma*, 25(1):38–51.

Majewska, A., Brown, E., Ross, J., and Yuste, R. (2000a). Mechanisms of calcium decay kinetics in hippocampal spines: role of spine calcium pumps and calcium diffusion through the spine neck in biochemical compartmentalization. *J Neurosci*, 20(5):1722–1734.

Majewska, A., Yiu, G., and Yuste, R. (2000b). A custom-made two-photon microscope and deconvolution system. *Pflugers Arch*, 441(2-3):398–408.

McConnell, G. C., Rees, H. D., Levey, A. I., Gutekunst, C.-A., Gross, R. E., and Bellamkonda, R. V. (2009). Implanted neural electrodes cause chronic, local inflammation that is correlated with local neurodegeneration. *J Neural Eng*, 6(5):056003.

McIntosh, T. K., Smith, D. H., Meaney, D. F., Kotapka, M. J., Gennarelli, T. A., and Graham, D. I. (1996). Neuropathological sequelae of traumatic brain injury: relationship to neurochemical and biomechanical mechanisms. *Lab Invest*, 74(2):315–342.

Nadal, A., Fuentes, E., Pastor, J., and McNaughton, P. A. (1995). Plasma albumin is a potent trigger of calcium signals and dna synthesis in astrocytes. *Proc Natl Acad Sci U S A*, 92(5):1426–1430.

Nadal, A., Sul, J. Y., Valdeolmillos, M., and McNaughton, P. A. (1998). Albumin elicits calcium signals from astrocytes in brain slices from neonatal rat cortex. *J Physiol*, 509 (Pt 3):711–716.

Narayan, R. K., Michel, M. E., Ansell, B., Baethmann, A., Biegon, A., Bracken, M. B., Bullock, M. R., Choi, S. C., Clifton, G. L., Contant, C. F., Coplin, W. M., Dietrich, W. D., Ghajar, J., Grady, S. M., Grossman, R. G., Hall, E. D., Heetderks, W., Hovda, D. A., Jallo, J., Katz, R. L., Knoller, N., Kochanek, P. M., Maas, A. I., Majde, J., Marion, D. W., Marmarou, A., Marshall, L. F., McIntosh, T. K., Miller, E., Mohberg, N., Muizelaar, J. P., Pitts, L. H., Quinn, P., Riesenfeld, G., Robertson, C. S., Strauss, K. I., Teasdale, G., Temkin, N., Tuma, R., Wade, C., Walker, M. D., Weinrich, M., Whyte, J., Wilberger, J., Young, A. B., and Yurkewicz, L. (2002). Clinical trials in head injury. *J Neurotrauma*, 19(5):503–557.

Nishimura, N., Schaffer, C. B., Friedman, B., Lyden, P. D., and Kleinfeld, D. (2007). Penetrating arterioles are a bottleneck in the perfusion of neocortex. *Proc Natl Acad Sci U S A*, 104(1):365–70.

Purcell, E. K., Seymour, J. P., Yandamuri, S., and Kipke, D. R. (2009). In vivo evaluation of a neural stem cell-seeded prosthesis. *J Neural Eng*, 6(2):026005.

Rohatgi, P., Langhals, N. B., Kipke, D. R., and Patil, P. G. (2009). In vivo performance of a microelectrode neural probe with integrated drug delivery. *Neurosurg Focus*, 27(1):E8.

Schmidt, E. M., Bak, M. J., and McIntosh, J. S. (1976). Long-term chronic recording from cortical neurons. *Exp Neurol*, 52(3):496–506.

Schwartz, A. B., Cui, X. T., Weber, D. J., and Moran, D. W. (2006). Brain-controlled interfaces: movement restoration with neural prosthetics. *Neuron*, 52(1):205–220.

Seymour, J. P. and Kipke, D. R. (2007). Neural probe design for reduced tissue encapsulation in cns. *Biomaterials*, 28(25):3594–3607.

Shen, Y., Jacobs, J. M., Camp, D. G., Fang, R., Moore, R. J., Smith, R. D., Xiao, W., Davis, R. W., and Tompkins, R. G. (2004). Ultra-high-efficiency strong cation exchange lc/rplc/ms/ms for high dynamic range characterization of the human plasma proteome. *Anal Chem*, 76(4):1134–1144.

Subbaroyan, J., Martin, D. C., and Kipke, D. R. (2005). A finite-element model of the mechanical effects of implantable microelectrodes in the cerebral cortex. *J Neural Eng*, 2(4):103–113.

Svoboda, K. and Yasuda, R. (2006). Principles of two-photon excitation microscopy and its applications to neuroscience. *Neuron*, 50(6):823–839.

Szarowski, D. H., Andersen, M. D., Retterer, S., Spence, A. J., Isaacson, M., Craighead, H. G., Turner, J. N., and Shain, W. (2003). Brain responses to micro-machined silicon devices. *Brain Res*, 983(1-2):23–35.

Tsai, P. S., Kaufhold, J. P., Blinder, P., Friedman, B., Drew, P. J., Karten, H. J., Lyden, P. D., and Kleinfeld, D. (2009). Correlations of neuronal and microvascular densities in murine cortex revealed by direct counting and colocalization of nuclei and vessels. *J Neurosci*, 29(46):14553–14570.

Turner, J. N., Shain, W., Szarowski, D. H., Andersen, M., Martins, S., Isaacson, M., and Craighead, H. (1999). Cerebral astrocyte response to micromachined silicon implants. *Exp Neurol*, 156(1):33–49.

Tyrrell, J. A., Mahadevan, V., Tong, R. T., Brown, E. B., Jain, R. K., and Roysam, B. (2005). A 2-d/3-d model-based method to quantify the complexity of microvasculature imaged by in vivo multiphoton microscopy. *Microvasc Res*, 70(3):165–178.

Unterberg, A. W., Stover, J., Kress, B., and Kiening, K. L. (2004). Edema and brain trauma. *Neuroscience*, 129(4):1021–9.

Zhang, K. and Sejnowski, T. J. (2000). A universal scaling law between gray matter and white matter of cerebral cortex. *Proc Natl Acad Sci U S A*, 97(10):5621–6.

Zhang, S., Boyd, J., Delaney, K., and Murphy, T. H. (2005). Rapid reversible changes in dendritic spine structure in vivo gated by the degree of ischemia. *J Neurosci*, 25(22):5333–8.

Zipfel, W. R., Williams, R. M., and Webb, W. W. (2003). Nonlinear magic: multiphoton microscopy in the biosciences. *Nat Biotechnol*, 21(11):1369–77.

CHAPTER IV

Integrated implantable organic stealthy ultra-small microthread electrophysiological biosensor for long-term *in vivo* neural recordings

Abstract

Implantable neural microelectrodes that record extracellular biopotentials from small, targeted groups of neurons are one of the critical technologies in neuroscience research and emerging clinical applications such as brain-controlled prosthetic devices. The critical materials dependent problem is to make implantable microelectrodes that record neural activity from the same neurons for years with high fidelity and reliability. Here, we report an integrated composite electrode consisting of a carbon fiber core, a poly(p-xylylene)-based thin-film coating that acts as dielectric barrier and is functionalized to control intrinsic biological processes, and a poly(thiophene)-based recording pad. The resulting implants are an order of magnitude smaller and more mechanically compliant with brain tissue than traditional recording electrodes and were found to elicit negligible chronic reactive tissue responses and have excellent recording characteristics in acute and chronic experiments in rats. This technology establishes a new development path for highly selective and long-lasting stealthy neural interface materials and devices.

4.1 Introduction

Obtaining selective, high fidelity, long lasting readouts of brain activity is critical technology across basic and applied neuroscience. Since the pioneering work of Strumwasser demonstrating the ability to chronically record neural activity using microwires in hibernating squirrels (Strumwasser, 1958), there has been an ongoing push to improve implantable microelectrode technologies (Kipke et al., 2008; Schmidt et al., 1976). Today. most implantable neural biosensors trace back to the three historical microelectrode technology: 1) microwires, 2) thin-film, planar probe in silicon or polymer substrates, or 3) bulk micromachined array layouts. While incremental progress has been steady, there are still no definitive solutions for creating stable, long lasting devices that elicit little or no deleterious tissue responses in the brain (Grill et al., 2009; Kipke et al., 2008). In each of these technologies, it is difficult to meet the aggressive size, strength, bioactive, and electrical characteristics that are coming to the forefront through a recent marked increase in the understanding of brain tissue responses (Biran et al., 2005; Henze et al., 2000; Ward et al., 2009; McConnell et al., 2009; Purcell et al., 2009; Rousche and Normann, 1998).

Recent studies in advanced biomaterials (Ludwig et al., 2006) and chronic neural interfaces (Biran et al., 2005; Polikov et al., 2005; Szarowski et al., 2003; Turner et al., 1999) support a data-driven exploration of new paradigms for improving long-term implantable neuronal biosensors. While carbon fiber microelectrodes have been extensively used to record extracellular/intracellular neural activity, and changes in chemical concentrations, they are insulated in glass capillaries or fused silica tubes which increase the implanted device's footprint and stiffness (Clark et al., 2010; Matsumura et al., 1996; van Horne et al., 1990) and limit its

capabilities for chronic *in vivo* single unit recordings. Studies of the probe-tissue interface suggest that flexible probes may help to minimize perpetual mechanical trauma caused by physiological motion between the probe and surrounding tissue (LaPlaca et al., 2005; Lee et al., 2005; Neary et al., 2003; Subbaroyan et al., 2005; Gilletti and Muthuswamy, 2006). To this end, biocompatible polymers have been employed in increasingly flexible probes (Kim et al., 2008, 2010; Lacour et al., 2010; Suzuki et al., 2003; Takeuchi et al., 2005; Viventi et al., 2010). Furthermore, new fabrication techniques leveraging softer advanced materials have allowed for sophisticated types of probe architectures with sub-cellular sized features demonstrating a reduction of the encapsulation response (Seymour and Kipke, 2007). However, reduction of recording sites causes an inverse effect of increasing impedance despite its ideal characteristics for isolating single unit neural activity. Therefore, advanced organic conductive polymers such as poly(3,4-ethylenedioxythiophene) (PEDOT) have been used to improve the recording characteristics of small recording sites (Cui et al., 2003; Ludwig et al., 2006). More recently, functional organic bioactive surface materials have shown promise of improving chronic interfaces in new ways (Azemi et al., 2008, 2011). The emerging engineering model based on these studies point to innovating advanced composite materials that are specifically designed to achieve aggressive sets of functional requirements across multiple dimensions that were previously limited by intrinsic size, strength, flexibility, electrical, and biocompatibility tradeoffs.

Our objective in this study was to fabricate and test an ultra-small organic electrical biosensor that has a sub-cellular cross-sectional dimension, but is flexible, stronger, and with sufficient electrical characteristics for neural recording and advanced bioactive capabilities for controlling intrinsic biological processes. We developed innovative technology through advanced composite materials that are specifi-

cally engineered to aggressively extend the biosensor design space to achieve a set of functional requirements for long-term performance that previously were limited by intrinsic size, strength, and electrical tradeoffs of conventional technologies. The reulsting Microthread Electrodes (MTEs) were prepared by mounting 7 μm diameter (tensile modulus 234 GPa) carbon fibers onto a microelectrode printed circuit board. The carbon fiber was then coated with an 800 nm poly(p-xylylene) coating via chemical vapor deposition (CVD) polymerization (Fig. 4.1A). Poly(p-xylylene) (also know under the trade name Parylene-N) was selected for its very low dissipation factor, high dielectric strength, and low dielectric constant that is also invariant with frequency. An additional 50 nm thick layer of the functionalized polymer coating poly[(p-xylylene-4-methyl-2-bromoisobutyrate)-co-(p-xylylene)] was deposited onto the device via CVD polymerization (Fig. 4.1B)(Lahann, 2006). This polymer provides initiator groups for subsequent atom transfer radical polymerization (ATRP). (Jiang et al., 2008) After ATRP, a ~200 nm thick poly(ethylene glycol methacrylate) (PEGMA) top layer was formed, which rendered the neuronal probe devices protein-resistant (Fig. 4.1C)(Jiang et al., 2008; Katira et al., 2007). Finally, a recording site was created by electrochemical deposition of poly(3,4-ethylenedioxythiophene) poly(styrenesulfonate) (PEDOT/PSS) onto the tip of the neuronal probe, from which the poly(p-xylylene) and poly(ethylene glycol) methacrylate coatings were previously removed (Fig. 4.1D). The primary innovation of this technology is the combination of advanced materials to result in an ultra-small organic interface that has the approximate size of a single trace of a conventional silicon neural probe, but sufficient strength and flexibility to act as a stand-alone electrode.

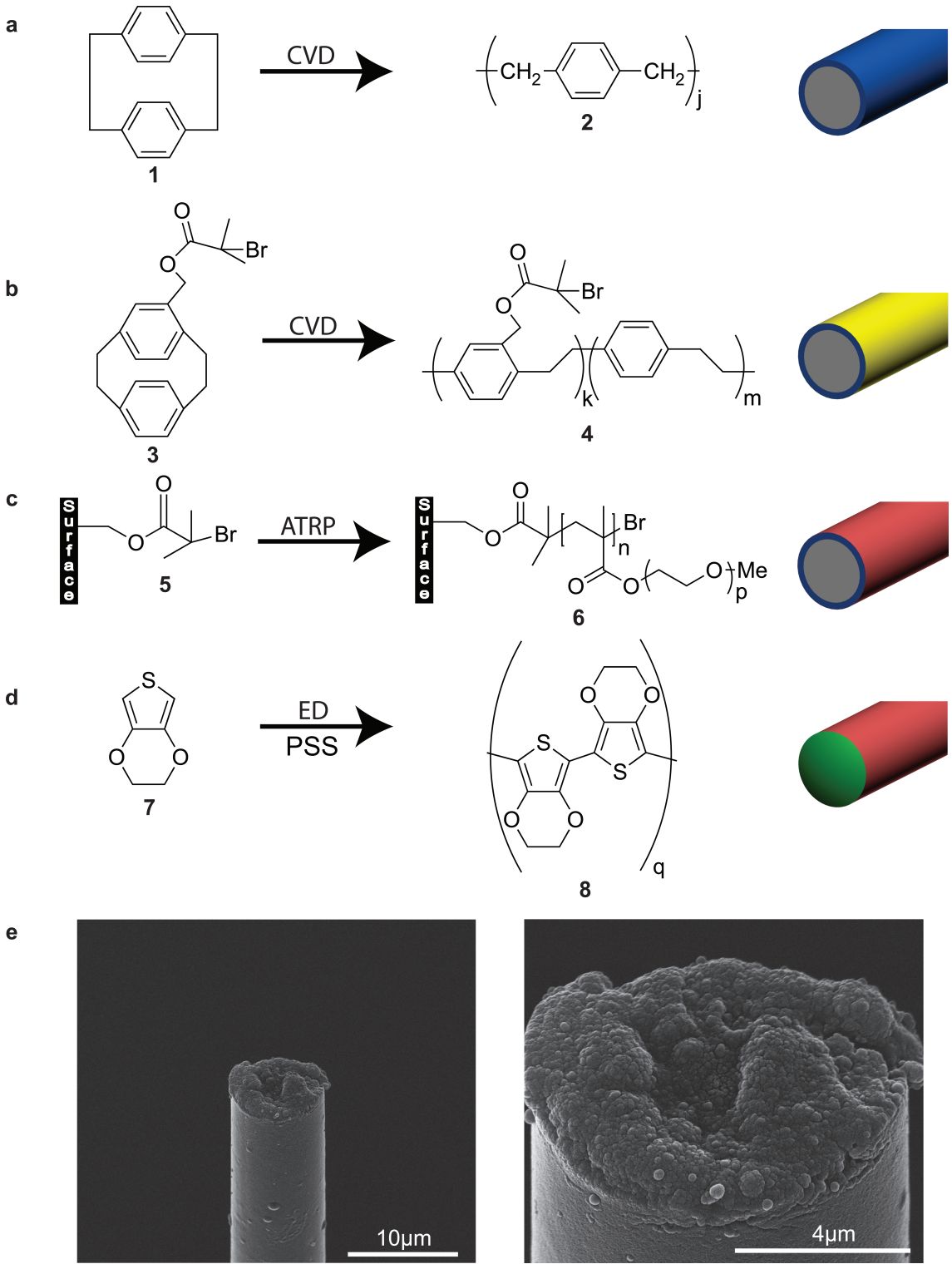

Figure 4.1: Preparation of a MTE; (A) carbon fibers are coated with 800 nm poly(p-xylylene). (B) the fiber is further coated with a 50 nm layer of poly[(p-xylylene-4-methyl-2-bromoisobutyrate)-co-(p-xylylene)]. (C) PEG is covalently grafted onto poly[(p-xylylene-4-methyl-2-bromoisobutyrate)-co-(p-xylylene)] through ATRP. (D) Insulation is removed by cutting away the tip to expose a carbon site, and then electrodeposited with PEDOT. (E) SEM of a modified MTE. (F) Size comparison of a 5 mm Michigan style electrode, 50 μm diameter microwire and a MTE.

4.2 Methods

4.2.1 Carbon Fiber Microthread Electrodes

One, two, or three individual 7 μm diameter (tensile modulus = 234 GPa) carbon fibers were mounted onto a NeuroNexus A16 printed circuit board or a bare stainless steel wire using silver epoxy (WPI; Sarasota, Fl) and baked at 140 °C for 10 min. An ~800 nm thick poly(p-xylylene) insulator layer was then coated via CVD. One gram of paracyclophane was sublimed at 90-110 °C and 0.3 mbar and carried into the pyrolysis chamber by argon at a flow rate of 20 standard cubic centimeters per minute (sccm). After pyrolysis at 670 °C, the polymer was deposited on the substrate at 15 °C. The deposition rate, according to the QCM, was 0.6-1.0Å/s.

4.2.2 Atom Transfer Radical Polymerization

Poly(ethylene glycol methacrylate) was grafted onto the poly(p-xylylene) surface by atom transfer radical polymerization (ATRP). Poly[(p-xylylene-4-methyl-2-bromoisobutyrate)-co-(p-xylylene)] was used as initiator for ATRP because of its functional groups (Jiang et al., 2008). After CVD polymerization of poly[(p-xylylene-4-methyl-2-bromoisobutyrate)-co-(p-xylylene)], MTEs were incubated under inert conditions with a degassed aqueous solution of oligo(ethylene glycol) methyl ether methacrylate, with CuBr/CuBr^2/bpy as the catalyst. The polymerizations proceeded at room temperature for 4 h. MTEs were thoroughly rinsed after the reaction.

4.2.3 Microscopic Raman Spectroscopy

The carbon nanotube samples were analyzed using a Bruker SENTERRA Raman system (Bruker Optik GmbH, Ettlingen, Germany) based on an Olympus BX 51 microscope (Olympus Corp. Tokyo, Japan), and an Olympus UIS-2 LMPlanFL N 100x/0.80 objective (Olympus Corp. Tokyo, Japan) with 2 μm resolution for the

lateral and axial direction was used. The equipped 532 nm laser was chosen for the measurements of the sample surfaces. In order to avoid thermal decomposition of the sample, the laser power was attenuated to 2mW for the analysis. The spectra were recorded in the region from 100 to 4000 $cm^{-}1$ for each sample.

4.2.4 EDX Analysis

Energy-dispersive X-ray spectroscopy (EDX) is a technique for elemental analysis of a sample. This technique is based on the fundamental principle that each element has a distinct atomic structure, which emits a unique characteristic X-ray to be analyzed. It relies on analyzing X-rays emitted by the sample upon hitting with charged particles. The inner shell electrons of the atoms in ground state could be ejected by the high energy particles. The outer shell higher energy electrons would replace the hole from the ejected electron. An X-ray would be emitted during this process due to the difference in the energy between the inner and outer electrons. The number and energy of the X-rays emitted from a sample can be measured by an energy-dispersive spectrometer, and this allows the elemental composition of the sample to be measured.

4.2.5 Grafting to Functionalized Coating: Active Ester

Poly(p-xylylene carboxylic acid pentafluorophenolester-co-p-xylylene) is a polymer with an active ester group which can readily react with primary amine (Lahann et al., 2001). After chemical vapor deposition of poly(p-xylylene carboxylic acid pentafluorophenolester-co-p-xylylene), MTEs were incubated in 10mM mPEG-NH2 (MW 10,000) PBS solution for 8h, followed by thorough rinses in PBS.

4.2.6 Protein Adsorption

Poly(p-xylylene)-coated and PEGMA-grafted devices were incubated in FITC-albumin in 2mg/ml Phosphate Buffer Saline (PBS) solution for 1 hour, then washed in PBS for 30m. Confocal images were taken with an SP2 confocal laser scanning microscope (Leica, USA). Immediately after, FITC-albumin was imaged with an Ar/ArKr laser at 488nm.

4.2.7 Recording Site

Poly(p-xylylene)-coated and PEGMA-grafted carbon fibers were then cut to a length of 0.3-0.5 cm. For PEDOT deposition, monomer 3,4-ethylenedioxythiophene (EDOT) (Bayer, Germany) was electrochemically polymerized and deposited onto the surface of the electrode sites together with the anions in the solution. Specifically, PEDOT/PSS was electropolymerized from a 0.1 M poly(sodium-p-styrenesulfonate) (PSS) (Acros Organics; Morris Plains, NJ) aqueous solution with an EDOT concentration of 0.01 M under galvanostatic conditions. In galvanostatic mode, the current was held at 100 pA.

4.2.8 SEM Imaging

SEM imaging was carried out on a FEI Quanta 200 3D Focussed Ion Beam Workstation. Samples were sputter coated with gold prior to imaging.

4.2.9 Surgery

The microthread probes were manually inserted into rat cerebral cortex to validate the insertion technique in a typical experimental preparation. Adult male Sprague-Dawley rats (Charles River Laboratories) weighing 300-350g were prepared for cortical implants using previously established methods (Ludwig et al., 2006). The animal

was anesthetized with a mixture of 50 mg/mL ketamine and 5 mg/mL xylazine administered intraperitoneally with an initial dosage of 0.125 mL/100 g of body weight and regular updates of ketamine. The depth of anesthesia was observed by monitoring heart rate and blood oxygen saturation. The animal was placed into a stereotaxic frame and a 2 mm by 2 mm craniotomy was made over the motor cortex. The dura was incised and resected. Sterile saline was used to keep the brain surface moist throughout the procedure. A stereotaxic frame mounted micromanipulator guided insertions of the MTE 2 mm into the cortex. Due to the stiffness of the carbon fiber, a 5-2.5 mm long fiber did not need additional assistance penetrating the cortex when aligned perpendicularly to the cortical surface. For chronic implants, a bone-screw grounded the electrode connected over parietal cortex using a stainless steel ground wire. Surgical closure was achieved with a combination of silicone (World Precision Instruments, Sarasota, FL), and Cerebond adhesive (MyNeurolab.com, St. Louis, MO). For chronic histology, a 5 mm Michigan Electrode (NeuroNexus Technologies, Ann Arbor, MI) was inserted 500 μm away from the MTE. Both probes were tethered to the skull using silicone and Cerebond adhesives. All procedures complied with the United States Department of Agriculture guidelines for the care and use of laboratory animals and were approved by the University of Michigan Committee on Use and Care of Animals.

4.2.10 *In vivo* Neural Recordings

For all animals in this study, electrophysiological data were acquired using a TDT RX5 Pentusa Recording System (Tucker-Davis Technologies, Alachua, FL). These neuronal signals were acquired through a head-stage buffer amplifier to avoid signal loss in data transmission. Signals were sequentially filtered by an anti-aliasing filter in the preamplifier, digitized at a $\sim$25-kHz sampling rate, and digitally band-pass

filtered from 2 to 5000 Hz. Wideband signals were acquired to capture both spiking and LFP activity. Signals were continuously recorded in segments ranging from 30 seconds to $>$ 10 minutes in duration.

Neural recording segments were analyzed offline to determine the number of neurons recorded, noise levels, and signal amplitudes using custom automated MATLAB (Mathworks Inc., MA) software, as described elsewhere (Ludwig et al., 2006). As an overview, the wide-band recordings were filtered in software to isolate the spike data (300-5000 Hz) from the LFP data (1-100 Hz). The LFP power spectral density plots were created using a Hamming window for smoothing with a 32768-point fast Fourier transform (FFT). Low frequency activity in the range typically observed for LFPs is presented. To identify individual units, the threshold for the high-frequency data was established by using a window set at 3.5 standard deviations below the mean of the data. A 3-msec waveform was extracted from the data stream at each threshold crossing. To group isolated waveforms to a single neuronal unit, principal component analysis was then completed, and the resultant components were separated into individual clusters by using Fuzzy C-means clustering. Units with sufficiently clustered principal components were plotted, and the signal-to noise ratio was calculated as the peak-to-peak amplitude of the mean waveform of the cluster divided by two times the standard deviation of the remaining data stream after all waveforms had been removed.

4.2.11 Impedance Spectroscopy Measurements

EIS and CV measurements were made using an Autolab potentiostat PGSTAT12 (Eco Chemie, Utrecht, The Netherlands) with associated frequency response analyzer and general purpose electrochemical system software (Metrohm, Westbury, NY), respectively. To obtain EIS and CV measurements, each probe was submerged in a

phosphate buffered saline (PBS) solution of 137mM sodium chloride, 2.7 mM potassium chloride, and 11.9mM phosphate buffer with a stainless steel rod serving as the counter electrode and a standard Ag—AgCl probe as the reference. Impedance measurements were taken between 10Hz and 31kHz at 25 mVrms. CV values were obtained by cycling three times from 0.8V to -0.6V at a sweep rate of 1 V/s and averaging the data. Charge storage capacity (CSC) of each site was calculated from the full area under the CV curve, scaled by the inverse of the scan rate. After implantation, a distant stainless steel (316-SS grade) bone screw was used as the reference and counter electrode.

4.2.12 Vasculature and BBB Disruption: Acute Histological Imaging

A 5 mm Michigan electrode was inserted into the cortex at least 49 μm away from all surface vessels24. Immediately after, a MTE was inserted into the cortex at least 1 mm away from the silicon electrode. 2 % evans blue (EB) at a dose of 2 ml/kg was injected intervenously into the tail vein at a rate of 0.45 ml/min. Brains were fixed with a transcardial perfusion with 100 ml of PBS followed by 250 ml of 4 % paraformaldehydesolution in pH 7.4 phosphate buffer, and then fixed in the same solution for another 24 h. Tissue was then rinsed with 1x PBS twice for 15 min to remove any excess paraformaldehyde. All procedures complied with the United States Department of Agriculture guidelines for the care and use of laboratory animals and were approved by the University of Michigan Committee on Use and Care of Animals.

The tissue sample was removed from the fixative and placed in 15 % sucrose w/v in 1X PBS until the brain sank to the bottom of the solution. The sample was then transferred to a 30 % sucrose solution until sunk. For 1-3 hr, the sample soaked in 30% sucrose:OCT embedding media (2:1) solution. A cryomold was filled with

20% sucrose:OCT embedding media (2:1) solution and the block of tissue placed within the mold. A weigh boat was filled with 2-Methylbutane and placed in dry ice for 15 min. After 15 min, the cryomold was placed in the weigh boat with the 2-methylbutane. Care was taken to ensure that the solution did not flood the inside of the mold. The sample was then allowed to slowly freeze. Upon complete freezing, sample was stored in a -80 °C freezer.

Samples were "thawed" to -20 °C at least 1 hour prior to sectioning. Each brain was then sliced on a cryostat into sections 30 μm thick and then, without further staining, placed on slides and coverslipped with ProLong Gold for microscopic examination.

The sections were imaged under a fluorescence microscope (Olympus BX51, MIL) for staining intensity. EB absorbs at 470 nm & 540 nm and emits at 680 nm. Dye indicates neural vasculature and locations in the brain where the microelectrode disrupted the vasculature and compromised the BBB.

4.2.13 Chronic Immunohistochemistry

Rats were perfusion-fixed with 4% paraformaldehyde two weeks after implant. Brains were then dissected with devices in place and block-fixed for 24 hr at 4 °C. Devices were removed; the brains were blocked, and 100-μm vibratome tissue slices were cut in a direction perpendicular to the long axis of the inserted device. Sections were then treated with 5 mg/mL sodium borohydride in HBHS for 30 min, followed by three rinses with HEPES-buffered Hanks saline (HBHS). In all steps involving HBHS, sodium azide (90 mg/L) was included. Tissue sections were then incubated in 0.5 % (v/v) Triton X-100 in HBHS for 30 min, followed by three washes with HBHS and then blocked overnight at room temperature with 5 % (w/v) goat serum. Sections were washed four times, for 30 min each, with HBHS. A multi-step immuno-

histochemical approach was needed due to cross reactivity seen when applying both the GFAP anti-rat primary and the Anti Rat Blood Brain Barrier (EBA) anti-mouse primary simultaneously. Our experience with the GFAP anti-rat primary antibody indicates that the anti-mouse primary and subsequent secondary needs to be applied first, followed by the GFAP primary and other primary anti-bodies. This method yields two complete separated channels for GFAP and EBA. The method is as follows: tissue was then incubated overnight at room temperature with the EBA primary antibody (1:300, Anti Rat Blood Brain Barrier, monoclonal anti-mouse; Covance SM171 lot 2) with 0.2% triton. After 24 hr, the sections were washed four times for 30 min each with HBHS. Sections were then incubated in a secondary antibody with 0.2% triton (1:200; Alexa Fluor 494 goat anti-mouse secondary antibody; Invitrogen, Carlsbad, CA), overnight at room temperature. After four 30 min washes, the tissue was incubated overnight at room temperature with the GFAP primary antibody (against astrocytes1:1000, anti rat; Invitrogen 1-0300 Lot 686276A), Iba-1 (against microglia, anti-rabbit, 1:800 Wako, 019-19741 Lot STN0674) containing 0.2% triton. After 24 hr, the sections were washed four times for 30 min each with HBHS. Sections were then incubated in a secondary antibody with 0.2% triton (1:200; Alexa Fluor 546 goat anti-rat, 1:200; Alexa Fluor 488 goat anti-rabbit secondary antibody; Invitrogen, Carlsbad, CA) and Hoechst 33342 (nuclei stain 1:150, Invitrogen H-1399 Lot 46C3-4), overnight at room temperature. After the final washes (four times for 30 min each with HBHS), tissue slices were mounted on slides with coverslips using Prolong Gold mounting media (Invitrogen). The slides remained covered (protected from light) at room temperature and allowed to clear for at least 12hrs prior to imaging.

4.2.14 Imaging and Image Processing

Images were obtained on a Leica TCS SP5 scanning laser multiphoton confocal microscope. All images were collected using a 40x objective (1.30 NA with a zoom of 1.25 = final 50x). Individual Z slices were acquired at 0.63 μm step sizes. The nuclei channel was collect in sequence using the multiphoton. Standard TIFF files were saved and were colorized using Image Pro Plus (Media Cybernetics, Bethesda, MD).

4.3 Results

4.3.1 Fabrication validation

In order to validate each of our fabrication process (Fig. 4.1) surface materials after each step were characterized using Raman Spectroscopy (Figure 4.2). Characteristic peaks of carbon fiber, parylene-N, and PEDOT were labeled with their respective wavelengths. This demonstrates that the parylene insulation was present along the carbon fiber surface. Also, PEDOT was detected at the tip of the device, but not along the insulated sides of the microthread electrode. The Poly[(p-xylylene-4-methyl-2-bromoisobutyrate)-co-(p-xylylene)] and PEGMA coatings were not detectable using Raman Spectroscopy, perhaps due to relatively low thickness of these coatings. Therefore, EDX was also used to characterize the surface material after each fabrication step (Figure 4.3). Carbon fiber and parylene-N are both made of only carbon elements, so they were not discernable using EDX (Figure 4.3A, 4.3B). The bromine element could be detected after the 50 nm coating with Poly[(p-xylylene-4-methyl-2-bromoisobutyrate)-co-(p-xylylene)] (Figure 4.3C). An increase in oxygen was detected as expected after the PEGMA coating (Figure 4.3D). Sulfur was detected in PEDOT at the tip of the assemble Microthread Electrode (Figure

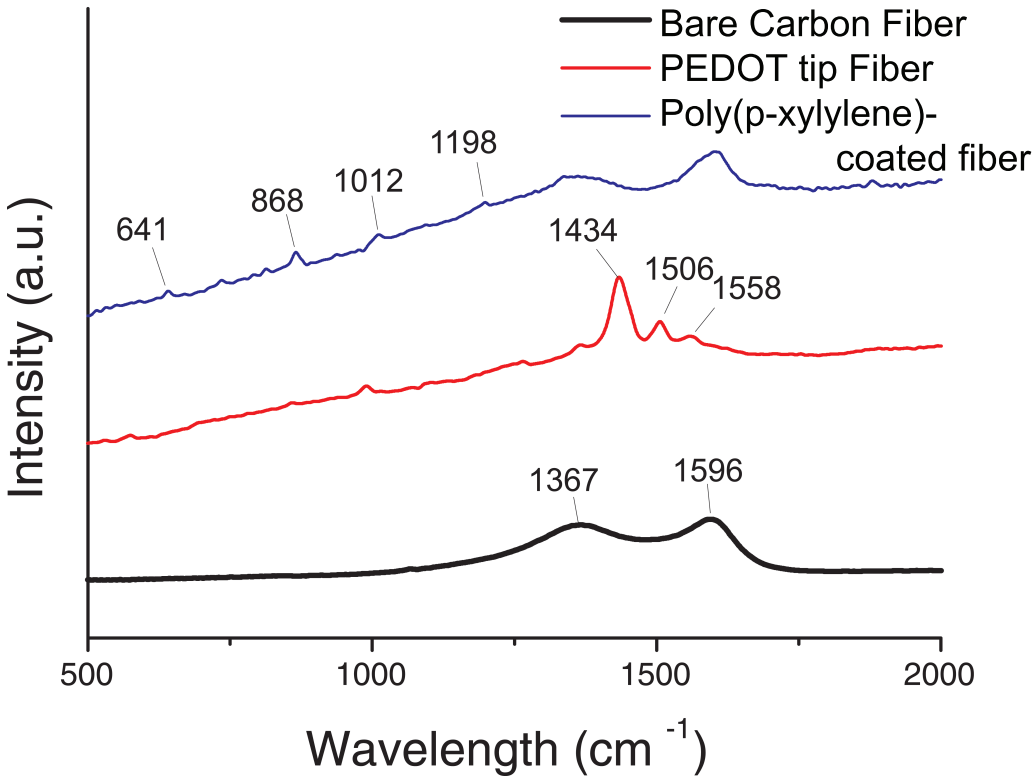

Figure 4.2: Raman Spectroscopy Analysis of Microthread Electrode components; bare carbon fibers (black), poly(p-xylylene) coating (blue), and PEDOT recording tip (red). Characteristic bands are labeled with their respective wavelengths.

4.3E). This suggests that each component of the fabrication is assembled into the Microthread Electrode.

4.3.2 *In vitro* characterization

The MTE electrical properties were characterized by impedance spectroscopy (EIS) and cyclic voltammetry (CV). Measurements were taken for two controls: poly(p-xylylene)-insulated carbon fibers, and poly(p-xylylene)-insulated fibers with a $\sim$38.5 μm^2 exposed cut carbon tip. Lastly, poly(p-xylylene)-insulated MTEs with increasing PEDOT/PSS deposited recording site were characterized. EIS measurements displayed a progressive decrease in impedance as the insulation at the tip was removed and then with increasing PEDOT deposition (Fig. 4.4A). The phase dia-

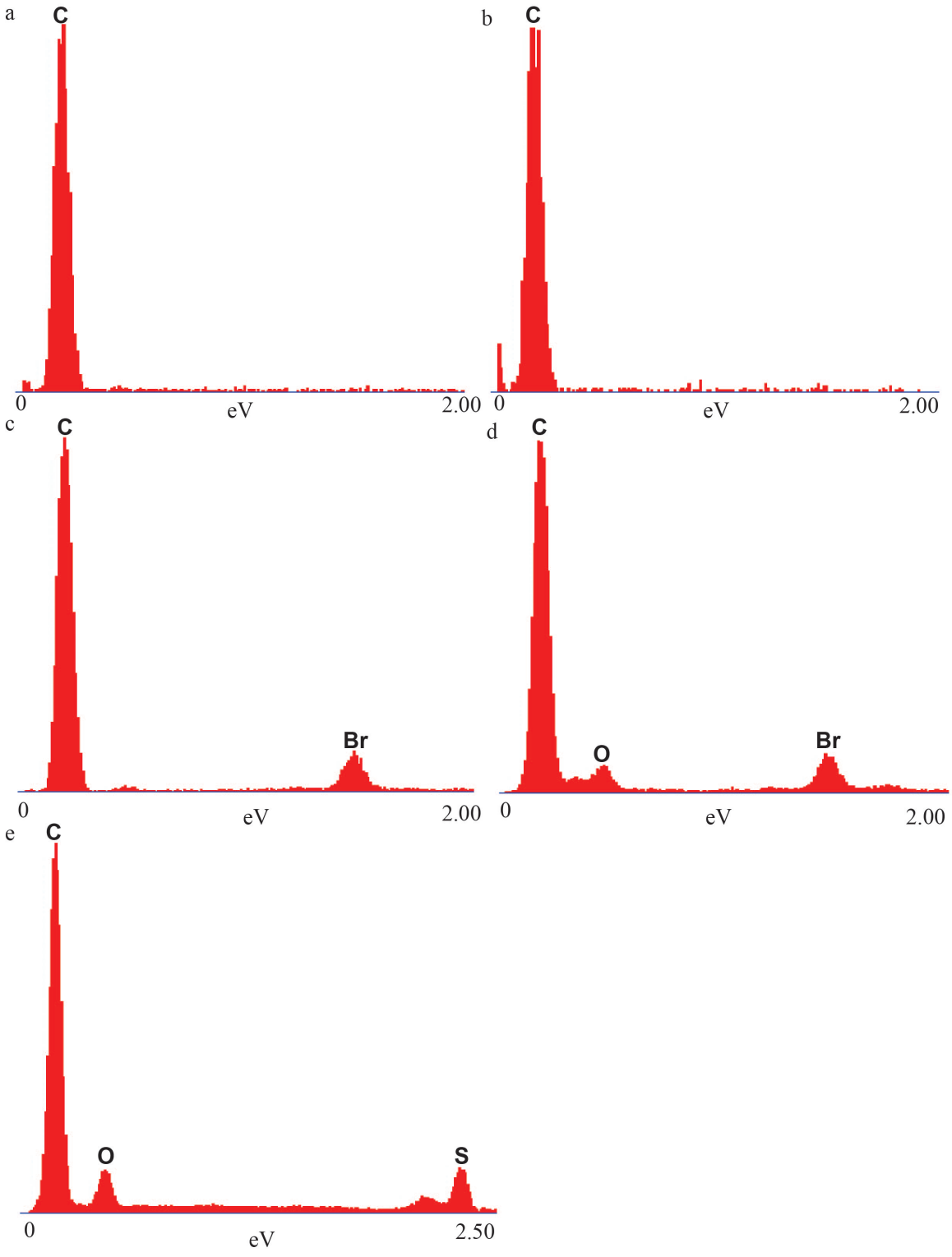

Figure 4.3: Stepwise EDX Analysis of Microthread Electrodes of MTE component throughout fabrication. (A) Carbon fiber, (B) Poly(p-xylylene), (C) Poly[(p-xylylene-4-methyl-2-bromoisobutyrate)-co-(p-xylylene)], (D) PEGMA, (E) PEDOT.

gram also shows decreasing phase delay with increasing PEDOT deposition which is indicative of PEDOT-coated electrical sites (Fig. 4.4B). CV measurements also showed increased charge storage capacity with increased PEDOT deposition (Fig. 4.4C). CV profiles indicate the presence of PEDOT on the recording site.

4.3.3 Stiffness

The MTEs also have a beneficial combination of mechanical properties for a neural probe in terms of stiffness, strength, and size. The stiffness (k) was calculated by:

$$k = \frac{AE}{l} \tag{4.1}$$

where A is the cross-sectional area, E is the elastic modulus, and l is the length of the device implanted into the cortex. The calculated k of a MTE is 4,540 N/m which is an order of magnitude smaller than a conventional silicon microelectrode of the same length, 151,000-246,000 N/m (Table 4.1) (Lee et al., 2005). Similarly, the spring constant k_c for a cantilever beam was calculated by:

$$k_{c(planar)} = \frac{Ewt^3}{4l^3} \tag{4.2}$$

or

$$k_{c(cylinder)} = \frac{3\pi E(d_o^4 - d_i^4)}{64l^3} \tag{4.3}$$

where E is the elastic modulus, w is the width of the probe, t is the thickness of the probe, d_o is the outer diameter, d_i is the inner diameter, and l is the length. k_c for a conventional silicon microelectrode is 2.13-3.46 N/m in the direction normal to the recording surface and 143-613 N/m in the lateral direction, while k_c for the MTE is 0.0106 N/m in all radial directions (Table 4.1, Fig. 4.5). This reduced

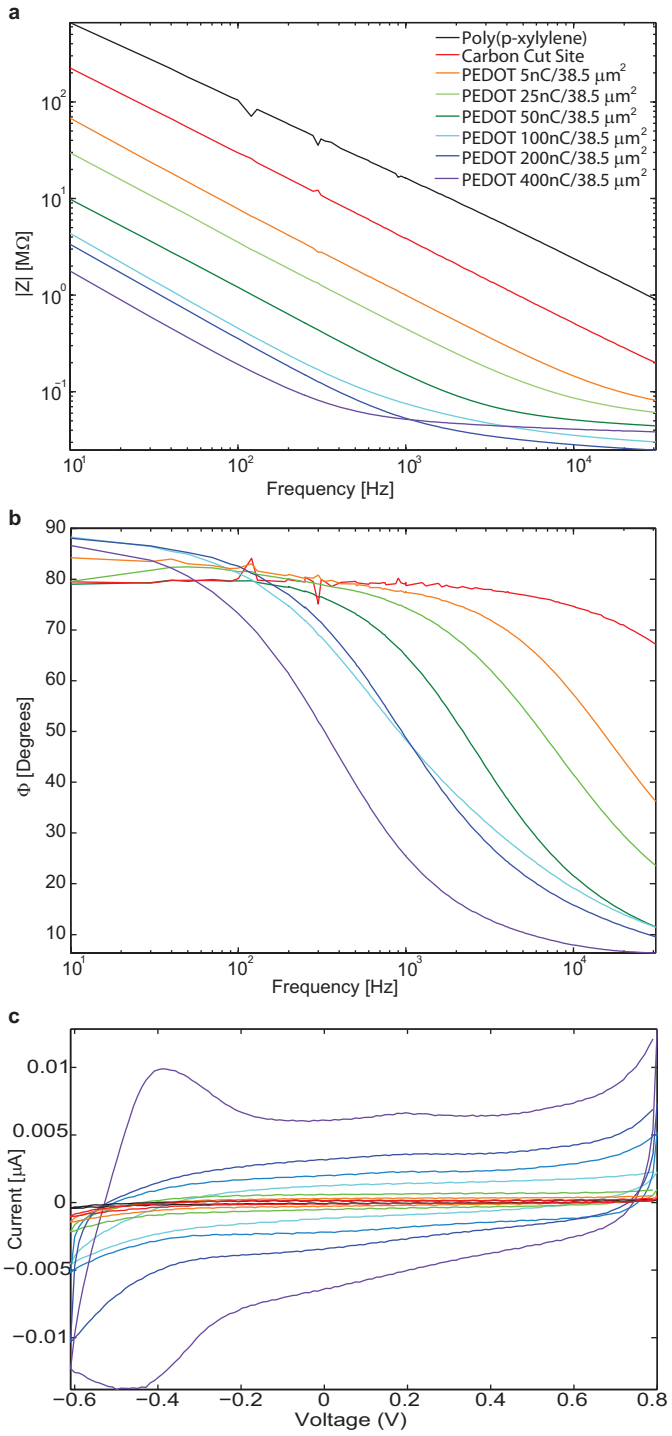

Figure 4.4: (A-B), Electrical characterization of poly(p-xylylene)-coated fiber, poly(p-xylylene)-coated carbon fiber with an exposed carbon tip, and poly(p-xylylene)-coated carbon fiber with an PEDOT/PSS recording site electrodeposited with 5 nC, 25 nC, 50 nC, 100 nC, 200 nC, 400 nC. a, Bode magnitude impedance plot. (B) Bode phase plot. The poly(p-xylylene)-insulated fiber without recording site was not plotted since a reliable signal could not be detected. (C) CV plot.

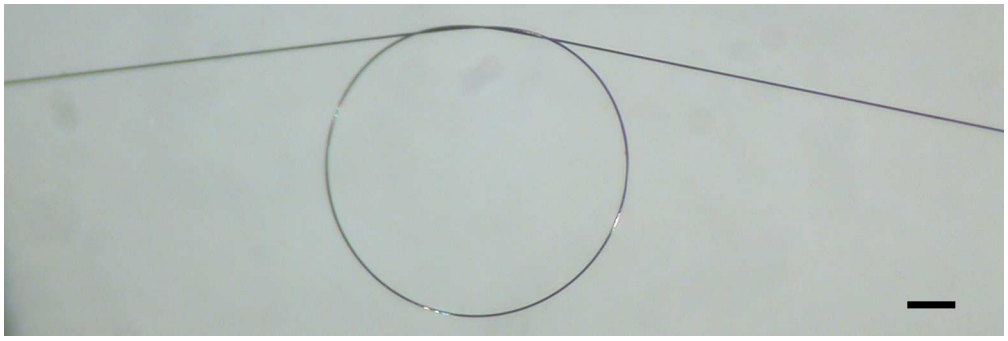

Figure 4.5: Demonstration of the flexibility and strength of Microthread electrodes. Scale indicates 100 μm.

k and k_c is primarily the result of the small diameter carbon fiber and the use of thin, parylene coating (Fig. 4.6A). Stiff implanted probes tethered to the skull may also cause rupture of nearby BBB during micromotion or physiological motion (Bjornsson et al., 2006; Subbaroyan et al., 2005).

Table 4.1: Stiffness of conventional silicon Michigan Electrode and Microthread Electrode.

Material	3mm-Si Elec	5mm-Si Elec	Parylene	C. Fiber	MTE
A (μm^2)	1,845	3,000	19.59	38.47	58.06
E (GPa)	164	164	4	234	
k (N/m)	151,000	246,000			4,540
$k_{c(planar)}$ (N/m)	2.13	3.46			0.0106
$k_{c(lateral)}$ (N/m)	143	615			0.0106

Length (l) was calculated for 2mm implants fixed to the skull at the surface of the brain

4.3.4 Anti-biofouling

The MTEs have a biofouling-resistant surface through functionalizing the outer poly(p-xylylene)-insulation with PEGMA, an anti-biofouling molecule. Although stab wound studies show limited chronic tissue damage (Biran et al., 2005), plasma protein adsorption onto the electrode may perpetuate the tissue response in chronically implanted neural electrodes. For example, albumin is a plasma protein that is, in part, responsible for inducing glial cell activation and proliferation (Ivens et al., 2007; Nadal et al., 1995, 1998). Within the central nervous system, anti-biofouling

coatings may only have to be stable long enough for cells to repair the BBB and clean up the plasma exudates. As such, covalently grafted functional bioactive surface materials may be more effective for improving chronic neural interfaces than rapidly dissolving anti-biofouling hydrogels. The organic PEGMA surface material demonstrated improved anti-biofouling properties from FITC-albumin adsorption compared to the native poly(p-xylylene) surface *in vitro* (Fig. 4.6B, 4.6C). The covalently grafted PEGMA layer has an added benefit of further minimizing the biosensor footprint compared to traditional drug eluting hydrogels that acutely push tissue away from the electrode surface. To the authors' knowledge, this is the first demonstration of functionalized poly(p-xylylene) coating in a functional neural biosensor. These properties are especially important when chronic use of the probes is intended.

4.3.5 Acute histology

One important aspect of the unique integration of novel functional materials is that it enables a significant reduction in footprint (Fig. 4.6A) that minimizes insertion damage, while maintaining comparable performance data. During insertion, the highly regulated blood brain barrier (BBB) is compromised as the implantation of microelectrodes punctures and tears neural vasculature (Bjornsson et al., 2006; Kozai et al., 2010) leading to plasma release into the surrounding parenchyma. BBB disruption caused by probe insertion leads to a net increase in extracellular water content(Unterberg et al., 2004) and intracranial pressure (Barzo et al., 1997) often associated with tissue damage (Dixon et al., 1991). This acute trauma leads to the release of erythrocytes, and inflammatory factors from disrupted blood vessels, which facilitate recruitment of activated microglia and astrocyte in a broad region around the inserted probe(Grill et al., 2009; Ivens et al., 2007; Szarowski et al., 2003;

Turner et al., 1999). Minimizing the device footprint is important for minimizing insertion trauma by reducing infiltration of blood components and pro-inflammatory signaling, especially when not using a positional guide to avoid large vasculature deep in the cortex (Kozai et al., 2010). It can also minimize disrupting arterioles from insertion causing loss of perfusion to tissue below the disrupted region, where the recording sites are located, leading to additional neuronal damage by means of ischemia (Kozai et al., 2010; Nishimura et al., 2007). Furthermore, the smaller feature size reduces the increase in intracranial pressure caused by tissue displacement from the probe footprint, which can improve recordings in acute experiments. However, the challenge with silicon technology is the difficultly in scaling to a single trace sub-cellular size while maintaining structural and electrical integrity when fixed to the skull. The novel MTEs have a total ~8.5 μm diameter which allows for a sub-cellular cross-section. Acute histological analysis shows that bleeding is limited around MTE probes (Fig. 4.6D, 4.6E, 4.6F). It also demonstrates that these biosensors can be implanted into the cortex. On the other hand, substantial bleeding can be observed around a conventional silicon probe (Fig. 4.6G, 4.6H, 4.6I). The diameter of the probe tract created by the MTE can be smaller than some major blood vessels in the cortex. The improved sub-cellular structure enabled by the composite material, may enhance the interface across multiple dimensions. To the authors' knowledge, this is the smallest electrical biosensor to be implanted in cortex as a stand-alone biosensor.

4.3.6 Acute *in vivo* electrophysiology

Two fiber Microthread Arrays (MTA) as well as single MTEs were implanted into rat motor cortex (Fig. 4.7A). MTAs contained one carbon recording site and one PEDOT recording site. MTEs contained either a carbon recording site or a

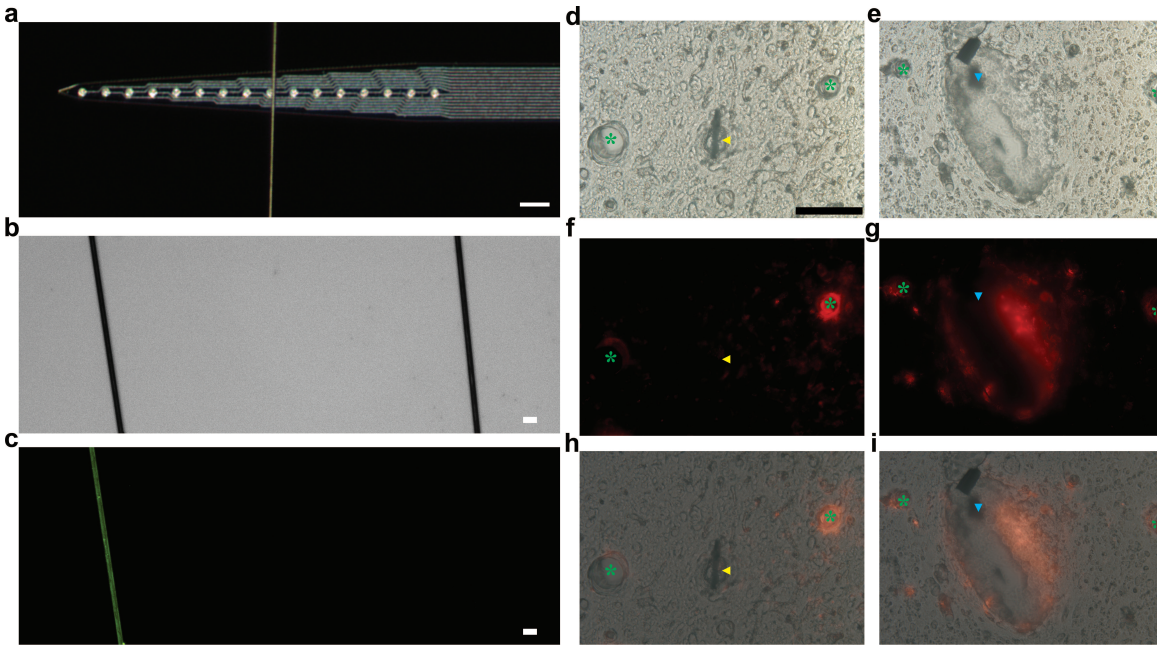

Figure 4.6: (A) Comparison of a MTE to a 5 mm Michigan Electrode. Scale bar indicates 100 m. (B) FITC-albumin adsorbed onto poly(p-xylylene)-coated device (left) and ATRP PEGMA surface coated device (right). Scale bar indicates 20 m. (C) Same image as above under fluorescent microscopy showing less protein adsorption onto the PEGMA surface (right) compared to the poly(p-xylylene) surface (left). (D)-(I), Comparison of acute BBB disruption from probe insertion in rat cortex. (D) Differential interference contrast (DIC) image of rat motor cortex section around a MTE foot print. MTE probe is indicated by a yellow arrow. Scale bar indicates 100 m. (E) A BBB impermeable fluorescent dye was used to image vasculature and bleeding around the MTE. (F) Overlay of image (D) and (E). (G) DIC image of a 5mm silicon Michigan probe in the same section. (H) Bleeding around the silicon probe. (I)Overlay of image (G) and (H). Green asterisk indicate large blood vessels.

PEDOT recording site. *In vivo* cortical recordings with PEDOT/PSS deposited poly(p-xylylene)/carbon fibers were able to record neural spikes (Fig. 4.7B). In all *in vivo* trials, the PEDOT/PSS-coated MTE was acutely able to detect at least one neuronal spike with a signal-to-noise ratio (SNR) greater than four standard deviations. On the other hand, poly(p-xylylene)-insulated carbon fibers with a cut carbon exposed recording site were unable to record any neuronal spike with an SNR greater than four standard deviations (Fig. 4.7B). Finally, an uninsulated carbon fiber implanted 2 mm into the cortex was able to record local field potential (LFP), but unable to discriminate any single unit spikes (Data not shown). Figure 4.7C-E show sorted single unit activity; pile plot (Fig. 4.7C), principle component analysis (Fig. 4.7D), and the mean waveform (Fig. 4.7E). On the other hand, simultaneous LFP recordings indicated that both materials are able to detect similar activity; however the PEDOT/PSS recording site was able to detect LFPs with higher amplitude (Fig. 4.7F). Phase differences between carbon and PEDOT/PSS sites between the LFP ranges (Fig. 4.4B) also verified that carbon and PEDOT/PSS recording sites can detect similar LFP activities. This is also demonstrated by the power spectral density plot of the neural recordings showing the intensity of the recordings as a function of frequency (Fig. 4.7G). Peak observed around 9-Hz is representative of low-frequency synchronous activity in the alpha band. These recordings demonstrate the ability to insert and record-high-quality unit activity from viable neurons located close to the MTE. To the authors' knowledge, this is the smallest recording site, approximately the size of a cell body, but with excellent electrical characteristics.

An alternative PEGMA grafting-to technique to ATRP was explored using an active ester functionalized parylene, Poly(p-xylylene carboxylic acid pentafluorophenolester-co-p-xylylene) (Lahann et al., 2001). Acutely, this alterna-

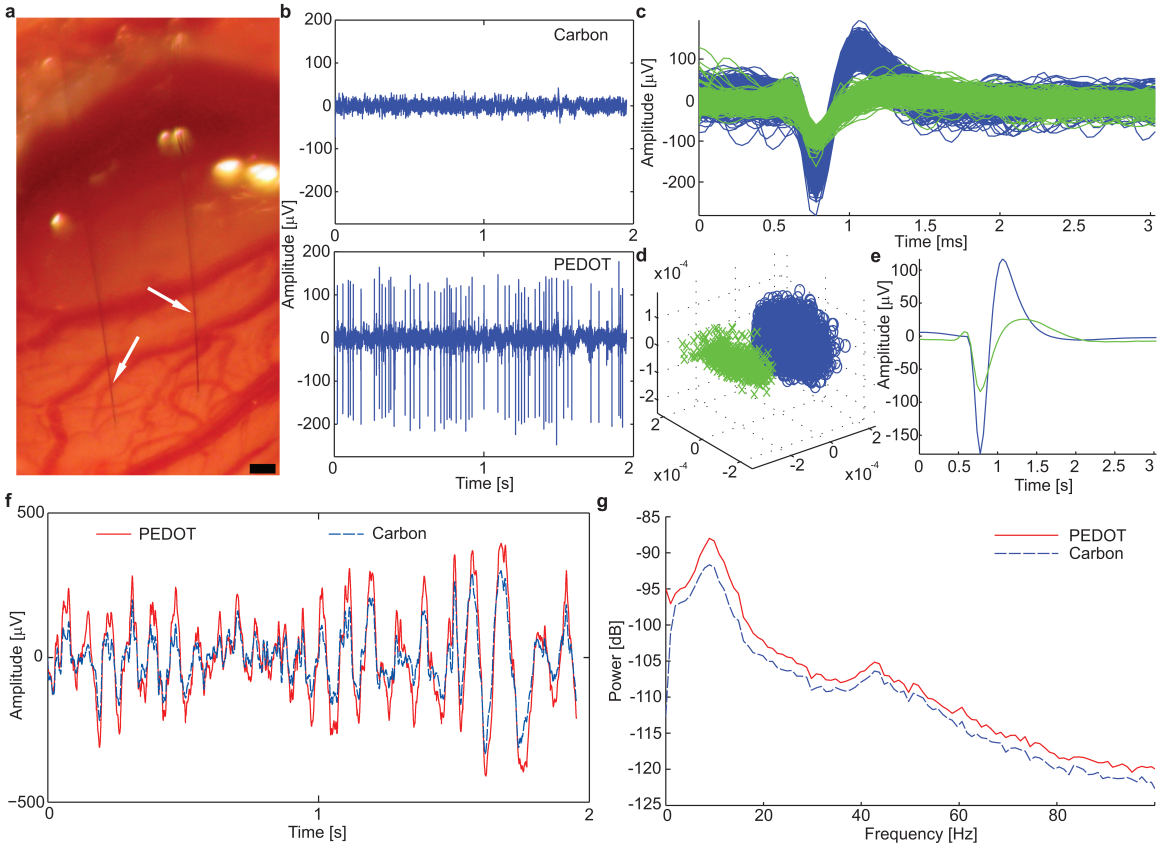

Figure 4.7: (A) Stereotrode MTA implanted 1.6 mm deep into cortex. (B) Representative example of two seconds of high-speed recordings taken simultaneously on the same array. Recordings on the carbon site channel shows an signal-to-noise ratio of 0 and noise floor of 16.6 μV (top), while recordings taken on the channel with the PEDOT/PSS site shows signal-to-noise rations of 12.7 and 4.71 and noise floor of 23.4 μV (bottom). (C) Piled single unit neural recordings over three minutes from a poly(p-xylylene)-coated PEDOT/PSS device. (D) Results from principal component analysis showing two distinct clusters. (E) Mean waveform for each unit spike. (F) Raw LFP simultaneously recorded across both channels. The PEDOT/PSS site channel recrorded a noise floor of 332 μV (solid red), while the carbon site channel recorded a noise floor of 233 μV (dash blue). (G) Power density spectra across the LFP range showing that for the LFP range both recording materials are similar.

tive coating technique demonstrated no noticeable difference in electrophysiological recording performance compared to ATRP PEGMA MTEs (Figure 4.8).

4.3.7 Chronic *in vivo* electrophysiology

Initial chronic neural recording studies suggest that these biosensors are stable over several weeks in the brain. MTEs demonstrated high yield across animals for detecting single unit activity overtime (Fig. 4.9A), which is comparable or better than the yield of conventional silicon devices (Ludwig et al., 2006) or wire microelectrode arrays (Williams et al., 1999). The mean SNR of the largest discernable single unit detected by each MTE shows the stability of the chronic single unit recordings (Fig. 4.9B, 4.10). During the initial inflammation period, the SNR decreases, then increases temporarily to a peak around one week before stabilizing. Tissue response to stab wounds subsides by four weeks (Biran et al., 2005) suggesting stabilization of the tissue after surgery. For this reason, electrophysiological recordings were continued up to five weeks. By the second week the single units appear to stabilize as indicated by the decreased fluctuation and standard deviation. This is stabilization period is similar to previously reported studies (Ludwig et al., 2006; Williams et al., 1999). Deconstructing the mean SNR of the largest discernable single unit to the units' amplitude and the electrodes' noise floor shows that the fluctuations in SNR in the first two weeks is due to fluctuations largely in signal amplitude as opposed to fluctuations in noise floor (Fig. 4.9C). Examining individual electrodes for SNR or signal amplitude fluctuations further demonstrate the large variability observed in the first week after implantation, and stabilization after the second week (Fig. 4.9D, 4.10). Figure 4.9E-F and Figure 4.9I-L demonstrate two examples of 5+ week chronic recordings from two different animals. These initial chronic recording studies suggest that these biosensors remain intact in the brain over moderate lengths

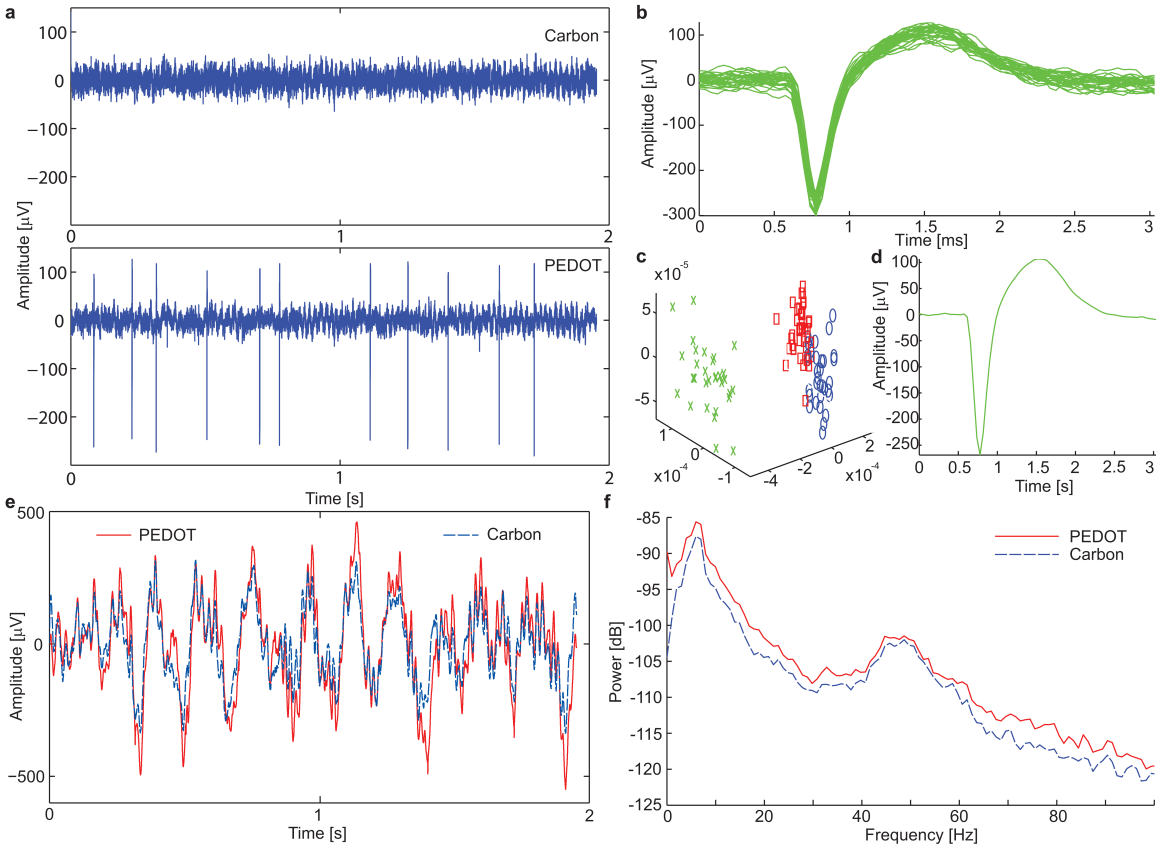

Figure 4.8: *In vivo* single unit recording capabilities of active ester grafted PEGMA coated MTE. (A) Two-fiber Microthread Array implanted 1.6mm deep into cortex. (B) Representative example of two seconds of high-speed recordings taken simultaneously on the same array. Recordings on the carbon site channel shows an signal-to-noise ratio of 0 and a noise floor of 21.9 μV (top), while recordings taken on the channel with the PEDOT site shows signal-to-noise rations of 19.3 and peak-to-peak noise of 19.4 μV (bottom). (C) Piled single unit neural recordings over three minutes from a parylene-N coated PEDOT MTE. (D) Results from principal component analysis showing three distinct clusters. (E) Mean waveform for each unit spike. (F) Raw local field potential simultaneously recorded across both channels. The PEDOT site channel recorded a noise floor of 254 μV (solid red), while the carbon site channel recorded a noise floor of 283 μV (dash blue). (G) Power density spectra across the LFP range showing that for the LFP range both recording materials are similar.

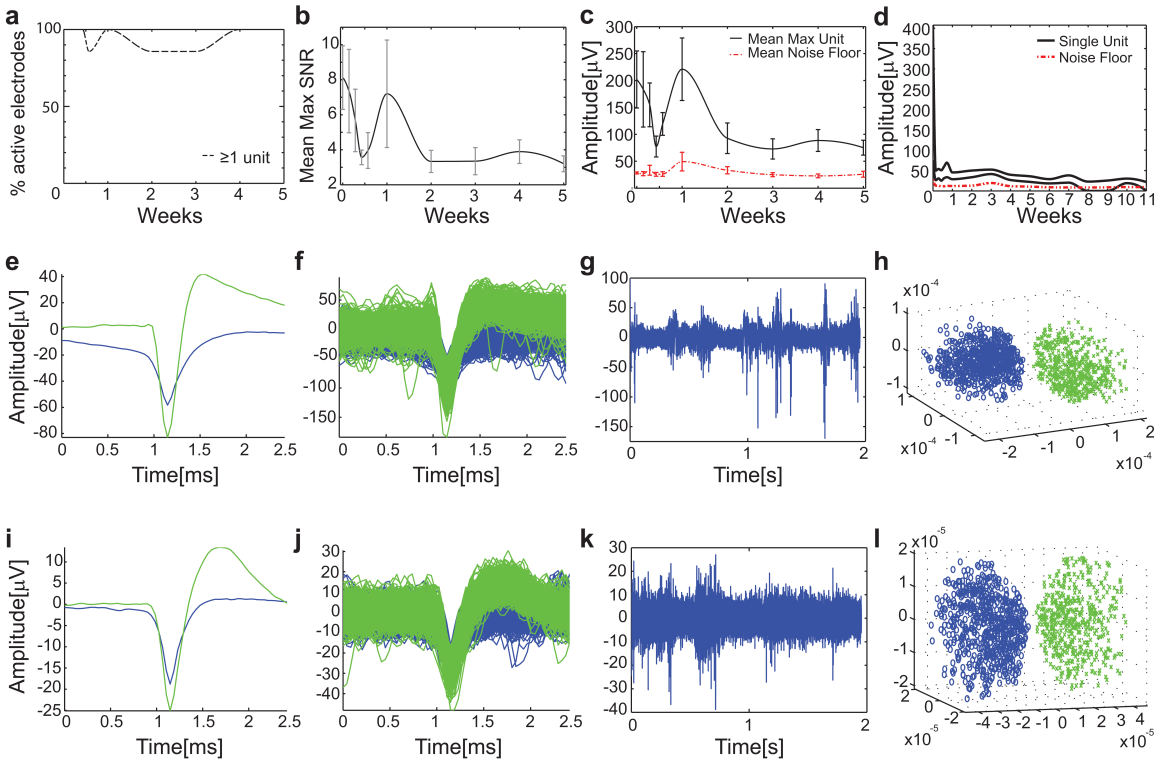

Figure 4.9: (A) Percent of active chronicly implanted MTEs able to detect at least 1 single unit (dashed line) as a function of weeks post-implant (n=7). (B) Mean SNR of the largest single unit detected on each electrode. (C) Mean amplitude of largest single unit detected on each electrode (solid, black), and the mean noise floor of each electrode (dashed, red). (D) Amplitude of single units from longest implant (solid, black). Amplitude of noise floor from same animal (dashed, red). (E-H), Electrophysiological recordings taken from a rat with a MTE implanted in M1 five weeks post-implant. (I-L), Electrophysiological recordings taken from a different rat implanted with a MTE in M1 seven weeks post-implant. (E), (I), Mean waveform of discernable single units. (F), (J), Piled single units from two minutes of recordings. (G), (K), Representative example of two seconds of high-speed recordings. (H), (L), Results from principal component analysis showing distinct clusters.

of time, without any electrophysiological evidence of signal degradation. They also have extremely high yield of unit recordings compared to SOA probes.

4.3.8 Chronic histology

Furthermore, there has recently been an improved understanding of the detailed reactive tissue responses to implantable biosensors (Polikov et al., 2005; Turner et al., 1999). Tissue encapsulation of the probe and neuronal death in the vicinity of the

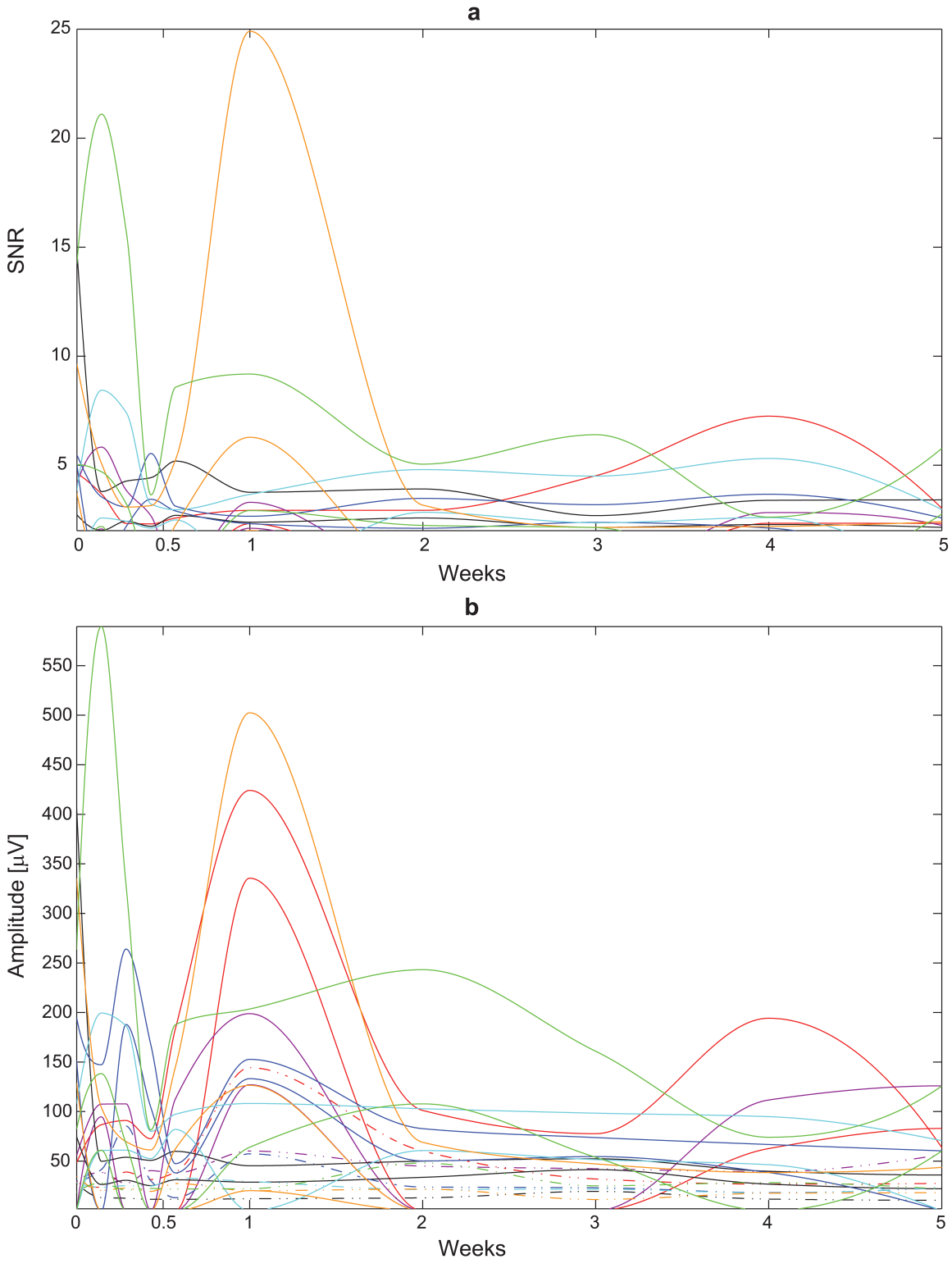

Figure 4.10: Individual chronic *in vivo* recording capabilities of Microthread Electrodes. (A) SNR of discernable single units detected on each electrode as indicated by color (red, orange, green, blue, cyan, purple, black). (B) Amplitude of discernable single unit detected on each electrode (solid), and the mean noise floor of each electrode (dashed) as indicated by color, respectively.

recording electrode has been implicated as the largest variables negatively impacting the stability and longevity of long-term neural recordings (Biran et al., 2005; Szarowski et al., 2003). Chronically implanted tethered MTEs show qualitatively reduced chronic tissue reponse. MTEs illicit a lesser GFAP response in astrocytes compared to the traditional silicon electrode (Fig. 4.11). More microglia can also be observed immediately adjacent to the planar silicon electrode compared to the MTE as indicated by Iba-1 and Hoechst labels (Fig. 4.11). EBA antigen labels healthy blood brain barrier, therefore blood vessels around the silicon electrode shows substantial injury compared to the MTE (Fig. 4.11). Neuronal densities around the silicon electrode are also diminished while several neurons can be observed adjacent to the Microthread electrode (4.12). The MTEs show reduced chronic tissue response across several histological outcomes. These histological data demonstrates the ability of MTEs to have markedly improved microenvironment in neural interfaces within the recording volume of the MTE and suggest progress towards a'stealthy' interface with the brain.

4.4 Discussion

This study demonstrated that novel ultramicroelectrodes with reduced footprint were able to record single unit spikes. To the authors' knowledge this is; 1) the smallest stand-alone implantable neuronal ultramicroelectrode, 2) the first functionalized poly(p-xylylene) surface on an neural biosensor, 3) the smallest recording electrode site size to deposit PEDOT/PSS and successfully record chronic single unit activity in the cortex. Current efforts are substituting the carbon fiber core with a stronger, more flexible carbon nanotube composite material than platinum that is also compatible with traditional microfabrication processes to enable manufacturing

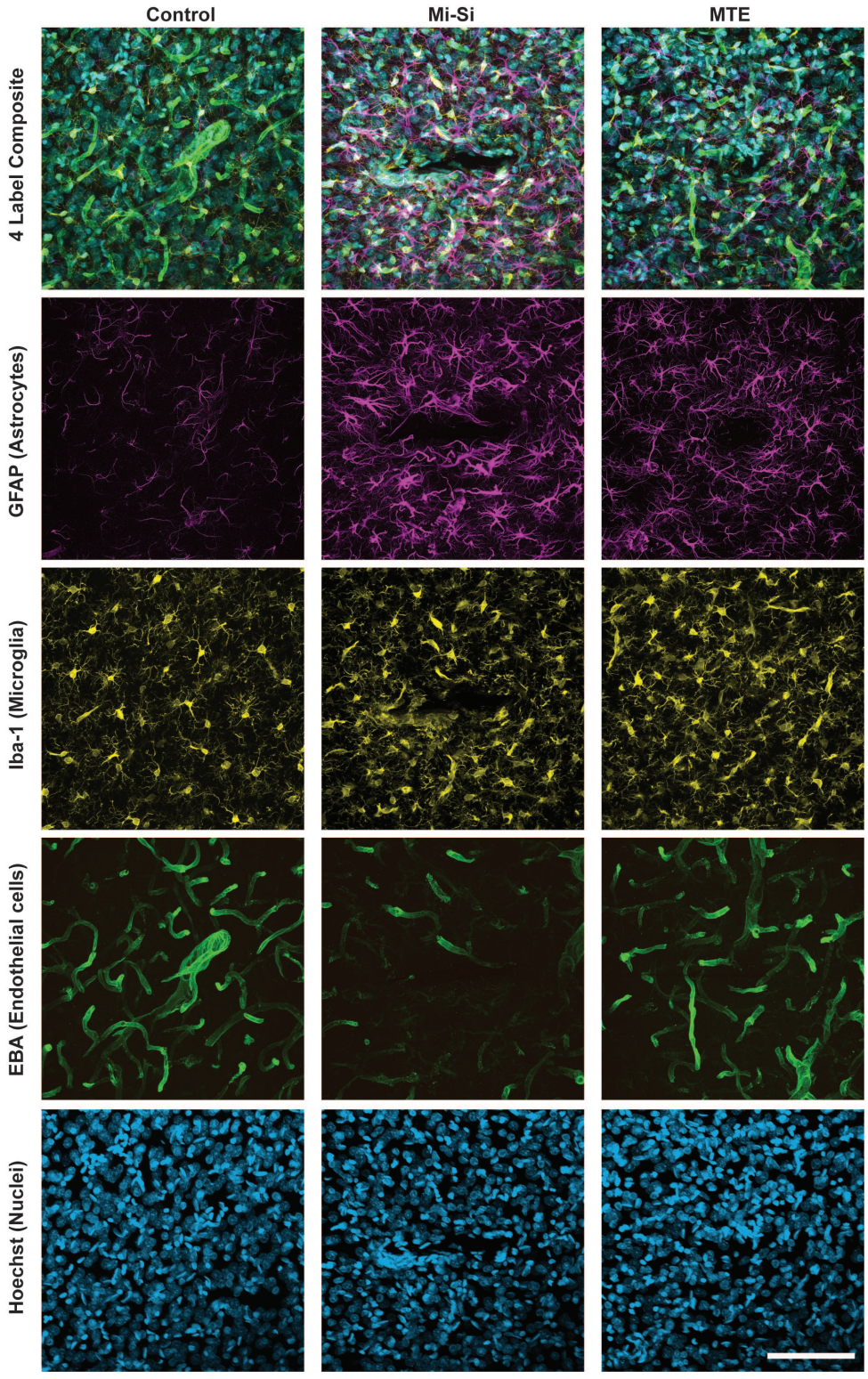

Figure 4.11: Tissue response in motor cortex to two week implanted planar silicon electrode (center), MTE (right), and negative control from the contralateral hemisphere (left). Tissue are labeled with astrocytes (purple), microglia (yellow), BBB/endothelial cells (green), nuclei (blue). Scale bar indicates 100 μm.

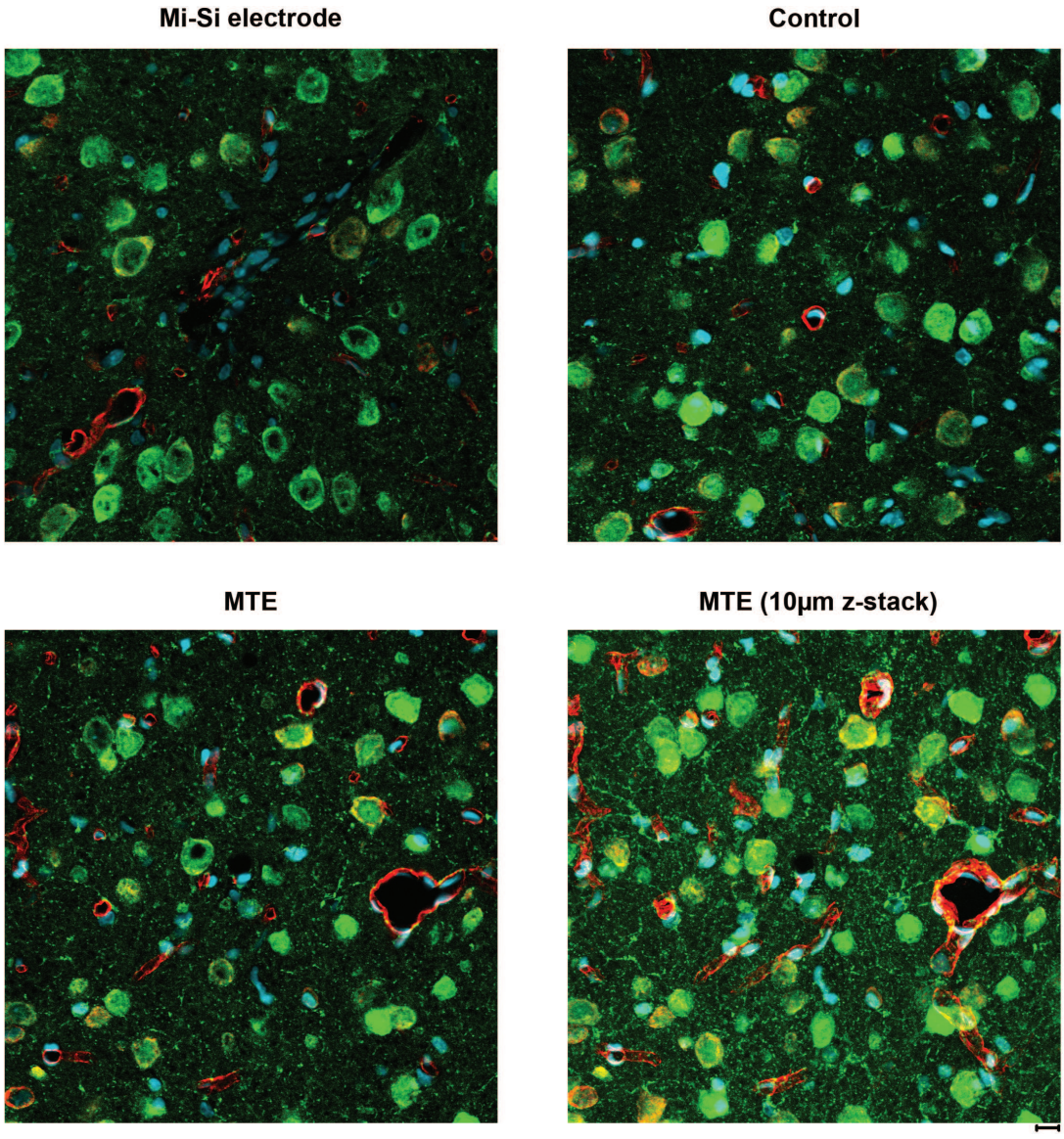

Figure 4.12: Tissue response in motor cortex to two week implanted planar silicon electrode (center), MTE (right), and negative control from the contralateral hemisphere (left). Tissue are labeled with astrocytes (purple), microglia (yellow), BBB/endothelial cells (green), nuclei (blue). Scale bar indicates 100 μm.

of high density arrays (Shim et al., 2007). These devices will be implanted into the brain by leveraging existing and emerging insertion techniques (Jaroch et al., 2009; Kozai and Kipke, 2009). In the future, more complex molecules may be grafted onto the insulation substrate to provide a more bio-mimetic, bio-integrating interface to further blur the line between biotic and abiotic, perhaps with a combination of lipids, growth factors, cell adhesion molecules, drugs, and/or enzymes (Azemi et al., 2011).

The capability of monitoring specific neuronal ensembles for long periods of time with great precision would be a powerful tool in neuroscience research for linking low-level neuronal circuits to high-level brain function, such as learning, memory, and perception. Because of its small size, it is also attractive for use with emerging optical technologies, such as *in vivo* multi-photon microscopy since it produces negligible optical shadows. These biosensors can also easily grafted with a fluorescent label for *in vivo* multi-photon deep tissue microscopy neuroscience studies. Its subcellular footprint also limits the impact of diffusion on biochemical and bioelectrical signaling around the device. Developing smaller and more flexible neural probes with advanced surface materials for long-term, high quality and selective neural recording could potentially lead to paradigm shifts in both neuroscience research and clinical neurotechnologies. The organic integrated composite biosensor technology may be further tuned to other disciplines, such as cardiology, peripheral nerve injury, or transdermal biosensors, to establish stealthy bio-interfaces for monitoring and controlling of intrinsic biological pathways.

4.5 Acknowledgements

This work was financially supported by a National Institutes of Health (NIH) Challenge Grant in Health and Science Research from the National Institute of

Neurological Disorders and Stroke (NINDS, 1RC1NS068396-0110) and the Center for Neural Communication Technology, a P41 Resource Center funded by the National Institute of Biomedical Imaging and Bioengineering (NIBIB, P41 EB002030). Amisha Agarwal and Firas S. Midani assisted in chronic probe assembly/packaging, chronic surgery, and chronic electrophysiological recordings. Amanda L. Ryan and Dr. Sampa Saha conducted ATRP. Dr. Hsien-Yeh Chen carried out Raman Spectroscopy. Immunohistochemistry of chronic implants was conducted by Wadsworth Center Advanced Light Microscopy & Image Analysis Core. Dr. Leah Hains cut the tissue and conducted preliminary immunohistochemistry. N.A.K. and D.R.K. acknowledge partial financial support of this work from DARPA STTR grant (W31P4Q-08-C-0426).

4.6 References

Azemi, E., Lagenaur, C. F., and Cui, X. T. (2011). The surface immobilization of the neural adhesion molecule l1 on neural probes and its effect on neuronal density and gliosis at the probe/tissue interface. *Biomaterials*, 32(2011):681–92.

Azemi, E., Stauffer, W. R., Gostock, M. S., Lagenaur, C. F., and Cui, X. T. (2008). Surface immobilization of neural adhesion molecule l1 for improving the biocompatibility of chronic neural probes: In vitro characterization. *Acta Biomater*, 4(5):1208–1217.

Barzo, P., Marmarou, A., Fatouros, P., Hayasaki, K., and Corwin, F. (1997). Contribution of vasogenic and cellular edema to traumatic brain swelling measured by diffusion-weighted imaging. *J Neurosurg*, 87(6):900–907.

Biran, R., Martin, D. C., and Tresco, P. A. (2005). Neuronal cell loss accompanies the brain tissue response to chronically implanted silicon microelectrode arrays. *Experimental Neurology*, 195(1):115 – 126.

Bjornsson, C. S., Oh, S. J., Al-Kofahi, Y. A., Lim, Y. J., Smith, K. L., Turner, J. N., De, S., Roysam, B., Shain, W., and Kim, S. J. (2006). Effects of insertion conditions on tissue strain and vascular damage during neuroprosthetic device insertion. *J Neural Eng*, 3(3):196–207.

Clark, J. J., Sandberg, S. G., Wanat, M. J., Gan, J. O., Horne, E. A., Hart, A. S., Akers, C. A., Parker, J. G., Willuhn, I., Martinez, V., Evans, S. B., Stella, N., and Phillips, P. E. M. (2010). Chronic microsensors for longitudinal, subsecond dopamine detection in behaving animals. *Nat Methods*, 7(2):126–129.

Cui, X., Wiler, J., Dzaman, M., Altschuler, R. A., and Martin, D. C. (2003). In vivo studies of polypyrrole/peptide coated neural probes. *Biomaterials*, 24(5):777–87.

Dixon, C. E., Clifton, G. L., Lighthall, J. W., Yaghmai, A. A., and Hayes, R. L. (1991). A controlled cortical impact model of traumatic brain injury in the rat. *J Neurosci Methods*, 39(3):253–262.

Gilletti, A. and Muthuswamy, J. (2006). Brain micromotion around implants in the rodent somatosensory cortex. *J Neural Eng*, 3(3):189–195.

Grill, W. M., Norman, S. E., and Bellamkonda, R. V. (2009). Implanted neural interfaces: biochallenges and engineered solutions. *Annu Rev Biomed Eng*, 11:1–24.

Henze, D. A., Borhegyi, Z., Csicsvari, J., Mamiya, A., Harris, K. D., and Buzski, G. (2000). Intracellular features predicted by extracellular recordings in the hippocampus in vivo. *J Neurophysiol*, 84(1):390–400.

Ivens, S., Kaufer, D., Flores, L. P., Bechmann, I., Zumsteg, D., Tomkins, O., Seiffert, E., Heinemann, U., and Friedman, A. (2007). Tgf-beta receptor-mediated albumin uptake into astrocytes is involved in neocortical epileptogenesis. *Brain*, 130(Pt 2):535–547.

Jaroch, D. B., Ward, M. P., Chow, E. Y., Rickus, J. L., and Irazoqui, P. P. (2009). Magnetic insertion system for flexible electrode implantation. *J Neurosci Methods*, 183(2):213–222.

Jiang, X. W., Chen, H. Y., Galvan, G., Yoshida, M., and Lahann, J. (2008). Vapor-based initiator coatings for atom transfer radical polymerization. *Advanced Functional Materials*, 18(1):27–35.

Katira, P., Agarwal, A., Fischer, T., Chen, H. Y., Jiang, X., Lahann, J., and Hess, H. (2007). Quantifying the performance of protein-resisting surfaces at ultra-low protein coverages using kinesin motor proteins as probes. *Advanced Materials*, 19(20):3171–6.

Kim, D.-H., Ahn, J.-H., Choi, W. M., Kim, H.-S., Kim, T.-H., Song, J., Huang, Y. Y., Liu, Z., Lu, C., and Rogers, J. A. (2008). Stretchable and foldable silicon integrated circuits. *Science*, 320(5875):507–511.

Kim, D.-H., Viventi, J., Amsden, J. J., Xiao, J., Vigeland, L., Kim, Y.-S., Blanco, J. A., Panilaitis, B., Frechette, E. S., Contreras, D., Kaplan, D. L., Omenetto, F. G., Huang, Y., Hwang, K.-C., Zakin, M. R., Litt, B., and Rogers, J. A. (2010). Dissolvable films of silk fibroin for ultrathin conformal bio-integrated electronics. *Nat Mater*, 9(6):511–517.

Kipke, D. R., Shain, W., Buzski, G., Fetz, E., Henderson, J. M., Hetke, J. F., and Schalk, G. (2008). Advanced neurotechnologies for chronic neural interfaces: new horizons and clinical opportunities. *J Neurosci*, 28(46):11830–11838.

Kozai, T. D. Y. and Kipke, D. R. (2009). Insertion shuttle with carboxyl terminated self-assembled monolayer coatings for implanting flexible polymer neural probes in the brain. *J Neurosci Methods*, 184(2):199–205.

Kozai, T. D. Y., Marzullo, T. C., Hooi, F., Langhals, N. B., Majewska, A. K., Brown, E. B., and Kipke, D. R. (2010). Reduction of neurovascular damage resulting from microelectrode insertion into the cerebral cortex using in vivo two-photon mapping. *J Neural Eng*, 7(4):046011.

Lacour, S. P., Benmerah, S., Tarte, E., FitzGerald, J., Serra, J., McMahon, S., Fawcett, J., Graudejus, O., Yu, Z., and Morrison, B. (2010). Flexible and stretchable micro-electrodes for in vitro and in vivo neural interfaces. *Med Biol Eng Comput*, 48(10):945–954.

Lahann, J. (2006). Vapor-based polymer coatings for potential biomedical applications. *Polymer International*, 55(12):1361–1370.

Lahann, J., Choi, I. S., Lee, J., Jenson, K. F., and Langer, R. (2001). A new method toward microengineered surfaces based on reactive coating. *Angewandte Chemie-International Edition*, 40(17):3166–9.

LaPlaca, M. C., Cullen, D. K., McLoughlin, J. J., and Cargill, R. S. (2005). High rate shear strain of three-dimensional neural cell cultures: a new in vitro traumatic brain injury model. *J Biomech*, 38(5):1093–1105.

Lee, H., Bellamkonda, R. V., Sun, W., and Levenston, M. E. (2005). Biomechanical analysis of silicon microelectrode-induced strain in the brain. *J Neural Eng*, 2(4):81–89.

Ludwig, K. A., Uram, J. D., Yang, J., Martin, D. C., and Kipke, D. R. (2006). Chronic neural recordings using silicon microelectrode arrays electrochemically deposited with a poly(3,4-ethylenedioxythiophene) (pedot) film. *J Neural Eng*, 3(1):59–70.

Matsumura, M., Chen, D., Sawaguchi, T., Kubota, K., and Fetz, E. E. (1996). Synaptic interactions between primate precentral cortex neurons revealed by spike-triggered averaging of intracellular membrane potentials in vivo. *J Neurosci*, 16(23):7757–67.

McConnell, G. C., Rees, H. D., Levey, A. I., Gutekunst, C.-A., Gross, R. E., and Bellamkonda, R. V. (2009). Implanted neural electrodes cause chronic, local inflammation that is correlated with local neurodegeneration. *J Neural Eng*, 6(5):056003.

Nadal, A., Fuentes, E., Pastor, J., and McNaughton, P. A. (1995). Plasma albumin is a potent trigger of calcium signals and dna synthesis in astrocytes. *Proc Natl Acad Sci U S A*, 92(5):1426–1430.

Nadal, A., Sul, J. Y., Valdeolmillos, M., and McNaughton, P. A. (1998). Albumin elicits calcium signals from astrocytes in brain slices from neonatal rat cortex. *J Physiol*, 509 (Pt 3):711–716.

Neary, J. T., Kang, Y., Willoughby, K. A., and Ellis, E. F. (2003). Activation of extracellular signal-regulated kinase by stretch-induced injury in astrocytes involves extracellular atp and p2 purinergic receptors. *J Neurosci*, 23(6):2348–2356.

Nishimura, N., Schaffer, C. B., Friedman, B., Lyden, P. D., and Kleinfeld, D. (2007). Penetrating arterioles are a bottleneck in the perfusion of neocortex. *Proc Natl Acad Sci U S A*, 104(1):365–70.

Polikov, V. S., Tresco, P. A., and Reichert, W. M. (2005). Response of brain tissue to chronically implanted neural electrodes. *J Neurosci Methods*, 148(1):1–18.

Purcell, E. K., Seymour, J. P., Yandamuri, S., and Kipke, D. R. (2009). In vivo evaluation of a neural stem cell-seeded prosthesis. *J Neural Eng*, 6(2):026005.

Rousche, P. J. and Normann, R. A. (1998). Chronic recording capability of the utah intracortical electrode array in cat sensory cortex. *J Neurosci Methods*, 82(1):1–15.

Schmidt, E. M., Bak, M. J., and McIntosh, J. S. (1976). Long-term chronic recording from cortical neurons. *Exp Neurol*, 52(3):496–506.

Seymour, J. P. and Kipke, D. R. (2007). Neural probe design for reduced tissue encapsulation in cns. *Biomaterials*, 28(25):3594–3607.

Shim, B. S., Tang, Z. Y., Morabito, M. P., Agarwal, A., Hong, H. P., and Kotov, N. A. (2007). Integration of conductivity transparency, and mechanical strength into highly homogeneous layer-by-layer composites of single-walled carbon nanotubes for optoelectronics. *Chemistry of Materials*, 19(23):5467–5474.

Strumwasser, F. (1958). Long-term recording' from single neurons in brain of unrestrained mammals. *Science*, 127(3296):469–470.

Subbaroyan, J., Martin, D. C., and Kipke, D. R. (2005). A finite-element model of the mechanical effects of implantable microelectrodes in the cerebral cortex. *J Neural Eng*, 2(4):103–113.

Suzuki, T., Mabuchi, K., and Takeuchi, S. (2003). A 3d flexible parylene probe array for multichannel neural recording. In *Proc. First Int Neural Engineering IEEE EMBS Conf*, pages 154–156.

Szarowski, D. H., Andersen, M. D., Retterer, S., Spence, A. J., Isaacson, M., Craighead, H. G., Turner, J. N., and Shain, W. (2003). Brain responses to micro-machined silicon devices. *Brain Res*, 983(1-2):23–35.

Takeuchi, S., Ziegler, D., Yoshida, Y., Mabuchi, K., and Suzuki, T. (2005). Parylene flexible neural probes integrated with microfluidic channels. *Lab Chip*, 5(5):519–523.

Turner, J. N., Shain, W., Szarowski, D. H., Andersen, M., Martins, S., Isaacson, M., and Craighead, H. (1999). Cerebral astrocyte response to micromachined silicon implants. *Exp Neurol*, 156(1):33–49.

Unterberg, A. W., Stover, J., Kress, B., and Kiening, K. L. (2004). Edema and brain trauma. *Neuroscience*, 129(4):1021–9.

van Horne, C. G., Bement, S., Hoffer, B. J., and Gerhardt, G. A. (1990). Multichannel semiconductor-based electrodes for in vivo electrochemical and electrophysiological studies in rat cns. *Neurosci Lett*, 120(2):249–252.

Viventi, J., Kim, D.-H., Moss, J. D., Kim, Y.-S., Blanco, J. A., Annetta, N., Hicks, A., Xiao, J., Huang, Y., Callans, D. J., Rogers, J. A., and Litt, B. (2010). A conformal, bio-interfaced class of silicon electronics for mapping cardiac electrophysiology. *Sci Transl Med*, 2(24):24ra22.

Ward, M. P., Rajdev, P., Ellison, C., and Irazoqui, P. P. (2009). Toward a comparison of microelectrodes for acute and chronic recordings. *Brain Res*, 1282:183–200.

Williams, J. C., Rennaker, R. L., and Kipke, D. R. (1999). Long-term neural recording characteristics of wire microelectrode arrays implanted in cerebral cortex. *Brain Res Brain Res Protoc*, 4(3):303–313.

CHAPTER V

Conclusion

5.1 Discussion

This dissertation describes the technology and biology of implantable cortical neural interfaces. These studies employ a multidisciplinary approach that combines molecular biology, biochemistry, chemical engineering, material science, neuroscience, optics, and electrical engineering into the neural engineering discipline to better understand the biological structure and bio-machinery. This approach is applied to produce not only biocompatible devices, but push the envelope to innovate bio-integrating interfaces. The data in this dissertation provides better insight to the details at the brain-machine interface and generates new questions on what actually occurs in the microenvironment surrounding the implant. It also equips the scientific field with new tools to probe these questions so that better intervention strategies may be developed.

In Chapter II, we discussed the development and characterization of an insertion strategy for implanting ultra-flexible polymer neural probes into soft brain tissue. This study applied the use of an electronegative self-assembled monolayer (SAM) as a coating on a stiff insertion shuttle to carry a polymer probe into the cerebral cortex, and then the detachment of the shuttle from the probe by altering the shuttle's

hydrophobicity. The results show that Polydimethylsiloxane (PDMS) and polyimide probes could be inserted into an agarose *in vitro* brain model using the SAM coated silicon insertion shuttles. SAM-coated shuttles were further validated through their use to reliably insert PDMS probes in the cerebral cortex of rodents. This study found that SAM-coated silicon shuttles are a viable method for accurately and precisely inserting flexible neural probes into the brain.

In Chapter III, we studied the acute tissue damage caused by implantation of cortical probes with specific focus on the vasculature disruption during probe implantation. This trauma can cause abnormal electrophysiological responses, elicit temporary increases in neurotransmitter levels, and perpetuate chronic immune responses. This study overcame the challenges for investigators to examine neurovascular features below the surface of the brain *in vivo* by employing 3D multiphoton imaging. Localized bleeding resulting from inserting microscale neural probes into the cortex was investigated and approaches were explored to minimize blood vessel disruption through insertion methods. 3D TPM images of cortical neurovasculature were obtained from mice and used to select preferred insertion positions for probe implantation to reduce neurovasculature damage. The results show significant reduction in neurovascular damage for probes inserted in regions devoid of major sub-surface vessels. Also, the deviation of surface vessels from the vector normal to the surface as a function of depth and vessel diameter was measured and characterized. 68% of the major vessels were found to deviate less than 49 μm from their surface origin up to a depth of 500 μm. Inserting probes more than 49 μm from major surface vessels can reduce chances of severing major sub-surface neurovasculature without using TPM.

Chapter IV reported an integrated composite electrode consisting of a carbon fiber

core, a poly(p-xylylene)-based thin-film coating that acts as dielectric barrier and is functionalized to control intrinsic biological processes, and a poly(thiophene)-based recording pad. The resulting devices were an order of magnitude smaller than currently available neural interfaces and more mechanically compliant with brain tissue than traditional recording electrodes. These microthread electrodes were found to elicit negligible chronic reactive tissue responses and have excellent recording characteristics in acute and chronic experiments in rats. Developing smaller and more flexible neural probes with advanced surface materials for long-term, high quality and selective neural recording could potentially lead to paradigm shifts in both neuroscience research and clinical neurotechnologies by allowing researchers to explore new paradigms in novel ways.

5.2 Future directions of dissertation studies

5.2.1 Insertion shuttle

The insertion shuttle designed in chapter 2 is difficult to handle for inexperienced users and is unable to penetrate dura. Next generation shuttles could be modified to be narrower and thicker to improve handling and decrease the chance of fracture within the tissue. While 15 μm thickness silicon shuttles are unable to penetrate the dura, 50 μm thick silicon shuttles (Escamilla-Mackert et al., 2009) or 40 μm thick C1095 spring steel shuttles can penetrate the dura, and may enable flexible polymer probe insertions through the dura as well as improve robustness and ease of use. Alternative materials may also be titanium or tungsten for deeper insertions in human or monkey brains.

One potential problem with increasing the size of the device is that it may increase insertion trauma. Damage from insertion shuttles may be minimal in chronic implantations since the shuttle is immediately removed similar to a stab wound

(Biran et al., 2005). Additionally, sustained tissue responses have been shown to be similar for two different style probes with an order of magnitude different cross-sectional area (Szarowski et al., 2003), which suggests that a slightly larger shuttle may not produce a noticeable difference in chronic tissue response. However, the specific relationship between shuttle size and stab wound on chronic tissue response has not been determined.

Furthermore, fluidic channels or grooves on the surface of the insertion shuttle could improve separation of the PDMS probe from the insertion shuttle. Additionally, the shape of the shuttle tip could be optimized to reduce mechanical trauma to the tissue during insertion. Incorporating this shuttle approach for controlled insertion techniques with motorized insertions may lead to minimally damaging insertions (Bjornsson et al., 2006; Johnson et al., 2007). Probes and shuttle systems for 3D flexible probes will also need to be designed. Future investigations should also include characterizing adhesion forces between the polymer probe and shuttle before and after release.

Many polymers are currently available for the fabrication of microelectrodes. These polymers have unique characteristics such as flexibility, structural stability, electrical properties, surface chemistry, and biocompatibility. Flexible microelectrode technologies have been underdeveloped in part because investigators lack a precise and efficient method to implant and validate these flexible microelectrodes *in vivo*. The ability to quickly and precisely implant polymer probes into the cortex will promote future polymer microelectrode development. Furthermore, microelectrode geometries (Szarowski et al., 2003), tip shapes, and insertion speeds influence mechanical and chemical strain on the tissue (Bjornsson et al., 2006; Johnson et al., 2007). Uncoupling the biocompatibility and neural integration requirements of probes from

the mechanical and handling requirements for reliably inserting the probe into the brain can allow a new degree of freedom to explore flexible microelectrode designs. Microelectrode tip shape, anchor, stiffness, size, and surface chemistry can be designed for biocompatibility independent of the requirements to minimize insertion trauma. This can in turn open opportunities for innovative microelectrode designs that focus solely on improving the chronic device-tissue interface, such as a flexible planar sinusoidal microelectrode array.

5.2.2 Vascular insertion trauma

The technique developed in chapter 3 to specifically target large subsurface blood vessels enables the ability to control the experimental test space and allows researchers to better understand the effects of blood brain barrier disruption on the electrode-tissue interface. This study enables and motivates subsequent experiments to determine if reducing acute vascular disruption can reduce variability in long-term recording capabilities and tissue reaction. Even within the same microelectrode array, recording sites can fail as early as several weeks or last as long as a few years (Williams et al., 1999; Rousche and Normann, 1998). Further understanding this variability in long-term recording capabilities may improve the efficacy of implanted neural microelectrode sites and provide insight on the molecular level for developing strategies to further prolong long-term recording capabilities.

Furthermore, by using advanced multiphoton microscopy techniques, it is possible to study how neurovascular damage affects encapsulation and how encapsulation grows around an electrode track. Chronic TPM studies may reveal where encapsulation originates: at the probe tip, the probe base (pia), at the largest severed blood vessel, near all severed blood vessels, and/or from nearby large uncut leaking blood vessels suffering from chronic violation, such as micromotion. It may also re-

veal the time course for encapsulation and answer how long encapsulation takes to grow around the entirety of the electrode shaft. Further, understanding the role of the BBB, the mechanisms of BBB disruption, and the physiological mechanisms of its repair on the reactive tissue response may open new revenues of investigation. Findings from these continuation studies can help investigators focus and test their intervention strategies to further improve chronic recordings as well as generate new treatments for other neurodegenerative diseases, such as certain types of multiple sclerosis.

Avoiding neurovasculature during probe insertion may have additional benefits for neural implants since neuronal nuclei statistically lie further away from vessels than would be expected from a random spatial distribution (Tsai et al., 2009). Therefore, by avoiding subsurface neurovasculature near electrode recording sites, there is an increased likelihood of being closer to neuronal nuclei. Newer studies from this group suggest that high densities of neurons may lie in the center of a cortical column while larger vessels tend to penetrate between columns. In any case, a better understanding of patterns of vascular deviation as vessels leave the surface to extend into the parenchyma will allow neurosurgeons to not only optimize their implant locations for cortical prostheses in order to obtain better long-term efficacy, but potentially help to minimize adverse side effects due to cortical vascular disruption and bleeding resulting from trauma of deep brain electrode implantation.

If an association between vascular disruption and long-term recording capabilities is assumed, these results imply that anti-biofouling coatings will be an important part of chronic implantable microelectrodes. Additionally, chronic microelectrodes should be designed to have a small footprint and perhaps be made of a flexible substrate suitable for navigating between or around major penetrating blood ves-

sels. Alternatively, chronic probes designed to have small flexible shanks and tips designed to deflect off diving vessels may allow probes to bend to follow a vessel into the cortex rather than penetrate the vessel. This study suggests that the use of multi-shank electrodes could increase the random chance of having at least some shanks implanted outside 'no implant' zones. However, it also increases the odds that some shanks will not be well positioned. If any shank disrupts a major arteriole during probe insertion, it can cause additional broad range of neuronal damage, by means of ischemia, through loss of perfusion to tissue downstream of the disrupted vessel, causing extended neural loss (Nishimura et al., 2007) and affecting other recording sites. On the other hand, single shank multi-site microelectrodes allow easier navigation of neurovasculature, but it limits the horizontal region in which one can record from the cortex. An alternative design may be a multi-shank microelectrode in which each shank can be individually positioned. Additionally, it may be possible to develop insertion assist devices that perfectly align stereotaxic frames for perpendicular insertions into the surface of the brain by finely controlling the x and y rotational axes. Alternatively, it may be possible to generate and align, perhaps automatically or by generating input coordinates, stereotaxic micropositioners for an optimal angled insertion that will run parallel to a penetrating major vessel. The tradeoff is complexity and surgical time unless an automated system can be developed.

If vascular disruption turns out to not be correlated with long-term recording capabilities, it would allow investigators to focus on other aspects of chronic probe design such as growth factor coatings (Azemi et al., 2008, 2011), stem cell seeding (Purcell et al., 2009), drug delivery (Rohatgi et al., 2009), advanced probe architectures (Seymour and Kipke, 2007), and flexibility (Kozai and Kipke, 2009; Subbaroyan et al., 2005; Lee et al., 2005). The final probe design that addresses the

chronic interface problem is likely to be a fine-tuned combination of these many parameters. However, further investigation of vascular disruption to long-term recording capabilities will allow investigators to prioritize or eliminate these parameters in future probe designs.

5.2.3 Microthread electrode

The data from chapter 4 shows that there are substantial fluctuations in the amplitude of the recording electrode but relatively low changes in noise. Studies focused on understanding the mechanism of this instability may lead to the development of better chronic electrode designs. In order to do this, chronic tracking of the interface will be necessary. Advances in optics, multiphoton microscopy, optrode electrodes, and genetics will provide the technology to enable these studies. In the future, more complex molecules may be grafted onto the insulation substrate to provide a more bio-mimetic, bio-integrating interface to further blur the line between biotic and abiotic, perhaps with a combination of lipids, growth factors, cell adhesion molecules, drugs, and/or enzymes. Another focus will be on substituting the carbon fiber core with a carbon nanotube composite material that is stronger and more flexible than platinum that is also compatible with traditional microfabrication processes to enable manufacturing of high density arrays (Shim et al., 2007), perhaps with integrated circuitry (Viventi et al., 2010; Kim et al., 2008). These devices will be implanted into the brain by leveraging existing and emerging insertion techniques (Jaroch et al., 2009; Kozai and Kipke, 2009). As devices become smaller, packaging becomes an issue. Considerations for packaging will be making the devices easy to handle, easy to deliver to the target region, and easy to reliably extract data. This will be especially true for arrays of flexible sub-cellular electrodes.

The capability of monitoring specific neuronal ensembles for long periods of time

with great precision would be a powerful tool in neuroscience research for linking low-level neuronal circuits to high-level brain function, such as learning, memory, and perception. Because of its small size, it also produces negligible optical shadows making it ideal for use with emerging optical technologies, such as *in vivo* multi-photon microscopy, particularly when the probe surface is grafted with a fluorescent label. Its subcellular footprint also limits the impact of diffusion on biochemical and bioelectrical signaling around the device. Developing smaller and more flexible neural probes with advanced surface materials for long-term, high quality and selective neural recording could potentially lead to paradigm shifts in both neuroscience research and clinical neurotechnologies by allowing researchers to explore new paradigms in novel ways. The organic integrated composite biosensor technology may be further tuned to other disciplines to establish stealthy bio-interfaces for monitoring and controlling of intrinsic biological pathways against injury, disease, or even biochemical warfare.

5.2.4 Other avenues

While large stimulation microelectrode for gross activation of a population of neurons is currently clinically available, precise sensory or feedback stimulation will require smaller microelectrodes. This form of feedback has been shown to have some advantages over stimulating a natural perception, such as hearing (Otto et al., 2005). Controlled activation of small groups of neurons will require smaller microelectrodes. Small stimulating microelectrodes have challenges producing meaningful activation of neurons without causing a large faradaic reaction at the electrode. As biotechnology advances, organic interfaces will become more important.

Glial cells have perhaps been the most poorly understood cellular component in the brain (Streit, 2000; Barres, 2008; Allen and Barres, 2009) as well as the reactive

tissue response. This is further complicated by the fact that microglia have versatile roles in normal brain function (ve Tremblay et al., 2010; Research-Highlights, 2010). New techniques targeting glial cells with optogenetics may provide a new investigative tool for getting closer to these answers (Gourine et al., 2010). Furthermore, advances in genetically labeled optical markers, *in vivo* microscopy, and optogenetics have provided the ground work for technological development in optical microfabcrication. As this technology matures, new implantable optical monitoring tools and techniques will be developed.

5.3 Concluding remarks

Neural prostheses have the potential to provide function to individuals who are injured or suffering from conditions that they were born with. Unfortunately, this technology is still currently in its infancy and suffers from a lack of stable long-term reliability. The current research focus is on minimizing the reactive tissue response to implants and maintaining a level of biocompatibility with the device. However, for long-term stable interfaces, understanding the mechanisms of both reactive tissue response and healthy tissue, and then developing intervention strategies that biointegrate with the host tissue will be necessary. In order to achieve this level of integration, one needs to shift and blur the traditional interface line that separates the body and the machine (or device).

Biology is perhaps the most robustly engineered system existing to date. Molecular biomachineries (enzymes, rybozymes, etc) are perhaps the fastest, most precise nanomachines while cells and organisms are robust systems with self-repairing and reproducing capabilities. Sometimes these systems get damaged beyond repair, genetically, developmentally, or through other injury. The aim is to repair, replace, or

substitute the damaged components while minimally impacting the healthy components.

While stem cell, genetics, and matrix scaffold research may someday surpass BCI's ability to treat these patients and ultimately find cures for them, humanity may take a very long journey not only to unlock the secrets of nature, but also to discuss and navigate through important inhibitions of ethics and regulation before reaching such medical utopia. Even centuries beyond such medical breakthroughs, these biohybrid interfaces may take on different forms to provide people with unprecedented control over their surroundings. Furthermore, the bionic interface technologies developed today will always remain valuable in some shape or form as diagnostic and research tools.

As we continue to improve our understanding of science and evolve our technology, it will become more imperative to apply a multidisciplinary philosophy to research and development. Applying cutting-edge inorganic science, such as optics, to unlocking the mechanism of biology at a molecular, cellular, and systems level will accelerate our understanding of nature. Each scientific and engineering discipline will provide fundamental building blocks that when combined with these new understandings will enable intelligent bio-design, for example through molecular structures, bio-templating, and bio-mimicry. A diverse multidisciplinary background with depth in molecular biochemistry and engineering will provide a powerful marriage to generate unique research tools and medical devices with more intimate biological interfaces to better mankind.

5.4 References

Allen, N. J. and Barres, B. A. (2009). Neuroscience: Glia - more than just brain glue. *Nature*, 457(7230):675–677.

Azemi, E., Lagenaur, C. F., and Cui, X. T. (2011). The surface immobilization of the neural adhesion molecule l1 on neural probes and its effect on neuronal density and gliosis at the probe/tissue interface. *Biomaterials*, 32(2011):681–92.

Azemi, E., Stauffer, W. R., Gostock, M. S., Lagenaur, C. F., and Cui, X. T. (2008). Surface immobilization of neural adhesion molecule l1 for improving the biocompatibility of chronic neural probes: In vitro characterization. *Acta Biomater*, 4(5):1208–1217.

Barres, B. A. (2008). The mystery and magic of glia: a perspective on their roles in health and disease. *Neuron*, 60(3):430–440.

Biran, R., Martin, D. C., and Tresco, P. A. (2005). Neuronal cell loss accompanies the brain tissue response to chronically implanted silicon microelectrode arrays. *Experimental Neurology*, 195(1):115 – 126.

Bjornsson, C. S., Oh, S. J., Al-Kofahi, Y. A., Lim, Y. J., Smith, K. L., Turner, J. N., De, S., Roysam, B., Shain, W., and Kim, S. J. (2006). Effects of insertion conditions on tissue strain and vascular damage during neuroprosthetic device insertion. *J Neural Eng*, 3(3):196–207.

Escamilla-Mackert, T., Langhals, N. B., Kozai, T. D. Y., and Kipke, D. R. (2009). Insertion of a three dimensional silicon microelectrode assembly through a thick meningeal membrane. *Conf Proc IEEE Eng Med Biol Soc*, 2009:1616–1618.

Gourine, A. V., Kasymov, V., Marina, N., Tang, F., Figueiredo, M. F., Lane, S., Teschemacher, A. G., Spyer, K. M., Deisseroth, K., and Kasparov, S. (2010). Astrocytes control breathing through ph-dependent release of atp. *Science*, 329(5991):571–575.

Jaroch, D. B., Ward, M. P., Chow, E. Y., Rickus, J. L., and Irazoqui, P. P. (2009). Magnetic insertion system for flexible electrode implantation. *J Neurosci Methods*, 183(2):213–222.

Johnson, M. D., Kao, O. E., and Kipke, D. R. (2007). Spatiotemporal ph dynamics following insertion of neural microelectrode arrays. *J Neurosci Methods*, 160(2):276–287.

Kim, D.-H., Ahn, J.-H., Choi, W. M., Kim, H.-S., Kim, T.-H., Song, J., Huang, Y. Y., Liu, Z., Lu, C., and Rogers, J. A. (2008). Stretchable and foldable silicon integrated circuits. *Science*, 320(5875):507–511.

Kozai, T. D. Y. and Kipke, D. R. (2009). Insertion shuttle with carboxyl terminated self-assembled monolayer coatings for implanting flexible polymer neural probes in the brain. *J Neurosci Methods*, 184(2):199–205.

Lee, H., Bellamkonda, R. V., Sun, W., and Levenston, M. E. (2005). Biomechanical analysis of silicon microelectrode-induced strain in the brain. *J Neural Eng*, 2(4):81–89.

Nishimura, N., Schaffer, C. B., Friedman, B., Lyden, P. D., and Kleinfeld, D. (2007). Penetrating arterioles are a bottleneck in the perfusion of neocortex. *Proc Natl Acad Sci U S A*, 104(1):365–70.

Otto, K. J., Rousche, P. J., and Kipke, D. R. (2005). Microstimulation in auditory cortex provides a substrate for detailed behaviors. *Hear Res*, 210(1-2):112–117.

Purcell, E. K., Seymour, J. P., Yandamuri, S., and Kipke, D. R. (2009). In vivo evaluation of a neural stem cell-seeded prosthesis. *J Neural Eng*, 6(2):026005.

Research-Highlights (2010). Neurobiology: Trimming brain connections. *Nature*, 468(7321):136–137.

Rohatgi, P., Langhals, N. B., Kipke, D. R., and Patil, P. G. (2009). In vivo performance of a microelectrode neural probe with integrated drug delivery. *Neurosurg Focus*, 27(1):E8.

Rousche, P. J. and Normann, R. A. (1998). Chronic recording capability of the utah intracortical electrode array in cat sensory cortex. *J Neurosci Methods*, 82(1):1–15.

Seymour, J. P. and Kipke, D. R. (2007). Neural probe design for reduced tissue encapsulation in cns. *Biomaterials*, 28(25):3594–3607.

Shim, B. S., Tang, Z. Y., Morabito, M. P., Agarwal, A., Hong, H. P., and Kotov, N. A. (2007). Integration of conductivity transparency, and mechanical strength into highly homogeneous layer-by-layer composites of single-walled carbon nanotubes for optoelectronics. *Chemistry of Materials*, 19(23):5467–5474.

Streit, W. J. (2000). Microglial response to brain injury: a brief synopsis. *Toxicol Pathol*, 28(1):28–30.

Subbaroyan, J., Martin, D. C., and Kipke, D. R. (2005). A finite-element model of the mechanical effects of implantable microelectrodes in the cerebral cortex. *J Neural Eng*, 2(4):103–113.

Szarowski, D. H., Andersen, M. D., Retterer, S., Spence, A. J., Isaacson, M., Craighead, H. G., Turner, J. N., and Shain, W. (2003). Brain responses to micro-machined silicon devices. *Brain Res*, 983(1-2):23–35.

Tsai, P. S., Kaufhold, J. P., Blinder, P., Friedman, B., Drew, P. J., Karten, H. J., Lyden, P. D., and Kleinfeld, D. (2009). Correlations of neuronal and microvascular densities in murine cortex revealed by direct counting and colocalization of nuclei and vessels. *J Neurosci*, 29(46):14553–14570.

ve Tremblay, M., Lowery, R. L., and Majewska, A. K. (2010). Microglial interactions with synapses are modulated by visual experience. *PLoS Biol*, 8(11):e1000527.

Viventi, J., Kim, D.-H., Moss, J. D., Kim, Y.-S., Blanco, J. A., Annetta, N., Hicks, A., Xiao, J., Huang, Y., Callans, D. J., Rogers, J. A., and Litt, B. (2010). A conformal, bio-interfaced class of silicon electronics for mapping cardiac electrophysiology. *Sci Transl Med*, 2(24):24ra22.

Williams, J. C., Rennaker, R. L., and Kipke, D. R. (1999). Long-term neural recording characteristics of wire microelectrode arrays implanted in cerebral cortex. *Brain Res Brain Res Protoc*, 4(3):303–313.